Localization of Carbon Nanotube in Multi-Phase Polymer Composites

RUJIREK WIWATTANANUKUL

Japan Advanced Institute of Science and Technology

Doctoral Dissertation

Localization of Carbon Nanotube in Multi-Phase Polymer Composites

by

RUJIREK WIWATTANANUKUL

Submitted to
Japan Advanced Institute of Science and Technology
in partial fulfillment of the requirements
for the degree of
Doctor of philosophy

Supervisor: Prof. Dr. Masayuki Yamaguchi

School of Materials Science
Japan Advanced Institute of Science and Technology

September 2016

Referee-in-chief : **Professor Dr. Masayuki Yamaguchi**
Japan Advanced Institute of Science and Technology

Referees : **Professor Dr. Tatsuo Kaneko**
Japan Advanced Institute of Science and Technology

Associate Professor Dr. Ken-ichi Shinohara
Japan Advanced Institute of Science and Technology

Associate Professor Dr. Kazuaki Matsumura
Japan Advanced Institute of Science and Technology

Professor Dr. Shuichi Maeda
Yamaguchi University

Preface

Carbon nanotube (CNT) is one of the great materials with superior electrical, thermal and mechanical properties and high aspect ratio. Consequently, CNT-polymer nanocomposites are promising for high-performance applications in various industrial fields. The final properties of polymeric nanocomposites are widely determined by the localization of CNTs in the materials, *i.e.*, in one of component polymer phases or at the interface, during processing.

In this thesis, the processing condition for controlling the localization of multi-walled carbon nanotubes (MWCNTs) in immiscible polymer blends is presented. By carefully adjusting the mixing temperature and/or the addition of thermal stabilizer under inert atmosphere, the dispersion states of MWCNTs can be designed, which have a significant effect on the mechanical and electrical properties of the obtained composites.

I hope this thesis will provide useful information to understand the transfer and localization of CNTs in multi-component systems and contributes the practicable process on CNT-polymer nanocomposite applications in industry.

Rujirek Wiwattananukul

Contents

Chapter 1

General Introduction

1.1 Polymer nanocomposite

Nanotechnology is one of the most popular fields in current studies and required for industrial development due to its remarkable and novel properties. It becomes a significant part of science and technology recently such as biomaterial, drug delivery, fuel cell electrode and polymeric material. In the field of polymer science, new materials have been generated constantly every year and are expected to be developed further in the near future because of their usefulness in industry and daily life [1]. Although polymer materials have many attractive properties such as lightweight, good processability and low production cost, their mechanical properties, *i.e.*, modulus and strength, are much lower than those of metals and ceramics. It is well known that an effective method to improve mechanical properties of a polymer is the addition of nanoscale fillers, *i.e.*, nanofillers, because they have created many opportunities to overcome inadequate properties of traditional polymer components, which significantly expands the range of their applications [2, 3]. Nanofillers are considered as the rigid materials whose dimension is in the range of 1-100 nm.

Among several nanofillers, carbon nanotube (CNT), which was firstly discovered by Iijima in 1991 [4], has outstanding properties in producing nanostructured materials with high potential properties and thereby, has become a hot topic for nanocomposites. It became one of the most attractive candidates to reinforce polymer materials because of the unique structure accompanying with the extreme combination of mechanical, electrical and thermal properties [5, 6]. From all features, CNTs have been considered as one of the most interesting materials to be employed in polymer nanocomposite applications. In essence, the aspect ratio and dispersion state in a polymer matrix, including the alignment, are important for material design [7].

1.2 Carbon nanotube (CNT)

1.2.1 Structure of CNT

CNT is a hollow cylinder of a graphite sheet that has been rolled up into seamless tubes with a small diameter and a length from a few nanometers to several microns. The repeating unit for CNTs is arranged in a hexagonal "honeycomb" mesh of sp^2-hybridized carbons [8, 9].

There are two main types of CNTs, *i.e.*, single-walled carbon nanotubes (SWCNTs) and multi-walled carbon nanotubes (MWCNTs), as illustrated in Fig. 1-1.

SWCNTs consist of one rolled-up graphene sheet with diameter range from 0.7 to 2 nm and a length in micrometer scale. Therefore, these nanotubes have a large aspect ratio, *i.e.*, 10^4-10^5. MWCNTs consist of two or more cylindrical graphene sheets with an interlayer separation of 0.34 nm. The structure is similar to "Russian doll", where weak van der Waals forces bind the tubes together. The diameter of nanotubes is in the range from several nanometers up to about 200 nm [4, 10-12].

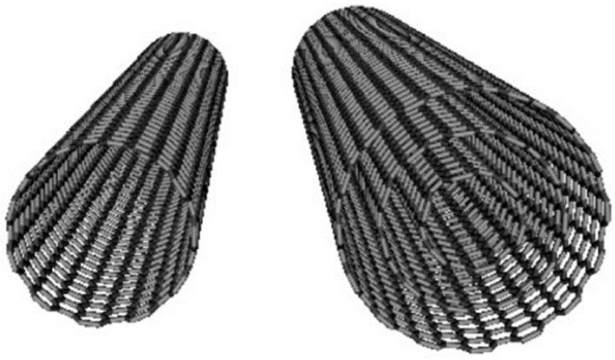

Fig. 1-1 Schematic illustration of (a) SWCNT and (b) MWCNT [13].

By rolling up a graphene sheet in different ways, various configurations of CNTs, *i.e.*, zigzag, armchair and chiral, can be produced as shown in Fig. 1-2. CNTs may be capped at the end by a fullerene hemisphere as presented in Fig. 1-3.

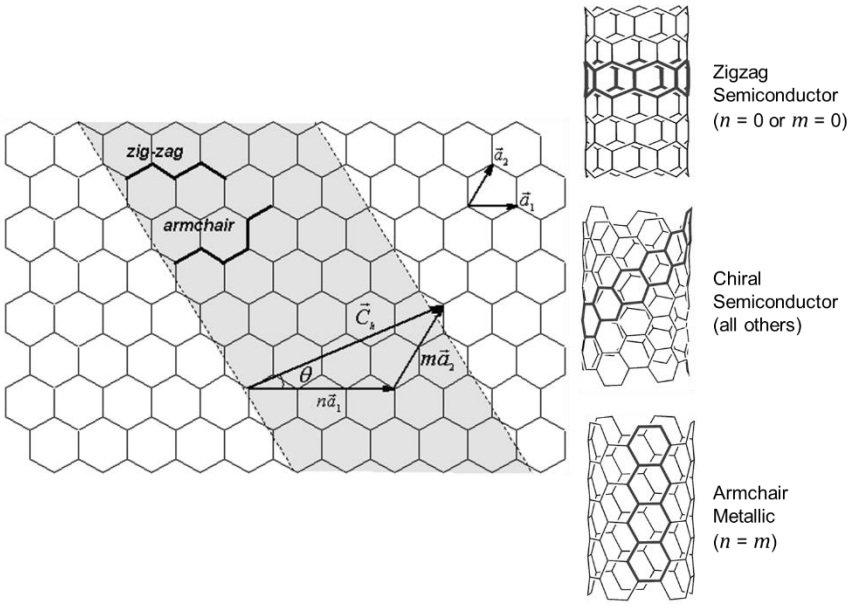

Fig.1-2 Chiral vector on a graphene sheet and possible configurations of CNTs [10].

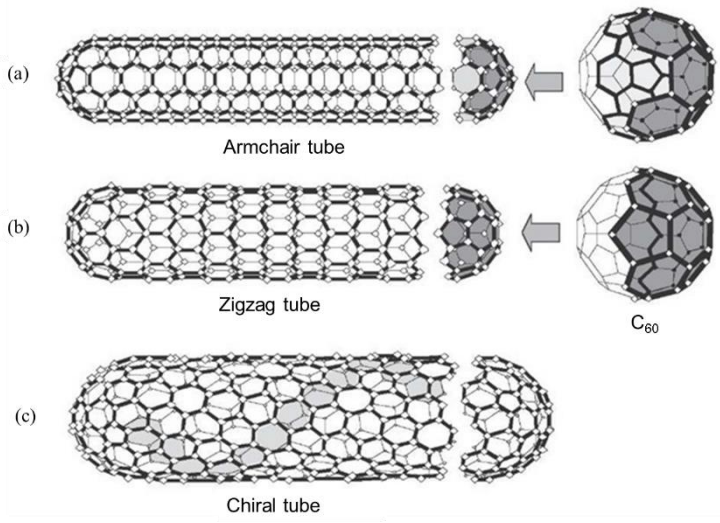

Fig. 1-3 Schematic illustration of nanotube structures: (a) armchair, (b) zigzag and (c) chiral. The cylinders capped with a half of a fullerene molecule are also shown [14].

The properties of CNTs are strongly dependent on their structures, which are typically described in term of a helicity or chirality. The chirality at which the graphene is rolled can be defined by a chiral vector $\vec{C}_h$ and a chiral angle θ. The $\vec{C}_h$ is presented in the term of the lattice translational indices (*n, m*) where *n* and *m* describe the number of the repeating unit in the chiral vector, and the unit vectors $\vec{a}_1$ and $\vec{a}_2$ of the hexagonal lattice correspond to a cross section of the nanotube perpendicular to the long axis.

$$\vec{C}_h = n\vec{a}_1 + m\vec{a}_2 \quad (n \text{ and } m \text{ are integers, } \ 0 \le |m| \le n) \tag{1.1}$$

Chiral angle θ is defined as the angle between the vectors $\vec{C}_h$ and $\vec{a}_1$, with values of θ in the range $0° \le |m| \le 30°$.

$$cos\theta = \frac{\vec{C}_h \cdot \vec{a}_1}{\left|\vec{C}_h\right| \cdot \left|\vec{a}_1\right|} = \frac{2n+m}{2\sqrt{n^2+m^2+nm}} \tag{1.2}$$

The radius of the CNTs is given by L/π, in which L is the circumferential length of CNTs:

$$2b = L/\pi \tag{1.3}$$

$$L = \left|\vec{C}_h\right| = \sqrt{\vec{C}_h \cdot \vec{C}_h} = a\sqrt{n^2+m^2+nm} \tag{1.4}$$

There are three types of structures: the armchair ($n = m$), zigzag ($n = 0$ or $m = 0$) and chiral ($n \neq m$). The chirality of a nanotube is significantly important for its electronic properties. Armchair CNTs are metallic, while other configurations provide semiconducting character [10, 14-16].

1.2.2 Manufacturing methods

CNTs can be manufactured by different methods which are divided into two main groups: high-temperature evaporation using arc discharge or laser ablation, and chemical vapor deposition (CVD) or catalytic growth processes. The produced CNTs with high purity, large amount, uniformity and low cost are highly required for the production. Schematic representation of these processes is shown in Fig. 1-4.

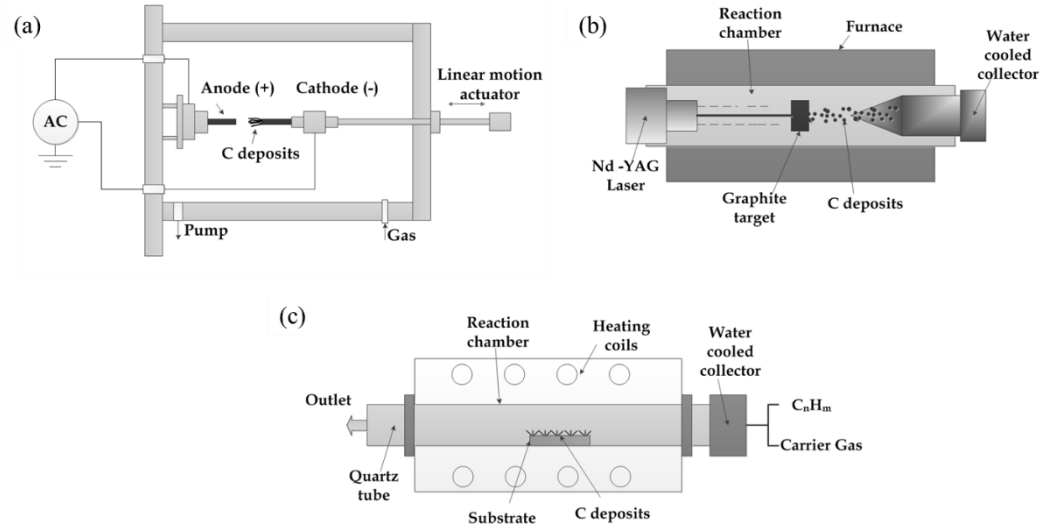

Fig. 1-4 Schematic illustrations of methods used for CNT production: (a) acr discharge, (b) laser ablution and (c) chemical vapor decomposition (CVD) [17].

Arc discharge method

This method was firstly developed to produce both SWCNTs and MWCNTs. The electric arc discharges have a diameter range from 5 to 20 nm, and the gap between electrodes, which consist of graphite, is around 1 mm. The production requires a low-voltage (~12 to 25 V) but high temperature (> 5,000 °C) under an inert gas atmosphere, *e.g.*, argon and helium. Although this method is tangled with poor control, it is possible to selectively grow SWCNTs or MWCNTs by controlling the variation of parameters, *e.g.*, temperature, pressure, gas species and catalyst, employed in this technique [6, 14]. The obtained CNTs are short with diameters of 1.2-1.4 nm (SWCNTs) and 1-3 nm (MWCNTs).

Laser ablation

A graphite target is vaporized by laser irradiation under an inert gas atmosphere at a high temperature (1,200 °C). The received CNTs are very pure, but the production rate is low because only bundles of SWCNTs with 5-10 μm in length and 1-2 nm in diameter are being produced. Therefore, it is not effective for a large-scale synthesis [18, 19].

Chemical vapor deposition (CVD)

This technique is an alternative method in which CNTs are grown using a catalyst. The nanotubes are produced from the decomposition of a continuous carbon containing gas on the substrate with the presence of a metal catalyst (iron, nickel or cobalt). The precipitation of carbon from the saturated metal particles leads to the formation of CNTs. The produced CNTs with controlled length and diameter can also be achieved via this CVD method. Long nanotubes with diameters ranging from 0.4-5 nm (SWCNTs) and 10-200 nm (MWCNTs) can be obtained. Due to the continuous supply of a gas, a high purity CNTs can be produced in a large scale with a good yield. Therefore, it has a capability to scale up into a commercialized level [20].

All of these methods are still under development and every technique provides diverse advantages and disadvantages for the quality and manufacturing methods.

1.2.3 Properties of CNT

CNTs have gained much interest due to their remarkable physical properties with an extremely high aspect ratio. Furthermore, their low density (800-1,800 [kg/m^3]) should be focused for high potential applications. Details of the properties are given below.

Mechanical properties

CNTs have been recognized as one of the strongest materials in the world because of the covalent sp^2 bonds between the individual carbon atoms. A perfect arrangement of the carbon-carbon bonds along the cylinder axis provides significantly high mechanical properties. The properties of CNTs have been intensively studied by both experimental measurements and simulations [8, 14]. The elastic modulus is determined by three kinds of forces: two types of strong intralayer carbon-carbon bonds and one weak interlayer interaction (only for MWCNTs). The intralayer forces consist of strong σ-bonding and π-bonding between carbon atoms, which offer CNTs very high modulus and tensile strength. It has been reported that Young's modulus of SWCNTs is in the range of 0.32-1.47 TPa, while that of MWCNTs is over 1TPa. Furthermore, the tensile strength in the range of 10-200 GPa for MWCNTs, which is 10 to 100 times higher than that of the strongest carbon steel (1.2 GPa) [8, 12, 14, 21]. Due to the extremely high strength of CNTs, they can bend without breaking. Therefore, they give possibilities for the use of highly elastic and very strong composite fillers.

Thermal properties

CNTs are of the great interest for not only their excellent mechanical properties,

but also their thermal properties, in particular, high thermal conductivity. Theoretical predictions have revealed that CNTs are very good thermal conductors along the tube axis but good insulators in the transverse direction [22]. In the classical Debye model, the thermal conductivity depends on the following three parameters: the phonon free path, the phonon velocity and the phonon heat capacity. Due to the nanoscale structure of CNTs, the quantum effect is expected, and thermal conductivity shows evidence of 1D-quantization of the phonon band structure. The thermal conductivity of a defect-free CNT can be as high as 6,000 W/mK, while the thermal conductivities of diamond and graphite crystal are around 3,320 and 2,000 W/mK, respectively [23].

Electrical properties

CNTs possess unique electrical properties with a large band gap, and the properties are closely related to their molecular structure [4]. More specifically, a CNT's band structure depends on its chirality as previously mentioned in 1.2.1. Armchair CNTs ($n = m$) show metallic conducting behavior, while zigzag (n or $m = 0$) and chiral ($n \neq m$) are semiconductors [10, 14, 15, 24]. Additionally, MWCNTs are more complex than SWCNTs because each of their carbon shells can have a different chirality and electronic character. The metallic properties of the MWCNTs are due to their multiple-shell structure

consisting of tubes with various electrical properties. In general, however, most MWCNTs act as a good one-dimensional conductors [25]. Moreover, MWCNTs are predicted to have ballistic electron transport at room temperature, *i.e.*, zero resistance along their length. Therefore, they can have conductivities several times greater than metals such as silver and copper [26].

Optical properties

The experimental measurements of the optical adsorption of a bundle of SWCNTs demonstrate that there are several absorption peaks. Each peak is related to the geometry of CNTs. The peak absorbance strongly depends on the CNT diameter and its chirality [27-29]. Since CNT thin sheets with low absorption from the UV region to the near-infrared can be manufactured, a great interest has been focused to produce transparent electrodes.

1.3 Polymer composite containing CNTs

Polymer composites, which consist of a polymer matrix with nanofillers, are greatly interesting and researched areas in nanotechnology because they have demonstrated their potential as high-performance materials. In this dissertation, CNT is

considered as one of the most interesting nanofillers for future applications. However, in spite of superior properties of CNTs combined with their low density and high aspect ratio, the way to use this nanofiller is not easy. Because of their non-reactive surface, CNTs have a bond with a polymer through physical interaction rather than chemical interaction, resulting in a weak interaction between a polymer and CNTs, which limits the efficient load transfer [30]. Besides, CNTs are difficult to be dispersed individually in a polymer matrix because they form bundles due to strong van der Waals interaction between individual tubes. The origin of the attractive force between neighboring tubes is the π-π interaction that causes a high van der Waals force, leading to an agglomeration of CNTs [1, 5, 31].

In order to disperse CNTs individually and uniformly within a polymer without destroying their high aspect ratio and integrity, several methods are employed such as functionalization of CNT surfaces by strong acid or solvents, the use of polymers to coat the CNT surfaces, *in-situ* polymerization, ultrasonic dispersion in solution, melt processing, the use of surfactants and so on. These methods allow CNTs to interact better with a matrix and thus overcome the van der Waals interaction between each nanotube.

1.3.1 Preparation of polymer composite containing CNTs

Several processing techniques are presented for preparing polymer composites containing CNTs. A good filler dispersion is required to achieve an effective utilization of CNTs in composite applications. Commonly, there are three methods for preparation.

Melt-blending

This technique is an effective method for introducing fillers into a viscous polymer melt. High temperature and high shear force are required for this technique to enhance the dispersion of fillers. The advantages of this method are as followed; (1) the filler can be dispersed into the polymer directly without the use of a chemical solvent and (2) the re-agglomeration of fillers is prohibited by the high viscous polymer. Moreover, this method is suitable for current industrial manufacturing. Many studies have shown the successful application of melt-blending in dispersing CNTs into various polymer matrices, *e.g.*, polycarbonate (PC) [32], polypropylene (PP) [33] and polyamide 6 (PA6) [34, 35]. Furthermore, melt-blending can be performed in two ways: (i) direct incorporation of CNTs into a polymer during melt-mixing and (ii) dilution of a masterbatch, *i.e.*, a polymer composite with a large amount of CNTs. At both cases, the mixing performance is strongly influenced by processing parameters such as mixing temperature, mixing time

and applied flow field [32, 36, 37].

Solution blending

This is the most common method in an experimental scale for fabricating polymer composites, which involves three steps: (i) dispersing CNTs into a suitable solvent, (ii) mixing CNT suspension with a polymer and (iii) evaporating the solvent. This technique effectively provides relatively well-dispersed CNTs in a polymer matrix under high-power ultrasonication for a period of time. Note that high-power ultrasonication may shorten CNT length, which is disadvantageous for the composite properties [38]. Normally, CNTs tend to form bundles because of van der Waals forces and physical entanglements between the tubes. The presence of CNT aggregates makes these fillers insoluble in a solvent. In order to solve this drawback, the introduction of a functionalization of the CNT surface is used to enhance the interaction between fillers and a host matrix. On the other hand, the surface properties of CNTs can be impacted negatively by solution blending, and the scale-up should be concerned because of the residue chemical solvent [38, 39].

***In-situ* polymerization**

The fabrication starts by dispersing CNTs in a monomer followed by polymerizing monomers. This process is an essential method for preparation of thermoset and rubber-based composites. For instance, an epoxy nanocomposite has been extensively studied using this technique, where CNTs are firstly dispersed in the precursor resin and followed by curing by hardener [40, 41]. The advantage of this process is that polymer chains can be grafted on the CNT surface, which gives a good dispersion of CNTs and a good interfacial strength between them. It should be noted that the viscosity of a polymer medium increases, which may limit the degree of polymerization [40-44].

1.3.2 Properties of polymer composite containing CNTs

Mechanical properties

The unique structure of CNTs and their high aspect ratio, low density and superior mechanical properties provide an outstanding reinforcing ability for polymeric materials. In order to efficiently increase the ability, the load transfer between CNTs and a polymer matrix should be considered. If a load is effectively transferred to CNTs, the modulus will be similar to that of the composite containing randomly oriented short fibers, which shows tremendously high modulus and tensile strength [5]. The addition of CNTs

into a polymer is expected to enhance the Young's modulus and tensile strength significantly with a relatively small amount. For example, Breuer and Sundararaj found 25% improvement in the tensile strength of PS by 1 wt.% of MWCNTs [31]. Dondero et al. prepared PP/MWCNT composites using the melt-mixing method followed by melt-drawing, and found that the toughness and modulus of PP increase about 32 and 138%, respectively, with 0.25 wt.% of MWCNTs [45]. On the contrary, in many cases, the elongation at break is decreased after the addition of CNTs [46, 47].

The tensile modulus and strength of CNT-filled polymer composites are strongly influenced by the CNT content, dispersion state and alignment. However, the experimental results at low CNT loadings usually stand far behind the theoretical predictions from the rule of mixture such as the Halpin-Tsai model [48]. This model is generally used to predict an elastic modulus of reinforced composites and can also be used to describe a stiffening effect of the CNT or nanofillers with large aspect ratio in polymer nanocomposites.

$$\frac{E_c}{E_p} = \frac{1 + 2(L/D)\varsigma V_f}{1 - \varsigma V_f} \tag{1.5}$$

where E_c and E_p are moduli of the composite and polymer matrix, respectively, and V_f is the volume fraction of fillers (CNT in this case). L and D are defined as diameter and length of CNTs. ς is the filler orientation efficiency factor, which is defined by

$$\varsigma = \frac{(E_f/E_p)-1}{(E_f/E_p)+2(L/D)} \tag{1.6}$$

where E_f represents the Young's modulus of the filler.

Haggenmueller et al. demonstrated that the tensile modulus of PE fiber was enhanced from 0.65 to 1.25 GPa with the addition of 5 wt.% SWCNTs, while the Halpin-Tsai model predicts the modulus to be around 16 GPa at the same filler loading [49]. At higher CNT loading, the viscosity of a composite becomes high, which limits the ability of the improvement and resulting in void defect [41]. The difference between the prediction and experimental results is caused by imperfect dispersion of CNTs and poor load transfer. Additionally, the modulus of agglomerated CNTs is lower than that of isolated CNTs, because the agglomerates have small aspect ratio combined with poor dispersion in a matrix. They result in insufficient stress transfer, leading to a composite with low mechanical properties. Hence, extremely high modulus and strength without losing in elongation at break can be achieved only by a proper mixing.

Electrical properties

The utilization of CNTs to improve electrical properties of polymer composites has been successfully realized. It is well known that a polymer is an insulating material which is desired for many applications. Nevertheless, due to the rapid growth of electronic

applications, conductive plastic parts are also required in electric devices. In fact, conductive polymers can be obtained when the filler content exceeds a critical value, known as a "percolation threshold". At the percolation threshold, a three-dimensional conductive network is formed, leading to a sharp jump in the conductivity by several orders in magnitudes [12, 32, 50], as shown in Fig. 1-5.

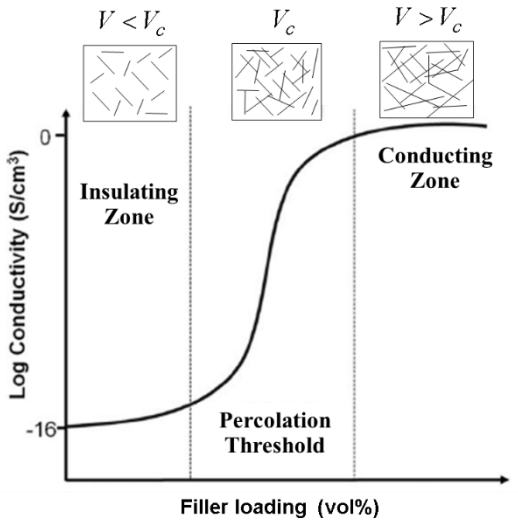

Fig. 1-5 Electrical conductivity as a function of CNT loading. When the filler content exceeds the critical filler content (V_c), the insulate-to-conductive transition will occur.

Presently, several fillers such as carbon black (CB) and carbon fiber (CF) are employed to improve the conductivity of a polymer. However, high loadings of such fillers are often needed to gain conductive materials. Furthermore, it increases the final

cost of the materials. In contrast, CNT/polymer composites exhibit an extremely low percolation threshold, which is attributed to the high aspect ratio and nanoscale dimension of CNTs. Consequently, a conductive material with a small amount loading is possible to achieve while the other performances of a polymer can be maintained.

The percolation threshold of polymer composites containing CNTs is affected by aspect ratio, dispersion and alignment of CNTs. In general, the percolation threshold is reduced by good dispersion [22]. This topic has been studied by Du et al. using a series of SWCNT/ poly(methyl methacrylate) (PMMA) composites, where the degree of CNT alignment was controlled by the melt spinning. At a constant SWCNT concentration, *e.g.*, 2 wt.%, it was found that high orientation of fillers significantly reduces the electrical conductivity of composites, which is attributed to the fewer contacts between SWCNTs, resulting in a higher percolation threshold [51, 52]. Besides, a chemical functionalization is widely used to improve the electrical properties of composites. Valentini et al. indicated that the amine-functionalized SWCNTs in an epoxy matrix allow transportation of intrinsic charges, leading to a good electrical conductivity [53].

Rheological properties

Rheological properties of polymer/CNT composites are very important to

understand the structure and their processability. In particular, rheological responses in the low-frequency region should be focused because they are sensitive to the structure, and thus have a close relationship with their electrical and mechanical properties in the solid state. In contrast, processability can be estimated roughly from the responses in the high-frequency or high shear rate region [54]. It should be noted that a significant change in the melt rheological behavior, *i.e.*, a visible increment in viscosity and a sudden increase in yield stress, occurs around at the percolation. These effects are more pronounced in storage shear modulus *G'* than in loss shear modulus *G"* [54, 55].

The non-terminal flow behavior, as often observed in composites with CNTs, is attributed to the formation of CNT network in a polymer matrix. As the CNT amount increases, nanotube-nanotube interactions begin to dominate, leading to the percolation and the formation of interconnected structure of CNTs, as shown by Pötschke et al. [32, 50, 56]. In other words, the rheological transition occurs from liquid-like ($G' \propto \omega^2$) to solid-like viscoelastic behaviors at the percolation threshold (*G'* and *G"* are independent of ω). It is well known that the rheological properties obey the power low near the sol-gel transition as follows.

$$\eta^* \propto (m - m_c)^a \tag{1.7}$$

$$G' \propto (m - m_c)^b \tag{1.8}$$

where η^* is the complex viscosity, *G'* is the storage modulus, *m* is the CNT loading, m_c is the rheological percolation threshold of the CNT loading, and, *a* and *b* are the critical exponents.

It is generally accepted that the rheological properties of composites also depend on dispersion and orientation of fillers and aspect ratio [57]. A good dispersion of fillers in a polymer matrix efficiently enhances *G'* and also reduces the rheological percolation threshold [22]. It has been also shown that the contacts between nanotube and nanotube decreases with increasing the orientation of CNTs. Hence, it can be concluded that the viscoelastic properties of composites are sensitive to the orientation of fillers [57, 58]. Moreover, it has been shown that the rheological percolation threshold is sensitive to the temperature, implying that rheology reflects a combined network of the polymer chains and CNTs [58, 59] (not only the interconnection between CNTs).

1.4 Polymer blend containing CNTs

1.4.1 Polymer blend

Polymer blends, *i.e.*, a mixture of at least two or more polymers, are generally used to develop a new material with different properties. The desired properties can be accomplished using this approach. Thermodynamically, there are two classifications of

polymer blends, *i.e.*, miscible and immiscible blends, defined by the following relation [60]:

$$\Delta G_{mix} = \Delta H_{mix} - T\Delta S_{mix} \quad (1.9)$$

where ΔG_{mix} is the Gibbs's free energy of mixing, ΔH_{mix} is the enthalpy of mixing and ΔS_{mix} is the entropy of mixing. One phase will be obtained in a blend in the equilibrium state when the Gibbs's free energy of mixing is negative. Though the entropy of mixing is always positive, the contribution is negligible because of the high molecular weight. Therefore, the sign and magnitude of ΔH_{mix} usually determine the sign of ΔG_{mix}. Due to high molecular weight, as mentioned above, the mixing entropy of a blend is extremely low, which can be regarded as 0. Further, the mixing enthalpy is positive for most polymer pairs. Consequently, the sign of ΔG_{mix} is positive, leading to phase separation for polymer-polymer blends. Therefore, most polymer blends show separated-phase morphology, *e.g.*, sea-island structure and co-continuous structure. The phase morphology of a polymer blend plays an important role in the final properties. In other words, a polymer blend with desired properties can be tailored by controlling its morphology.

In this thesis, CNTs are further added in immiscible polymer blends. The introduction of MWCNTs into commercial thermoplastic blends can be found such as polyethylene (PE)/PC [61], poly(ethylene terephthalate) (PET)/poly(vinylidene fluoride)

(PVDF) [62], PP/acrylonitrile-butadiene-styrene terpolymer (ABS) [63], etc. Mechanical and electrical properties of polymer blends can be greatly enhanced by the addition of a small amount of CNTs due to their superior structure.

When CNTs are introduced into a polymer blend, three cases of filler dispersion can take place (Fig. 1-6): (i) CNTs are randomly dispersed in both polymer phases, (ii) CNTs selectively reside in only one of phases and (iii) CNTs localize at the interface between phases [64-67]. In order to control the structure, the recipe of a polymer blend and processing conditions have to be appropriately selected.

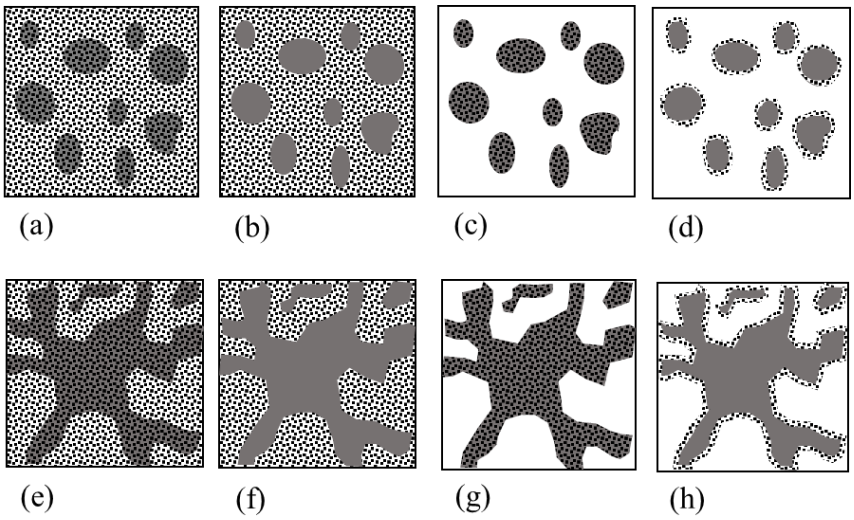

Fig. 1-6 Possible uneven distributions of CNTs in an immiscible polymer blend. (a) - (d) represent sea-island structure, while (e) - (h) show co-continuous structure with different CNT localizations.

It is noted that, although three types of the filler distribution can occur, the desired properties of polymer blends containing CNTs are usually obtained from two morphologies: (i) localization in one polymer phase [Fig. 1-6 (b, c, f and g)] and (ii) localization at the interphase between polymer phases [Fig. 1-6 (d and h)].

1.4.2 Localization of CNTs

As presented in Fig. 1-6, CNTs will reside in one phase or at the phase boundary. There are two main factors to determine the localization of the fillers: thermodynamic and kinetic effects.

1.4.2.1 Thermodynamic effect

The selective localization of CNTs in a polymer blend is related to the difference in interfacial tensions between the filler and polymers. Furthermore, the interfacial tension is determined by the difference in polarity and surface free energy (Fig. 1-7) [68].

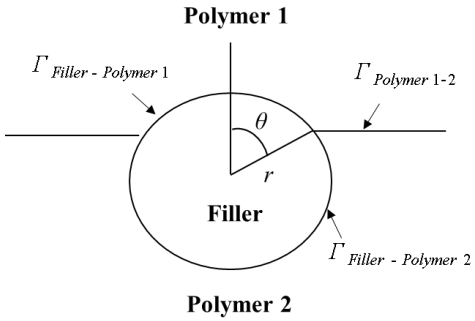

Fig. 1-7 Schematic representation of the interface between polymer 1, polymer 2 and filler.

Preferential localization of CNTs can be predicted by the wetting coefficient ω_a defined as Eq. 1.10 [68], that is obtained from the Young's equation.

$$\omega_a = \cos\theta = \frac{\Gamma_{Filler-Polymer\ 2} - \Gamma_{Filler-Polymer\ 1}}{\Gamma_{Polymer\ 1-2}} \tag{1.10}$$

where θ represents the contact angle, and $\Gamma_{Filler\text{-}Polymer\ 2}$, $\Gamma_{Filler\text{-}Polymer\ 1}$ and $\Gamma_{Polymer\ 1\text{-}2}$ represent the interfacial tensions between the filler and polymer 2, the filler and polymer 1, and the polymers 1 and 2, respectively.

This equation describes the adjustment of wetting angle on filler surfaces, and is the most common approach to predict the filler location after melt blending.

As described by Sumita et al. [64], fillers will locate in polymer 1 at $\omega_a > 1$ and in polymer 2 at $\omega_a < -1$. Fillers will reside at the interface between two polymers at $-1 < \omega_a < 1$. The last situation is possible to occur in a polymer blend composed of polymers

with a large interaction parameter or when the difference in the interfacial tension between filler and polymer is significantly small. This coefficient can be used as a thermodynamic indicator to predict the distribution of fillers in a specific area in a polymer blend with multiphase. Usually, interfacial tensions between polymers are estimated by the theoretical models, *i.e.*, Wu [69], Owens-Wendt [70] or Girifalco-Good [71] equations (Eqs. 1.11-1.13). Those equations are based on the measurement of the surface free energy of each component.

$$\Gamma = \gamma_1 + \gamma_2 - 4\left[\frac{\gamma_1^d \gamma_2^d}{\gamma_1^d + \gamma_2^d} + \frac{\gamma_1^p \gamma_2^p}{\gamma_1^p + \gamma_2^p}\right] \tag{1.11}$$

$$\Gamma = \gamma_1 + \gamma_2 - 2(\sqrt{\gamma_1^d \gamma_2^d} + \sqrt{\gamma_1^p \gamma_2^p}) \tag{1.12}$$

$$\Gamma = \gamma_1 + \gamma_2 - 2\sqrt{\gamma_1 \gamma_2} \tag{1.13}$$

The exponents *d* and *p* represent the dispersive and polar contributions to the surface free energy. Such calculations, based on the Owens-Wendt equation, have been done by Sumita et al. for PE/PP, PE/PMMA and PP/PMMA blends with CB [64, 72], by Elias et al. for silica dispersed PP/polystyrene (PS) and PP/EVA blends [73, 74], and by Göldel et al. for MWCNT dispersion in PC/poly(styrene-*co*-acrylonitrile) (SAN) blends [75]. It is important to note that the surface free energy of a polymer is dependent upon temperature [68]. However, almost interfacial tensions between a filler and a polymer are evaluated at room temperature, while the morphology is decided in the molten state. It suggests that

the thermodynamic equilibrium state may be difficult to reach and kinetic effects, such as mixing protocol and viscosity, should be taken into account.

1.4.2.2 Kinetic effect

Kinetic effect is directly attributed to the mixing process. It is known that the dispersion state of fillers in a polymer blend is often different from the equilibrium one because of its high viscosity. Fillers may reside in a polymer that has a lower viscosity or melting point, even though it has a lower interaction with fillers than another phase. Nevertheless, it has been shown that the localization can be changed by controlling kinetic factors.

Mixing protocol

The order in the component addition, *i.e.*, mixing protocol, is important and has a strong effect on the final distribution of CNTs. Generally, fillers can be introduced into a polymer blend by several methods:

(i) All components are simultaneously mixed in a mixing machine. As mentioned previously, the melting point of a polymer affects the distribution of fillers. If one polymer melts at a temperature apparently lower than the other polymer,

fillers may localize into the first one. [76].

(ii) Two polymers are mixed together and subsequently introduced fillers into the melt blend.

(iii) Fillers are firstly introduced into one polymer, *i.e.*, masterbatch, and diluted by another polymer.

Depending on the mixing orders, CNTs may transfer from one polymer to the other to reduce the free energy. For example, Zaikin et al. have varied the mixing order of polymer pairs with CB. They found that the mixing order significantly affects the localization of CBs, leading to different conductivity [77, 78]. Furthermore, Gubbles et al. studied the transfer behavior of CBs in co-continuous PS/PE blends as a function of duration of mixing. The CBs were firstly melt-mixed with PS, and then PE was further added. It was found that CBs tend to move from less preferred PS toward preferred PE phase with prolonged mixing, resulting in an obvious difference in resistivity. When CBs are localized at the interface, the resistivity is low. Then, the value gradually increases with the filler migration. With this strategy, an extremely low amount of CBs (0.4 wt.%) is enough to produce a conductive PS/PE blend. It implies that the preferential localization of fillers can be controlled by mixing condition [79, 80].

Viscosity

The viscosity ratio of component polymers is one of the major factors to determine the morphology of a polymer blend. When the selective localization of fillers in one phase in a phase-separated polymer blend occurs, the viscosity ratio between two polymers is also changed concurrently, leading to a significant change and/or evolution of the blend morphology. Feng et al. and Liebscher et al. proved that the viscosity ratio of polymers is important to determine the final morphology of the blend [81, 82]. For example, the viscosity ratio of PP and PMMA affects the dispersion state of CBs in the blends. CB resides in the PMMA phase when the viscosity of PMMA is low or at the boundary when the viscosity is medium. When PMMA has significantly high viscosity, CB will be selectively localized inside the PP phase [81]. These results agree with the studies reported by Clarke et al. [83] and Zhou et al. [84]. Besides CB, Wu et al. have demonstrated that a different localization behavior of CNTs in poly(lactic acid) (PLA)/polycarprolactone (PCL) blends. They found that CNTs are localized in the PCL phase or at the interface when the viscosity ratio is high. In contrast, a localization of CNTs in PLA is detected at a low viscosity ratio [85].

Moreover, surface roughness and aspect ratio of fillers also play an important role in the transfer behavior of fillers. Recently, Göldel et al. purposed a “slim-fast

mechanism" which describes the impact of filler shape and aspect ratio on kinetic transfer between polymers [86]. The high-aspect-ratio filler, *e.g.*, CNT, transfers from one phase to the other faster and more efficiently than low-aspect-ratio filler, *e.g.*, CB [75, 86, 87]. This is because low-aspect-ratio fillers have more resistance during transfer and are trapped at the blend interface [64, 79], as illustrated in Fig. 1-8

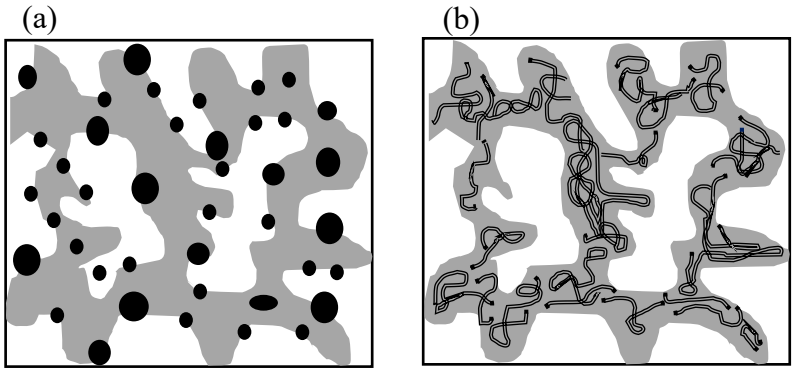

Fig. 1-8 Distribution state of (a) low and (b) high aspect ratio fillers in polymer blend after melt mixing. Fillers are firstly dispersed in polymer 1 (white) and subsequently mixed with polymer 2 (grey).

1.4.3 Theoretical background of CNT transfer in polymer blend

During melt-mixing process, the transfer of CNTs from one phase to the other can take place in two steps: (i) direct contact between CNTs and the blend interface and (ii) CNTs transfer through the interface [88]. In general, the filler movement and

localization can be induced by flow field and diffusion of fillers. At least in the latter case, the Brownian motion [67] is the driving force. The mechanism of CNT migration involves the combination of filler diffusion, shear induced collision and particle trapping during coalescence [88, 89]. The probability of the collision and coalescence strongly depends on the filler localization and blend morphology. In the case of sea-island morphology, these mechanisms can be used when fillers are located in the matrix. When fillers localize in the dispersed droplets, the transfer has to be provided by other mechanisms, which are still not understood.

From the concept of slim-fast mechanism, the subsequent transfer of fillers should be driven by the curvature of the blend interface, which is originated from the development of the wetting angle on the surface of fillers [86]. The mechanism is described in more detail by the following steps.

Diffusion

The important phenomenon to describe the CNT transfer is the Brownian motion. For an ideal cylinder filler with high aspect ratio, the motion of a filler surrounded by a molten polymer is relatively complex due to translational and rotational motions of the anisotropic filler.

Generally, a diffusion coefficient D of spherical fillers by Brownian motion is expressed by the Stokes-Einstein equation:

$$D = \frac{k_B T}{6\pi \eta_M r} \tag{1.14}$$

where k_B is the Boltzmann constant, T is the temperature, η_M is the viscosity of the medium and r is the radius of a spherical filler.

For a rigid rod filler, the rotational diffusion in a viscous liquid was theoretically discussed by Doi and Edwards [90]. The rotational diffusivity D_r is derived by the following equation:

$$D_r = \frac{k_B T}{\zeta_r} \tag{1.15}$$

where ζ_r is the rotational friction constant, which is provided by:

$$\xi_r = \frac{2\pi}{3}\eta_M L^3\left(1-\frac{1}{A^4}\right)\left[\frac{2A^2-1}{2A\left(A^2-1\right)^{1/2}} ln\left(\frac{A+\left(A^2-1\right)^{1/2}}{A-\left(A^2-1\right)^{1/2}}\right)-1\right]^{-1} \tag{1.16}$$

where L is the length of rigid rod and A is the aspect ratio ($A = L/r$). For $A > 2$, Eq. 1.16 is approximated as:

$$\xi_r = \frac{2\pi \eta_M L^3}{3\left[2ln(2A)-1\right]} \tag{1.17}$$

Using integration by parts, a translational diffusion coefficient $\overline{D}$ that consists of two kinds of motions, *i.e.*, parallel and perpendicular, to the rod's long axis can be estimated.

$$D_{//} = \frac{k_B T}{\xi_{//}} = \frac{k_B T ln(L/r)}{2\pi \eta_M L} \tag{1.18}$$

$$D_{\perp} = \frac{k_B T}{\xi_{\perp}} = \frac{k_B T \ln(L/r)}{4\pi \eta_M L} \tag{1.19}$$

Since $D_{//} > D_{\perp}$, a rod can move more easily in parallel direction to the axis than in perpendicular. The $\overline{D}$ of a Brownian rod in an isotropic medium is the average of the diffusion coefficients $D_{//}$ and $D_{\perp}$.

$$\overline{D} = \frac{1}{3}(D_{//} + 2D_{\perp}) \tag{1.20}$$

Finally, the translational motions of CNTs in a polymer melt can be explained.

Shear induced collision

Since fillers and polymers are moving during melt-mixing, a collision between a filler and the boundary of phases should occur. This phenomenon occurs obviously when CNTs are dispersed in a matrix and tend to move to the dispersed droplets. Based on the basic study on the droplet breakage and coalescence processes [91], the collision probability P_{col} between two droplets after breakage is approximately given by Eq. 1.21 [92]:

$$P_{col} = exp\left(-\frac{t_{col}}{t_{proc}}\right) = exp\left(-\frac{\pi}{8\dot{\gamma}\,\Phi_d\, t_{proc}}\right) \tag{1.21}$$

where t_{col} is the collision time, t_{proc} is the mixing time, Φ_d is the volume fraction of the dispersion and $\dot{\gamma}$ is the shear rate of the mixing process.

Particle trapping during coalescence

In this case, the coalescence between two droplets of a dispersed phase plays an important role in the transfer of the filler. Apart from the collision of a filler and the blend interface by external flow field, the coalescence process can be subdivided into three further steps [87, 89, 92].

(1) Free polymer droplets are moving and subsequently approaching each other, leading to a formation of a film between them.

(2) The film becomes thinner because the matrix is slowly drained away. Finally, the film is ruptured, which is attributed to the attractive van der Waals forces between two drops when it reaches a critical thickness.

(3) Since the film is ruptured, the coalescence will be completed by the development of neck between two droplets.

The coalescence probability P_{coa} can be estimated by Eq. 1.22 and the probability P_{drain} of a drained matrix film between the drops:

$$P_{coa} = P_{col} \cdot P_{drain} \tag{1.22}$$

With the ratio of the drain time t_{drain} to the collision time t_{col}, the probability of P_{drain} can be approximated:

$$P_{drain} = exp\left(-\frac{t_{drain}}{t_{col}} \right) \tag{1.23}$$

The P_{col} is obtained from Eq. 1.21 [92]:

$$P_{coa} = exp\left(-\frac{t_{col}}{t_{proc}} - \frac{t_{drain}}{t_{col}} \right) \tag{1.24}$$

In fact, it is difficult to obtain t_{drain} by the empirical model because of insufficient data for the estimation. The duration of film drainage is frequently described by simulations. Therefore, this mechanism should be kept in mind. The models and simulations still need to be further verified in experimental investigations.

1.5 Objective of this research

Due to its high aspect ratio with a combination of superior properties, CNT is a promising filler for a polymer including immiscible polymer blends to provide high-performance and novel functions. A variety of potential applications based on polymer blends containing CNTs has been widely established. Hence, this research field is presently one of the most explored areas in the material science and engineering.

It has been revealed from many studies that the transfer of CNTs from unfavorable phase to the other can occur during melt-mixing process, which strongly influences the morphology and localization of CNTs. Since the morphology directly decides the properties of composites, understanding and controlling the CNT localization are the keys to adjust the desired properties for new potential applications.

The objective of this dissertations is to study and control the localization of MWCNTs in immiscible polymer blends by adjusting the processing conditions. Although the localization of CNTs was studied intensively, the method presented in this research is different from the previous works. In most previous studies, the dispersion state of CNTs is controlled by surface modification of CNTs. On the contrary, the method in this study is free from the modification procedure. Furthermore, the effect of MWCNT localization on the composite properties, *i.e.*, mechanical and electrical properties, is considered. Four types of polymer blends are employed in this study: PC/PET, PC/PE, PC/ethylene-propylene copolymer (EPR) and PP/EPR blends. PC/PET is one of the most available engineering plastics used for housing of electric field. PP/EPR is the most important polymer blend in the commodity plastics, which is used in wide applications including automobile industry. PC/PE and PC/EPR are not conventional blends in industry. However, they are easy to characterize the morphology including the distribution state of MWCNTs.

Following this general introduction, the localization of MWCNTs in PC/PET blends is presented in Chapter 2. The effect of the preferential localization on the mechanical properties is reported. Contradictory transfer behaviors of MWCNTs during laminating and melt-mixing are discussed in Chapter 3. Meanwhile, the selective

adsorption of PE on the surface of MWCNTs is also shown in the same chapter. In Chapter 4, the effect of processing conditions on the localization of MWCNTs in PC/EPR and PP/EPR blends is investigated. Furthermore, the mechanical properties for composites with different distribution states of MWCNTs are also evaluated. Finally, the findings of this research are summarized in Chapter 5. It is expected that the finding in this research will affect the industry greatly.

1.6 References

1. L.S. Schadler, S.C. Giannaris, P.M. Ajayan, *Applied Physics Letters,* **73**, 3842 (1998).
2. S.S. Ray, M. Bousmina, A. Maazouz, *Polymer Engineering & Science,* **46**, 1121 (2006).
3. W. Li, A.K. Schlarb, M. Evstatiev, *Journal of Applied Polymer Science,* **113**, 1471 (2009).
4. S. Iijima, *Nature,* **354**, 56 (1991).
5. P.M. Ajayan, L.S. Schadler, C. Giannaris, A. Rubio, *Advanced Materials,* **12**, 750 (2000).
6. R. Saito, G. Dresselhaus, M.S. Dresselhaus, *Electronic Structure of Single-Wall Nanotubes,* Imperial College Press and World Scientific, London, (2011).
7. P.C. Ma, N.A. Siddiqui, G. Marom, J.K. Kim, *Composites Part A: Applied Science and Manufacturing,* **41**, 1345 (2010).
8. D. Qian, G.J. Wagner, W.K. Liu, M.F. Yu, R.S. Ruoff, *Applied Mechanics Reviews,* **55**, 495 (2002).
9. C. Thomsen, S. Reich, J. Maultzsch, *Electronic Properties of Carbon Nanotubes*, Wiley-VCH, Weinheim, (2007).
10. M.S. Dresselhaus, G. Dresselhaus, R. Saito, *Carbon,* **33**, 883 (1995).
11. J.C. Kearns, R.L. Shambaugh, *Journal of Applied Polymer Science,* **86**, 2079 (2002).
12. B.P. Grady, *Carbon Nanotube-Polymer Composites: Manufacture, Properties, and Applications*, John Wiley & Sons, Hoboken (2011).
13. M. Scarselli, P. Castrucci, M.D. Crescenzi, *Journal of Physics: Condensed Matter,*

24, 313202 (2012).

14. E.T. Thostenson, Z. Ren, T.W. Chou, *Composites Science and Technology,* **61**, 1899 (2001).
15. M.S. Dresselhaus, G. Dresselhaus, P.C. Eklund, *Science of Fullerenes and Carbon Nanotubes*, Academic Press, San Diego, (1996).
16. M. Meyyappan, *Carbon Nanotubes : Science and Applications,* CRC Press, Florida, (2005).
17. J.P. Gore, A. Sane, *Carbon Nanotubes - Synthesis, Characterization, Applications,* In Tech, Croatia, (2011).
18. A.G. Rinzler, J. Liu, H. Dai, P. Nikolaev, C.B. Huffman, F.J. Rodríguez-Macías, P.J. Boul, A.H. Lu, D. Heymann, D.T. Colbert, R.S. Lee, J.E. Fischer, A.M. Rao, P.C. Eklund, R.E. Smalley, *Applied Physics A,* **67**, 29 (1998).
19. Y. Zhang, S. Iijima, *Applied Physics Letters,* **75**, 3087 (1999).
20. Y.C. Choi, Y.M. Shin, Y.H. Lee, B.S. Lee, G.S. Park, W.B. Choi, N.S. Lee, J.M. Kim, *Applied Physics Letters,* **76**, 2367 (2000).
21. J. Bernholc, M. Buongiorno-Nardelli, J.L. Fattebert, D. Orlikowski, C. Roland, Q. Zhao, *Mechanical Properties and Electronic Transport in Carbon Nanotubes*, Springer, Boston, (2002).
22. M. Moniruzzaman, K.I. Winey, *Macromolecules,* **39**, 5194 (2006).
23. M.J. Biercuk, M.C. Llaguno, M. Radosavljevic, J.K. Hyun, A.T. Johnson, J.E. Fischer, *Applied Physics Letters,* **80**, 2767 (2002).
24. A.K.T. Lau, D. Hui, *Composites Part B: Engineering,* **33**, 263 (2002).
25. Y.J. Kim, T.S. Shin, H.D. Choi, J.H. Kwon, Y.C. Chung, H.G. Yoon, *Carbon,* **43**, 23 (2005).

26. A. Urbina, I. Echeverría, A. Pérez-Garrido, A. Díaz-Sánchez, J. Abellán, *Physical Review Letters,* **90**, 106603 (2003).

27. H. Kataura, Y. Kumazawa, Y. Maniwa, I. Umezu, S. Suzuki, Y. Ohtsuka, Y. Achiba, *Synthetic Metals,* **103**, 2555 (1999).

28. O. Jost, A.A. Gorbunov, W. Pompe, T. Pichler, R. Friedlein, M. Knupfer, M. Reibold, H.D. Bauer, L. Dunsch, M.S. Golden, J. Fink, *Applied Physics Letters,* **75**, 2217 (1999).

29. N. Minami, S. Kazaoui, R. Jacquemin, H. Yamawaki, K. Aoki, H. Kataura, Y. Achiba, *Synthetic Metals,* **116**, 405 (2001).

30. O. Lourie, H.D. Wagner, *Applied Physics Letters,* **73**, 3527 (1998).

31. O. Breuer, U. Sundararaj, *Polymer Composites,* **25**, 630 (2004).

32. P. Pötschke, A.R. Bhattacharyya, A. Janke, H. Goering, *Composite Interfaces,* **10**, 389 (2003).

33. A.R. Bhattacharyya, T.V. Sreekumar, T. Liu, S. Kumar, L.M. Ericson, R.H. Hauge, R.E. Smalley, *Polymer,* **44**, 2373 (2003).

34. T. Liu, I.Y. Phang, L. Shen, S.Y. Chow, W.D. Zhang, *Macromolecules,* **37**, 7214 (2004).

35. W.D. Zhang, L. Shen, I.Y. Phang, T. Liu, *Macromolecules,* **37**, 256 (2004).

36. P. Pötschke, A.R. Bhattacharyya, A. Janke, *European Polymer Journal,* **40**, 137 (2004).

37. I. Alig, D. Lellinger, M. Engel, T. Skipa, P. Pötschke, *Polymer,* **49**, 1902 (2008).

38. P.R. Sundararajan, S. Singh, M. Moniruzzaman, *Macromolecules,* **37**, 10208 (2004).

39. W. Bauhofer, J.Z. Kovacs, *Composites Science and Technology,* **69**, 1486 (2009).

40. J. Zhu, J. Kim, H. Peng, J.L. Margrave, V.N. Khabashesku, E.V. Barrera, *Nano Letters,* **3**, 1107 (2003).

41. J. Zhu, H. Peng, F. Rodriguez-Macias, J.L. Margrave, V.N. Khabashesku, A.M. Imam, K. Lozano, E.V. Barrera, *Advanced Functional Materials,* **14**, 643 (2004).

42. W. Feng, X.D. Bai, Y.Q. Lian, J. Liang, X.G. Wang, K. Yoshino, *Carbon,* **41**, 1551 (2003).

43. H. Huang, C.H. Liu, Y. Wu, S. Fan, *Advanced Materials,* **17**, 1652 (2005).

44. N.R. Raravikar, L.S. Schadler, A. Vijayaraghavan, Y. Zhao, B. Wei, P.M. Ajayan, *Chemistry of Materials,* **17**, 974 (2005).

45. W.E. Dondero, R.E. Gorga, *Journal of Polymer Science Part B: Polymer Physics,* **44**, 864 (2006).

46. O. Meincke, D. Kaempfer, H. Weickmann, C. Friedrich, M. Vathauer, H. Warth, *Polymer,* **45**, 739 (2004).

47. H. Zeng, C. Gao, Y. Wang, P.C.P. Watts, H. Kong, X. Cui, D. Yan, *Polymer,* **47**, 113 (2006).

48. J.N. Coleman, U. Khan, W.J. Blau, Y.K. Gun'ko, *Carbon,* **44**, 1624 (2006).

49. R. Haggenmueller, W. Zhou, J.E. Fischer, K.I. Winey, *Journal of Nanoscience and Nanotechnology,* **3**, 105 (2003).

50. P. Pötschke, T.D. Fornes, D.R. Paul, *Polymer,* **43**, 3247 (2002).

51. F. Du, J.E. Fischer, K.I. Winey, *Journal of Polymer Science Part B: Polymer Physics,* **41**, 3333 (2003).

52. F. Du, J.E. Fischer, K.I. Winey, *Physical Review B,* **72**, (2005).

53. L. Valentini, I. Armentano, D. Puglia, J.M. Kenny, *Carbon,* **42**, 323 (2004).

54. L.A. Utracki, *Polymer Composites,* **7**, 274 (1986).

55. J.M. Dealy, K.F. Wissbrun, *Linear Viscoelasticity*, Springer Netherlands, Dordrecht, (1999).

56. M. Abdel-Goad, P. Pötschke, D. Zhou, J.E. Mark, G. Heinrich, *Journal of Macromolecular Science, Part A,* **44**, 591 (2007).

57. F. Du, R.C. Scogna, W. Zhou, S. Brand, J.E. Fischer, K.I. Winey, *Macromolecules,* **37**, 9048 (2004).

58. D. Wu, L. Wu, M. Zhang, *Journal of Polymer Science Part B: Polymer Physics,* **45**, 2239 (2007).

59. P. Pötschke, M. Abdel-Goad, I. Alig, S. Dudkin, D. Lellinger, *Polymer,* **45**, 8863 (2004).

60. P.J. Flory, *The Journal of Chemical Physics,* **10**, 51 (1942).

61. P. Pötschke, A.R. Bhattacharyya, A. Janke, *Polymer,* **44**, 8061 (2003).

62. M. Wu, L.L. Shaw, *Journal of Power Sources,* **136**, 37 (2004).

63. R.A. Khare, A.R. Bhattacharyya, A.R. Kulkarni, M. Saroop, A. Biswas, *Journal of Polymer Science Part B: Polymer Physics,* **46**, 2286 (2008).

64. M. Sumita, K. Sakata, S. Asai, K. Miyasaka, H. Nakagawa, *Polymer Bulletin,* **25**, 265 (1991).

65. Y.P. Mamunya, *Journal of Macromolecular Science, Part B,* **38**, 615 (1999).

66. S.S. Ray, S. Pouliot, M. Bousmina, L.A. Utracki, *Polymer,* **45**, 8403 (2004).

67. H. Yoon, K. Okamoto, M. Yamaguchi, *Carbon,* **47**, 2840 (2009).

68. S. Wu, *Polymer Interface and Adhesion,* Marcel Dekker, New York, (1982).

69. S. Wu, *Journal of Macromolecular Science, Part C,* **10**, 1 (1974).

70. D.K. Owens, R.C. Wendt, *Journal of Applied Polymer Science,* **13**, 1741 (1969).

71. S. Ross, I.D. Morrison, *Colloidal Systems and Interfaces,* Wiley-Interscience,

New York, (1988).

72. M. Sumita, K. Sakata, Y. Hayakawa, S. Asai, K. Miyasaka, M. Tanemura, *Colloid Polymer Science,* **270**, 134 (1992).

73. L. Elias, F. Fenouillot, J.C. Majeste, P. Cassagnau, *Polymer,* **48**, 6029 (2007).

74. L. Elias, F. Fenouillot, J.C. Majesté, P. Alcouffe, P. Cassagnau, *Polymer,* **49**, 4378 (2008).

75. A. Göldel, G. Kasaliwal, P. Pötschke, *Macromolecular Rapid Communications,* **30**, 423 (2009).

76. Y. Mamunya, V. Levchenko, G. Boiteux, G. Seytre, M. Zanoaga, F. Tanasa, E. Lebedev, *Polymer Composites,* n/a (2015).

77. A.E. Zaikin, R.R. Karimov, V.P. Arkhireev, *Colloid Journal,* **63**, 53 (2001).

78. A.E. Zaikin, E.A. Zharinova, R.S. Bikmullin, *Polymer Science Series A,* **49**, 328 (2007).

79. F. Gubbels, S. Blacher, E. Vanlathem, R. Jerome, R. Deltour, F. Brouers, P. Teyssie, *Macromolecules,* **28**, 1559 (1995).

80. F. Gubbels, R. Jerome, E. Vanlathem, R. Deltour, S. Blacher, F. Brouers, *Chemistry of Materials,* **10**, 1227 (1998).

81. J. Feng, C.M. Chan, J.X. Li, *Polymer Engineering & Science,* **43**, 1058 (2003).

82. M. Liebscher, L. Tzounis, P. Pötschke, G. Heinrich, *Polymer,* **54**, 6801 (2013).

83. J. Clarke, B. Clarke, P.K. Freakley, I. Sutherland, *Plastics, Rubber and Composites,* **30**, 39 (2001).

84. P. Zhou, W. Yu, C. Zhou, F. Liu, L. Hou, J. Wang, *Journal of Applied Polymer Science,* **103**, 487 (2007).

85. D. Wu, D. Lin, J. Zhang, W. Zhou, M. Zhang, Y. Zhang, D. Wang, B. Lin,

Macromolecular Chemistry and Physics, **212**, 613 (2011).

86. A. Göldel, A. Marmur, G.R. Kasaliwal, P. Pötschke, G. Heinrich, *Macromolecules,* **44**, 6094 (2011).

87. A. Göldel, G.R. Kasaliwal, P. Pötschke, G. Heinrich, *Polymer,* **53**, 411 (2012).

88. L. Elias, F. Fenouillot, J.C. Majesté, G. Martin, P. Cassagnau, *Journal of Polymer Science Part B: Polymer Physics,* **46**, 1976 (2008).

89. F. Fenouillot, P. Cassagnau, J.C. Majesté, *Polymer,* **50**, 1333 (2009).

90. M. Doi, S.F. Edwards, *The Theory of Polymer Dynamics,* Clarendon Press, Oxford, (1986).

91. S.L. Ross, F.H. Verhoff, R.L. Curl, *Industrial & Engineering Chemistry Fundamentals,* **17**, 101 (1978).

92. H. Potente, M. Bastian, *Polymer Engineering & Science,* **40**, 727 (2000).

Chapter 2

Localization of CNTs in Polycarbonate and Poly(ethylene terephthalate) Blends

2.1 Introduction

Polymer blends have been intensively studied in both academic and industrial fields because of their potentially tailored properties with beneficial cost-performance [1, 2]. It has been established that a polymer blend has a capability to improve mechanical properties due to synergistic effect [3, 4]. Furthermore, properties of a polymer blend can be further enhanced by adding nanofillers such as organoclay, titanium dioxide and carbon black [5-7]. Carbon nanotube (CNT) is also a good candidate for polymer nanocomposites due to their excellent mechanical and electrical properties with a large aspect ratio [8, 9]. Besides, a selective localization of fillers is very important for the morphology design and property control of an immiscible polymer blend [10-12]. In general, filler dispersion in a blend strongly depends on both thermodynamic and kinetic effects [2, 13-16]. The thermodynamic effect governs the localization of fillers in one phase or at the interface, depending on the minimization of the interfacial tension between polymers and fillers. Thus, the filler location can be predicted. However, an equilibrium state of filler dispersion is uneasy to be obtained. Therefore, the kinetic effect, which

relates to the processing conditions and mixing protocol, becomes crucial in the preferential filler localization [17-19]. Moreover, fillers can act as compatibilizers to modify the morphology and properties of a polymer blend if they have a strong interfacial adhesion between two polymers. It has been reported that such fillers can reduce the interfacial tension, leading to an improvement of the compatibility of the different polymer species [17, 20, 21]. Pötschke et al. have investigated the localization of multi-walled CNT (MWCNT) for various blends prepared by melt-mixing process, where the main component was polycarbonate (PC) and the second component was polyethylene (PE) or polypropylene (PP) [11, 22, 23]. They found that MWCNTs preferentially localize in the thermodynamically preferred PC phase upon melt compounding. Besco et al. studied a double percolation for PC/acrylonitrile-butadiene-styrene terpolymer (ABS) with modified layered-silicates and MWCNTs. They indicated that MWCNTs reside in the PC phase and the layered-silicates hinder the formation of an electrically conducting MWCNT network [24]. Rejisha et al. exhibited that the addition of a small amount of MWCNTs into the blend of poly(butylene terephthalate) (PBT) and PC significantly improves mechanical and thermal properties of the blend [25]. Additionally, the mechanical and electrical properties of poly(ethylene terephthalate) (PET)/poly(vinylidene fluoride) (PVDF) blends can be improved by the incorporation of

CNTs. It was found that CNTs selectively distribute in the PET phase due to a small interfacial tension [26].

It should be noted that the location of nanofillers is usually not in the equilibrium state after processing. Consequently, they can transfer to other phase by Brownian motion [15, 27, 28]. It was found that the transfer of MWCNTs from PP to PC takes place during an annealing treatment of laminated sheets composed of PP/MWCNT and neat PC [15]. After the separation, a conductive PC sheet with a small amount of MWCNTs on the surface is obtained. On the contrary, the transfer of MWCNTs does not occur from PC to PP, indicating that the interfacial tension between PC and MWCNT is lower than that between PP and MWCNT.

Polymer blends find use in many engineering potential applications and exhibit exclusive features, *e.g.*, good mechanical properties, chemical resistance, and durability [29-31]. Since the enhancement of mechanical properties is crucial for advanced applications, such as automobile and aerospace, intense interest is focused on polymer blends with MWCNTs. Therefore, the work in this chapter focuses on the localization and interphase transfer of MWCNTs in the blends of PC and PET in order to establish the material design to control the morphology and also improve the mechanical properties by the addition of MWCNTs. These polymer blend systems have been already studied and

found to be immiscible [32-34]. However, the thermal treatment at the mixing process induces the transesterification. As a result, the blends can be partially miscible. Hence, in this study, the effect of MWCNTs on the miscibility between PC and PET is also examined.

2.2 Experiments

2.2.1 Materials

Polycarbonate (PC) (Panlite L-1225Y) and poly(ethylene terephthalate) (PET) were exployed in this study. PC was produced by Teijin (Japan) and PET was by Toray Industries (Japan). The zero-shear viscosities of the polymers at 280 °C are 943 Pa.s for PC and 30 Pa.s for PET. The number- and weight-average molecular weights as a polystyrene standard were characterized by a size exclusion chromatography (HLC-8020, Tosoh, Japan) with TSK-GEL® GMHXL. Chloroform was employed as a solvent for PC. The concentration was 1 mg/mL. In the case of PET, the sample was dissolved into hexafluoro-2-propanol at a concentration of 10 mg/mL. Then the solution was diluted by chloroform at a concentration of 1 mg/mL. It was found $M_n = 1.9 \times 10^4$ and $M_w = 9.7 \times 10^4$ for PC, and $M_n = 1.6 \times 10^4$ and $M_w = 3.0 \times 10^4$ for PET.

MWCNT (NT-7, Hodogaya Chemical, Japan), produced via a catalytic chemical

vapor deposition process using a floating reactant method and subsequent thermal treatment up to 2,600 °C, was employed [35, 36]. Typical diameters are ranging from 40 to 80 nm, while the lengths are between 10 and 20 μm as shown in Fig. 2-1. The density is approximately 2,300 [kg/m^3].

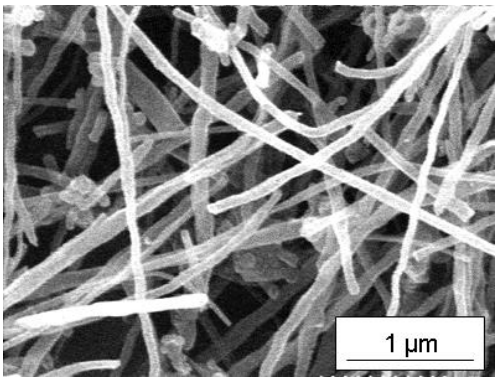

Fig. 2-1 SEM image of MWCNTs

The composite of PC with 20 wt.% of MWCNTs, *i.e.*, PC/MWCNT, was kindly provided by Hodogaya Chemical in a pellet form.

2.2.2 Sample preparation

Prior to melt mixing, pure PC and PC/MWCNT were dried at 120 °C for 8 h in a vacuum oven. Pure PET was also dried at 80 °C for 4 h in order to remove the moisture.

PC/MWCNT and PET were mixed using a 30 cc internal batch mixer at 280 °C

for 5 min with a blade rotation speed of 50 rpm. The blend ratios of PC/MWCNT to PET were 50/50 and 25/75 (w/w), *i.e.*, PC/MWCNT/PET = 44/11/44 and 20/5/75, respectively. Additionally, the blend samples composed of PC and PET without MWCNT were also prepared under the same condition at the blend ratios of 44/44 (= 50/50), 20/75 (= 21/79) and 0/100. The obtained samples were compressed into flat sheets with a thickness of 1 mm using a laboratory compression-molding machine (Table-type test-press, Tester Sangyo, Japan) at 280 °C under 10 MPa for 4 min and subsequently cooled at 25 °C for 4 min. The samples, except for the dynamic mechanical analysis, were annealed at 120 °C for 6 h in order to crystallize PET prior to the measurements. In the case of tensile testing, both non-annealed and annealed samples were used.

2.2.3 Measurements

The temperature dependence of the dynamic mechanical properties of the compressed sheets was measured using a dynamic mechanical analyzer (DMA) (Rheogel-E4000, UBM, Japan) at a heating rate of 2 °C/min in the temperature range from 50 to 200 °C. The frequency applied was 10 Hz.

The compressed sheets of PC/MWCNT, PC/PET and PC/MWCNT/PET were immersed in tetrahydrofuran (THF) to extract PC fraction at room temperature for a week.

After the dissolution of PC from the sample, the remained sheet, *i.e.*, insoluble part, was taken out and dried to measure the weight. The weight fraction of the soluble part *S* was calculated using equation 2.1:

$$S = \frac{w_i - w_f}{w_i} \times 100 \tag{2.1}$$

where w_i and w_f are the weights of the initial sample and the dried insoluble part, respectively.

The infrared spectra of pure PC, pure PET and the soluble part in THF were investigated using a Fourier-transform infrared (FTIR) spectrometer (Spectrum 100, Perkin Elmer, USA).

The morphology and distribution of MWCNTs in the blends were characterized using a scanning electron microscope (SEM) (S4100, Hitachi, Japan). The surface of a sheet sample fractured in liquid nitrogen was coated with Pt-Pd by a sputter coating machine prior to the observation.

The thermal behavior was measured using a differential scanning calorimetry (DSC) (DSC820, Mettler-Toledo International, Japan) under nitrogen atmosphere. The sample was heated from room temperature to 300 °C at a scanning rate of 10 °C/min to evaluate the crystallinity and the melting point T_m. After keeping the sample at 300 °C for 3 min, it was cooled to 50 °C at 10 °C/min to evaluate the crystallization temperature T_c.

The degree of crystallinity X_c of PET was calculated using equation 2.2 from the heating scan.

$$X_c = \frac{\Delta H_m}{\Delta H^0 W_{PET}} \times 100 \tag{2.2}$$

where ΔH_m is the measured enthalpy for melting, ΔH^0 is the melting enthalpy of 100% crystalline PET (144.664 J/g) [37], W_{PET} is the weight fraction of a polymer in the sample.

The mechanical properties were measured using a universal tensile testing instrument (LSC-50/300, Tokyo Testing Machine, Japan), according to ASTM D638. The specimens were in dumbbell shape (ASTM D638-V) (Fig. 2-2) with 0.3 mm thickness, 10 mm width and a gauge length of 10 mm. The tensile test was performed at a constant crosshead speed and a strain rate of 0.1 min^{-1}. The measurements were performed ten times, and the average value was reported.

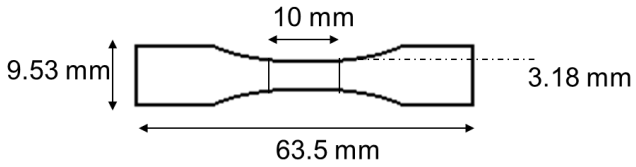

Fig. 2-2 Dimension of the dumbbell-shaped specimen.

2.3 Results and discussion

2.3.1 Miscibility of the blend

Temperature dependence of dynamic tensile moduli such as tensile storage modulus *E'* and loss modulus *E''* is shown in Fig. 2-3. In this experiment, the samples without annealing procedure were used to characterize the glass-to-rubber transition clearly.

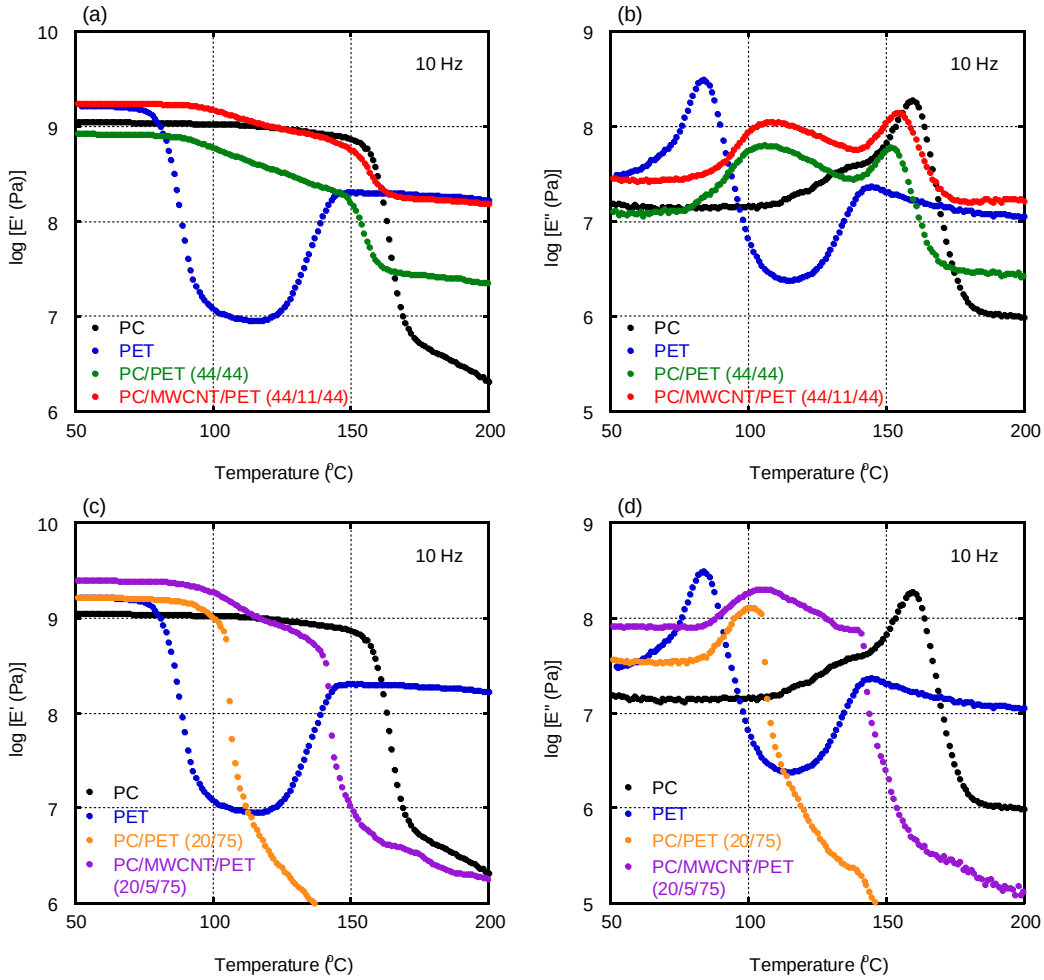

Fig. 2-3 Temperature dependence of dynamic tensile moduli such as storage modulus *E'* ((a) and (c)) and loss modulus *E"* ((b) and (d)) at 10 Hz; (a) and (b) PC, PET, PC/PET (44/44) and PC/MWCNT/PET (44/11/44); (c) and (d) PC, PET, PC/PET (20/75) and PC/MWCNT/PET (20/5/75).

It is clearly observed that both *E'* and *E"* increase with temperature around at 140 °C for PET, which is ascribed to the cold crystallization. Because of the cold crystallization, the sample becomes opaque after the measurement. It is found that *E'* of

PC/PET blends decreases with increasing the PC content. Moreover, *E'* of the blends is enhanced by the addition of MWCNTs due to the reinforcing effect, resulting in an increase in stiffness.

As shown in the figure, the *E"* peaks ascribed to T_g of neat PC and PET are located at 160 and 84 °C, respectively. There are double peaks in the *E"* curve for PC/PET blends, irrespective of the blend ratio, indicating that they are immiscible. This result corresponds with the SEM observation (Fig. 2-6). Besides, T_g of PET shifts to higher temperature and vice versa compared with the virgin polymers. It demonstrates that the compatibility between PC and PET increases probably owing to the transesterification reaction. In other words, PC and PET are dissolved each other to some degree, which has been reported previously [32, 38]. It is found that the peak intensity of PC in the PC/PET (20/75) blend is significantly lower than that of neat PC. Correspondingly, *E'* greatly drops beyond T_g of PET. This is reasonable because the PC-rich phase is floated in the PET-rich matrix. With increasing PC content to 44 wt.%, the peak intensity is enhanced, presumably owing to the co-continuous structure. Besides, it can be observed that the *E"* peak of the PC/PET blends become broader after the addition of MWCNTs. This can be explained by the reduced polymer chain mobility by marked crystallinity, which leads to a broad glass transition region.

In addition, it can be seen in Fig. 2-3(b) that T_g's of PET in PC/PET (44/44) and PC/MWCNT/PET (44/11/44) are 106 and 108 °C while T_g's of PC in those blends are 152 and 155 °C, respectively. In the case of PC/PET (20/75) and PC/MWCNT/PET (20/5/75), T_g's of PET in the samples are 101 and 105 °C while T_g's of PC in those blends are similar, *i.e.*, 139 °C. The results exhibit that T_g's of PET and PC in PC/MWCNT/PET are almost the same with those in the PC/PET blends. It implies that the presence of MWCNTs has no/little influence on the miscibility of the blends.

2.3.2 Localization of MWCNT

It is generally understand that the localization of MWCNTs in an immiscible polymer blend can be determined by the interfacial tension between MWCNT and polymer components [39]. The interfacial tension between them was calculated by the Girifalco-Good equation [40, 41].

$$\Gamma_{1-2} = \gamma_1 + \gamma_2 - 2\sqrt{\gamma_1\gamma_2} \tag{2.3}$$

where $\Gamma_{1\text{-}2}$ is the interfacial tension between components and γ_i is the surface free energy of *i-th* component.

It was reported that the surface free energies of PC and PET at 20 °C are 42.9 and 44.6 mN/m, respectively [42]. In the case of MWCNT, various values of the surface

tension were reported, which depend on the production method and/or surface treatment [43]. For example, Barber et al. reported that it is 27.8 mN/m at 20 °C [44], while Nuriel et al. found to be 45.3 mN/m [45]. Dujardin et al., reported that the value is around 130-190 mN/m [46, 47]. Unfortunately, the exact value of the MWCNT used in this study is not clear. Moreover, the surface tension is known to be a function of ambient temperature, suggesting that the discussion has to be carried out using the values at the mixing temperature. It is known that the preferential localization of fillers in an immiscible polymer blend is predicted by wetting angle. An equilibrium state of the MWCNT dispersion is described by the wetting coefficient ω_a, which was derived from the Young's equation [48].

$$\omega_a = \frac{\Gamma_{MWCNT-PC} - \Gamma_{MWCNT-PET}}{\Gamma_{PC-PET}} \tag{2.4}$$

where Γ_{A-B} is the interfacial tension between A and B.

When the value is lower than -1, MWCNTs are predicted to be localized in PC. In contrast, MWCNTs are distributed in PET when the value is larger than 1. At $-1 < \omega_a < 1$, MWCNTs reside at the interphase.

Assuming that the surface tension of MWCNTs is 27.8 mN/m [44], ω_a is calculated to be 1.81, indicating that MWCNTs are distributed in the PET phase. When the surface tension of MWCNTs is 45.3 mN/m [45], the value is -20. Therefore,

MWCNTs should be localized in the PC phase. Certainly, the conflicting prediction is attributed to the difference in the surface tension of MWCNTs.

In order to clarify the distribution state of MWCNTs in the blends, the solvent immersion experiments were carried out. The obtained sample sheets with a thickness of 1 mm, *i.e.*, PC/MWCNT (80/20), PC/PET (44/44), PC/PET (20/75), PC/MWCNT/PET (44/11/44) and PC/MWCNT/PET (20/5/75), were immersed into THF at room temperature for a week to remove PC fraction after exposure to annealing operation at 120 °C. It has been reported that crystallized PET is insoluble in THF [49], which was confirmed also for the present sample. The solution is presented in Fig. 2-4. Additionally, the weight measurement was performed to check the fraction of the insoluble part, as shown later.

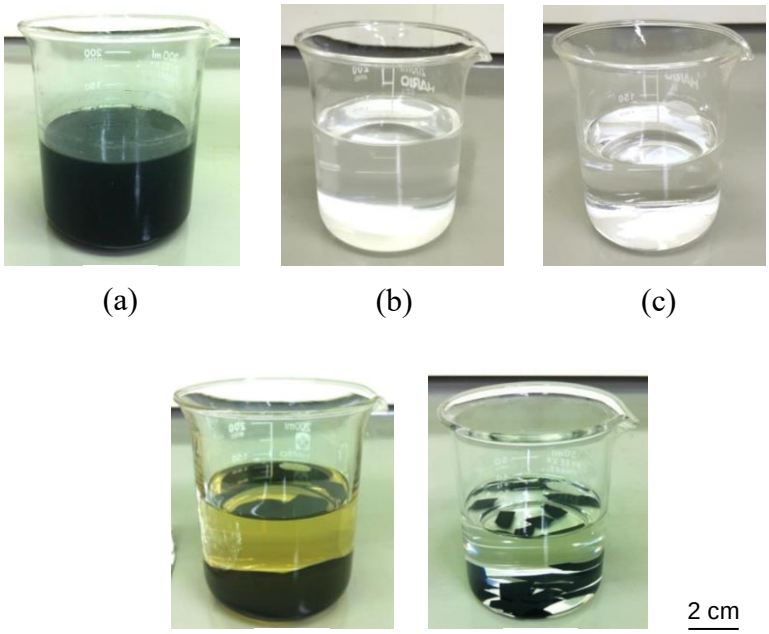

Fig. 2-4 Photographs of (a) PC/MWCNT (80/20), (b) PC/PET (44/44), (c) PC/PET (20/75), (d) PC/MWCNT/PET (44/11/44) and (e) PC/MWCNT/PET (20/5/75) after immersed in THF at room temperature for seven days.

As seen in Fig. 2-4(a), the solution of PC/MWCNT (80/20) is black. This is reasonable because MWCNTs are dispersed in the solvent after the dissolution of PC. For PC/PET (44/44) and (20/75) blends, the solutions are transparent. Since the sample was annealed prior to the solvent extraction, PET is crystallized and thus not dissolved in the solvent. In the case of PC/MWCNT/PET (44/11/44) and (20/5/75) composites, the solutions are fairy transparent, indicating that MWCNTs are barely dissolved into THF. However, the yellow color of the PC/MWCNT/PET solution implies that a small amount

of MWCNTs is dissolved into the solvent with PC.

The soluble part was collected and dried. Then, the sample was compressed into a thin film to examine the composition by FTIR as presented in Fig. 2-5.

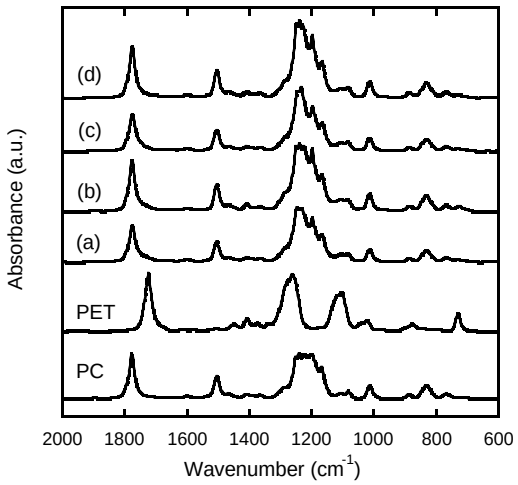

Fig. 2-5 Infrared spectra of soluble parts in THF at room temperature for seven days for (a) PC/PET (44/44), (b) PC/PET (20/75), (c) PC/MWCNT/PET (44/11/44) and (d) PC/MWCNT/PET (20/5/75). In the figure, the spectra of pure PC and PET are also shown as references.

It is found that PC is a major polymer fraction. The absorption peak of PET in the sample's spectra cannot be detected, demonstrating that PET is not dissolve into the solvent. Furthermore, it is found that the weight fractions of the insoluble part in THF, PET/MWCNT, are approximately 56 and 81 wt.%, which correspond with the total

amounts of PET and MWCNT in the original composites, *i.e.*, PC/MWCNT/PET (44/11/44) and (20/5/75). The experimental results indicate that the transfer of MWCNTs from PC to PET occurs during melt-mixing process, although PC and PET are partially dissolved each other by transesterification reaction. It can be concluded that MWCNTs are selectively localized in the PET phase owing to the better wetting.

Morphologies of the fractured surfaces of PC/PET and PC/MWCNT/PET with different PET compositions are shown in Fig. 2-6. The PC phase was extracted by THF.

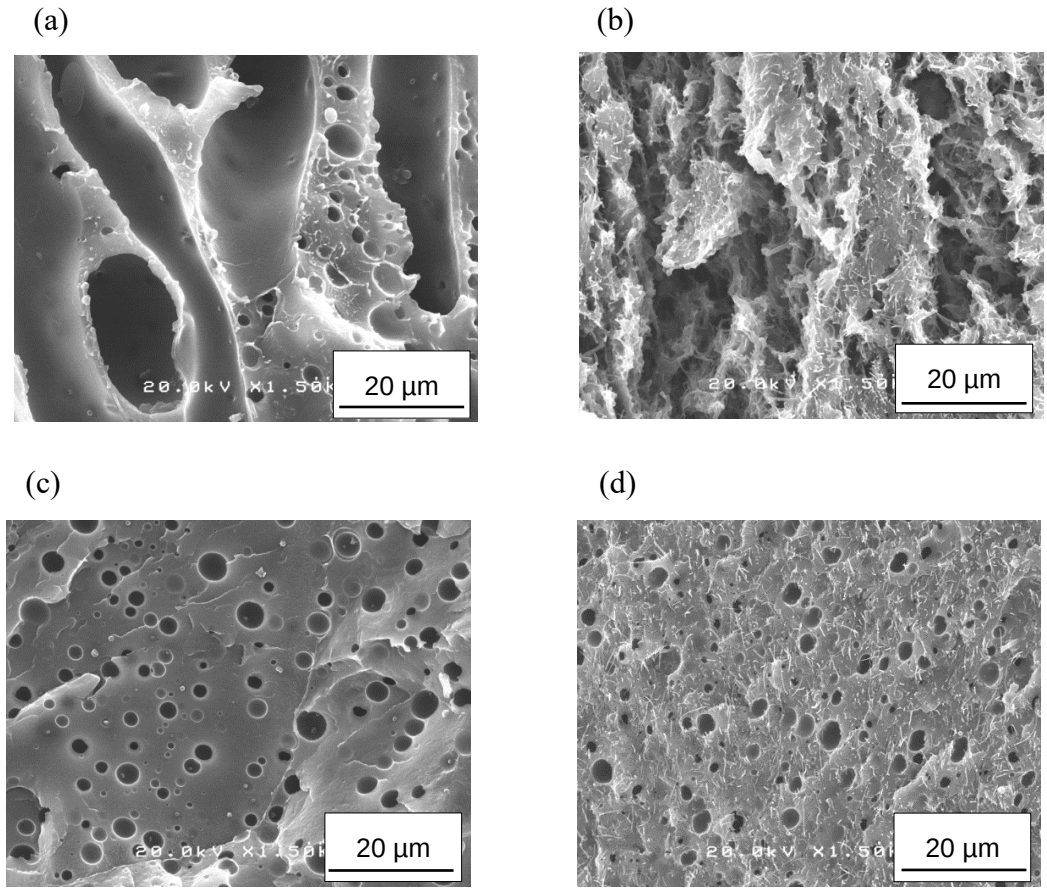

Fig. 2-6 SEM images of fractured surfaces of (a) PC/PET (44/44), (b) PC/MWCNT/PET (44/11/44), (c) PC/PET (20/75) and (d) PC/MWCNT/PET (20/5/75). PC fraction is removed by THF prior to Pt-Pd coating.

SEM images clearly indicate that all blends with different compositions have two-phase morphology, which corresponds with the dynamic mechanical properties. Co-continuous structure is generated at a blend ratio of 44/44 as illustrated in Fig. 2-6(a). As increasing the PET content from 44 to 75 wt.%, the blend shows sea-island structure with sperically dispersed PC. The uniform distribution of PC domains in the PET matrix can

be seen in Fig. 2-6(c). Furthermore, the morphologies exhibit that MWCNTs are preferentially localized within the PET phase as shown in Figs. 2-6(b) and (d), even though MWCNTs are firstly dispersed in PC. The result confirms that MWCNTs move from PC to PET during melt-mixing.

2.3.3 Thermal behavior

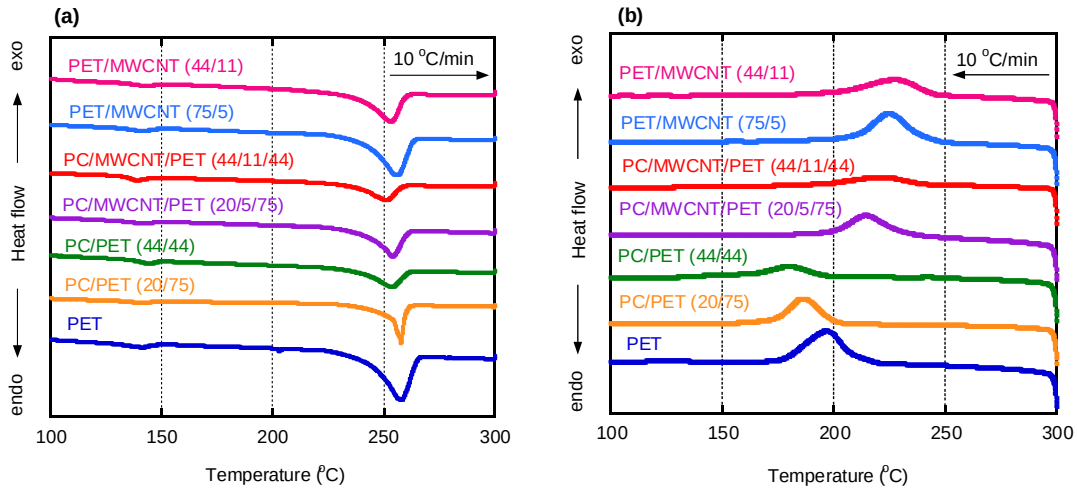

Fig. 2-7 DSC (a) heating and (b) cooling curves at 10 °C/min for PET, PC/PET, PET/MWCNT and PC/MWCNT/PET.

Fig. 2-7 shows the DSC thermograms of PET, PC/PET, PET/MWCNT and PC/MWCNT/PET. As shown in the figure, the cold crystallization of PET is not detected during heating in this study. This is attributed to the annealing treatment at 120 °C for 6

h. In other words, the annealing condition is sufficient to crystallize PET.

As shown in Fig. 2-7(a), the melting point T_m of PET in the PC/PET blends shifts to low temperature as compared to that of pure PET, which is attributed to the transesterification between PET and PC. However, the addition of MWCNTs has no impact on T_m of PET in the blend. In contrast, the MWCNT addition in pure PET, *i.e.*, PET/MWCNT (75/5) and PET/MWCNT (44/11), results in a slight decrease in T_m ($\leq$ 4 °C), but had a significant effect on both crystallization temperature T_c and crystallinity X_c of PET. Correspondingly, T_c of PET in the blends is much lower than that of pure PET, especially for PC/PET (44/44). This is reasonable because intermolecular reaction will be accelerated for PET when the PC content increases. The incorporation of MWCNTs to PC/PET blends results in a dramatic increase in T_c of PET, suggesting that MWCNTs act as an efficient nucleating agent for PET [50-53]. In general, the process of polymer crystallization is controlled by two factors: the number of nuclei and the crystal growth rate [54, 55]. The incorporation of MWCNTs usually may retard the molecular diffusion because MWCNT network restricts the polymer chains motion and therefore the formed crystal cannot grow properly. Therefore, the acceleration of crystallization by the MWCNTs addition is attributed to the increase in crystal nuclei sites for PET.

The crystallinity X_c of PET is determined by Eq. 2.2, which is summarized in Table 2-1.

Table 2-1 DSC characterization

Samples	T_m (°C)	ΔH_m (J/g)	X_c	T_c (°C)
Non-annealed				
PET	258	46.3	32	198
PC/PET (20/75)	256	29.7	26	191
PC/PET (44/44)	252	15.2	21	182
PC/MWCNT/PET (20/5/75)	253	31.5	29	216
PC/MWCNT/PET (44/11/44)	252	17.2	27	226
PET/MWCNT (75/5)	254	39.3	29	223
PET/MWCNT (44/11)	253	32.4	28	228
Annealed				
PET	257	49.2	34	197
PC/PET (20/75)	256	32.0	28	187
PC/PET (44/44)	253	17.4	24	181
PC/MWCNT/PET (20/5/75)	253	33.6	31	215
PC/MWCNT/PET (44/11/44)	251	19.0	30	222
PET/MWCNT (75/5)	255	44.8	33	225
PET/MWCNT (44/11)	253	35.8	31	228

Because of the transesterification reaction, PC/PET (44/44) shows a low value of X_c as compared with pure PET and PC/PET (20/75). The crystallinity increases by the MWCNT addition due to the rapid increase in the number of nuclei, which is attributed to the marked nucleating effect of MWCNTs for PET. Similar effect has also been

reported for PP, HDPE (high-density polyethylene) and PA6 (polyamide 6) [56-58].

2.3.4 Mechanical properties

The stress-strain curves of both non-annealed and annealed samples are shown in Fig. 2-8. Furthermore, the tensile properties determined from the stress-strain curves are summarized in Table 2-2.

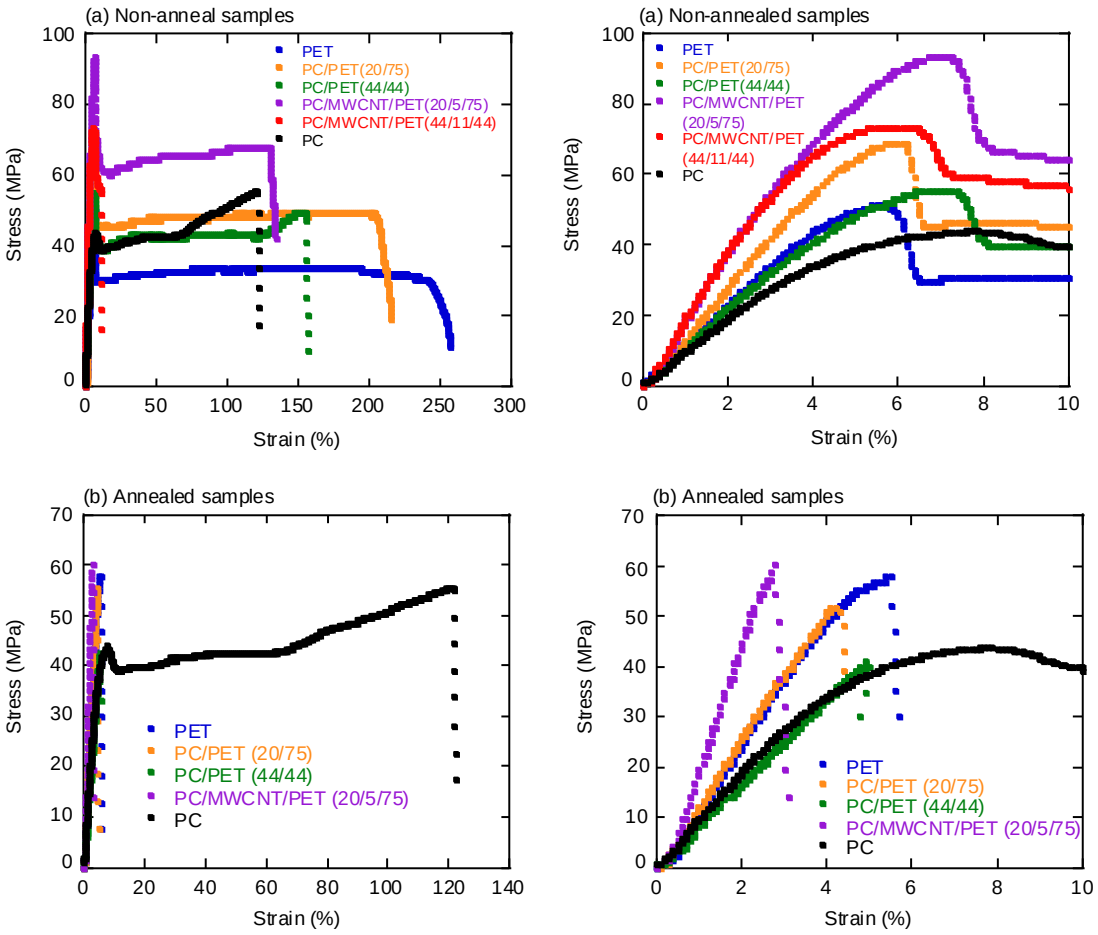

Fig. 2-8 Stress-strain curves of (a) non-annealed and (b) annealed samples. The initial parts are also shown in the right figure.

Table 2-2 Mechanical properties of non-annealed and annealed samples

Samples	Young's modulus [a] (MPa)	Yield strength [b] (MPa)	Strain at yield point [b] (%)	Ultimate strength [b] (MPa)	Elongation at break [b] (%)
Non-annealed					
PC	1560	55 ± 27	9 ± 2	48 ± 17	129 ± 9
PET	1660	51 ± 8	7 ± 1	44 ± 1	227 ± 60
PC/PET (20/75)	1690	54 ± 19	7 ± 1	44 ± 15	220 ± 77
PC/PET (44/44)	1650	52 ± 10	7 ± 1	46 ± 6	156 ± 26
PC/MWCNT/PET (20/5/75)	2050	90 ± 34	7 ± 1	66 ± 29	51 ± 47
PC/MWCNT/PET (44/11/44)	1770	57 ± 12	6 ± 1	54 ± 11	9 ± 3
Annealed					
PET	2530	-	-	57 ± 2	5.2 ± 1.0
PC/PET (20/75)	2370	-	-	50 ± 2	4.7 ± 0.4
PC/PET (44/44)	2050	-	-	43 ± 2	4.9 ± 0.4
PC/MWCNT/PET (20/5/75)	2670	-	-	62 ± 4	2.5 ± 0.1

a) as measured by DMA
b) as measured by tensile testing machine

The mechanical properties for both non-annealed and annealed PC/PET blends are between those for pure PC and PET. In the case of annealed PC/MWCNT/PET (44/11/44), a dumbbell-shaped specimen cannot be prepared because of the brittle fracture. As seen in the figure, pure PC shows the strain-hardening before rupture. All the non-annealed samples exhibit ductile failure with a distinct yield point followed by a necking

behavior, whereas annealed PET shows brittle behavior. The Young's moduli of the annealed blend samples are noticeably higher than those of non-annealed ones. This is reasonable because the degree of crystallinity for PET is enhanced. In addition, the modulus increases progressively with the PET content. Furthermore, as expected, Young's modulus, yield strength and ultimate strength are enhanced significantly by the introduction of MWCNTs. Considering the increament of Young's modulus by annealing and the MWCNT addtion, it is found that the effect of annealing treatment is more pronounced than in the latter case. Additionally, the MWCNT addition decreases the elongation at break, which is significant for PC/MWCNT/PET (44/11/44). Although it has reported that agglomeration of CNTs could take place during annealing [12], which may be responsible for the embrittlement of annealed samples, the SEM observation cannot detect large agglomerates after annealing in this study. Besides, the morphological change by the annealing, which also greatly affects the mechanical properties as reported [59, 60], is not detected in this experiment.

2.4 Conclusion

The selective localization of MWCNTs has been detected in the blends of PC and PET filled with MWCNTs, which can be explained by the interfacial tension between MWCNTs and polymers. The MWCNTs preferentially reside in the more favorable PET phase in all PC/MWCNT/PET blends. This is confirmed from the SEM observation and solvent extraction experiments. The MWCNT addition, however, has no/little effect on the miscibility/compatibility between PC and PET. As a result, T_g's of both PC and PET in the PC/MWCNT/PET blends are similar to those in PC/PET. The localization of MWCNTs in the PET phase is again confirmed from the DSC measurements. The incorporation of MWCNTs shifts T_c of PET to higher temperatures and crystallizes PET more, resulting in an increase in the crystallinity. Therefore, the Young's modulus and ultimate strength of blends are greatly improved, although it reduces the elongation at break of PC/PET.

2.5 References

1. L.A. Utracki, *Development of Polymer Processing*, Chapman and Hall, London, (1998).
2. D.R. Paul, C.B. Bucknall, *Polymer Blends: Formulation & Performance,* Wiley, New York, (2000).
3. O. Olabisi, L.M. Robeson, M.T. Shaw, *Properties of Miscible Polymer Systems*, Academic Press, New York, (1979).
4. M.J. Folkes, P.S. Hope, *Polymer Blends and Alloys,* Chapman and Hall, London, (1993).
5. J.G. Mallette, L.M. Quej, A. Marquez, O. Manero, *Journal of Applied Polymer Science,* **81**, 562 (2001).
6. S.S. Ray, M. Bousmina, A. Maazouz, *Polymer Engineering & Science,* **46**, 1121 (2006).
7. W. Li, A.K. Schlarb, M. Evstatiev, *Journal of Applied Polymer Science,* **113**, 1471 (2009).
8. S. Iijima, *Nature,* **354**, 56 (1991).
9. J. Sandler, M.S.P. Shaffer, T. Prasse, W. Bauhofer, K. Schulte, A.H. Windle, *Polymer,* **40**, 5967 (1999).
10. Y.P. Mamunya, *Journal of Macromolecular Science,* **38**, 615 (1999).
11. P. Pötschke, A.R. Bhattacharyya, A. Janke, *Polymer,* **44**, 8061 (2003).
12. A. Göldel, G.R. Kasaliwal, P. Pötschke, G. Heinrich, *Polymer,* **53**, 411 (2012).
13. I. Duvdevani, A. Tsou, M. Yamaguchi, C.G. Gogos, Prep. 161st Technical Meeting of Rubber Div., American Chemical Society, Georgia, (2002)

14. A. Göldel, G. Kasaliwal, P. Pötschke, *Macromolecular Rapid Communications,* **30**, 423 (2009).

15. H. Yoon, K. Okamoto, M. Yamaguchi, *Carbon,* **47**, 2840 (2009).

16. P. Médéric, J. Ville, J. Huitric, M. Moan, T. Aubry, *Polymer Engineering & Science,* **51**, 969 (2011).

17. F. Gubbels, R. Jerome, E. Vanlathem, R. Deltour, S. Blacher, F. Brouers, *Chemistry of Materials,* **10**, 1227 (1998).

18. F. Fenouillot, P. Cassagnau, J.C. Majesté, *Polymer,* **50**, 1333 (2009).

19. L. Zonder, A. Ophir, S. Kenig, S. McCarthy, *Polymer,* **52**, 5085 (2011).

20. A.E. Zaikin, E.A. Zharinova, R.S. Bikmullin, *Polymer Science Series A,* **49**, 328 (2007).

21. D. Wu, Y. Zhang, M. Zhang, W. Yu, *Biomacromolecules,* **10**, 417 (2009).

22. P. Pötschke, B. Kretzschmar, A. Janke, *Composites Science and Technology,* **67**, 855 (2007).

23. P. Pötschke, S. Pegel, M. Claes, D. Bonduel, *Macromolecular Rapid Communications,* **29**, 244 (2008).

24. S. Besco, M. Modesti, A. Lorenzetti, S. Donadi, T. McNally, *Journal of Applied Polymer Science,* **124**, 3617 (2012).

25. C.P. Rejisha, S. Soundararajan, N. Sivapatham, K. Palanivelu, *Journal of Polymers,* **2014**, 7 (2014).

26. M. Wu, L.L. Shaw, *Journal of Power Sources,* **136**, 37 (2004).

27. V.A. Doan, S. Nobukawa, M. Yamaguchi, *Composites Part B: Engineering,* **43**, 1218 (2012).

28. V.A. Doan, S. Nobukawa, S. Ohtsubo, T. Tada, M. Yamaguchi, *Journal of Polymer*

Research, **20**, 1 (2013).

29. S.S. Pesetskii, B. Jurkowski, V.N. Koval, *Journal of Applied Polymer Science,* **84**, 1277 (2002).
30. S.S. Pesetskii, O.V. Filimonov, V.N. Koval, V.V. Golubovich, *eXPRESS Polymer Letters,* **3**, 606 (2009).
31. A. Al-Jabareen, S. Illescas, M.L. Maspoch, O.O. Santana, *Journal of Materials Science,* **45**, 6623 (2010).
32. T. Suzuki, H. Tanake, T. Nishi, *Polymer,* **30**, 1287 (1989).
33. Y. Kong, J.N. Hay, *Polymer,* **43**, 1805 (2002).
34. P.S.C. Pereira, L.C. Mendes, R.E.R. Abrigo, *International Journal of Polymeric Materials and Polymeric Biomaterials,* **57**, 494 (2008).
35. Y.A. Kim, T. Hayashi, M. Endo, Y. Kaburagi, T. Tsukada, J. Shan, K. Osato, S. Tsuruoka, *Carbon,* **43**, 2243 (2005).
36. J. Chen, J.Y. Shan, T. Tsukada, F. Munekane, A. Kuno, M. Matsuo, T. Hayashi, Y.A. Kim, M. Endo, *Carbon,* **45**, 274 (2007).
37. X. Tang, W. Guo, G. Yin, B. Li, C. Wu, *Journal of Applied Polymer Science,* **104**, 2602 (2007).
38. R.S. Porter, L.H. Wang, *Polymer,* **33**, 2019 (1992).
39. R. Cardinaud, T. McNally, *European Polymer Journal,* **49**, 1287 (2013).
40. A.W. Adamson, A.P. Gast, *Physical Chemistry of Surfaces,* Wiley, New York, 348 (1997).
41. S. Ross, I.D. Morrison, *Colloidal Systems and Interfaces,* Wiley, New York, (1998).
42. J. Brandrup, E.H. Immergut, E.A. Grulke, D.R. Bloch, *Polymer Handbook,* Wiley,

New York, (1999).

43. L.Y. Meng, S.J. Park, *Carbon Letters,* **13**, 178 (2012).

44. A.H. Barber, S.R. Cohen, H.D. Wagner, *Physical Review Letters,* **92**, 186103 (2004).

45. S. Nuriel, L. Liu, A.H. Barber, H.D. Wagner, *Chemical Physics Letters,* **404**, 263 (2005).

46. E. Dujardin, T.W. Ebbesen, H. Hiura, K. Tanigaki, *Science,* **265**, 1850 (1994).

47. E. Dujardin, T.W. Ebbesen, A. Krishnan, M.M.J. Treacy, *Advanced Materials,* **10**, 1472 (1998).

48. M. Sumita, K. Sakata, S. Asai, K. Miyasaka, H. Nakagawa, *Polymer Bulletin,* **25**, 265 (1991).

49. S. Mori, H.G. Barth, *Size Exclusion Chromatography,* Springer, New York, (1999).

50. S. Tzavalas, V. Drakonakis, D.E. Mouzakis, D. Fischer, V.G. Gregoriou, *Macromolecules,* **39**, 9150 (2006).

51. Y. Wang, J. Deng, K. Wang, Q. Zhang, Q. Fu, *Journal of Applied Polymer Science,* **104**, 3695 (2007).

52. S. Tzavalas, D.E. Mouzakis, V. Drakonakis, V.G. Gregoriou, *Journal of Polymer Science Part B: Polymer Physics,* **46**, 668 (2008).

53. V.J. Cruz-Delgado, C.A. Ávila-Orta, A.B. Espinoza-Martínez, J.M. Mata-Padilla, S.G. Solis-Rosales, A.F. Jalbout, F.J. Medellín-Rodríguez, B.S. Hsiao, *Polymer,* **55**, 642 (2014).

54. F.W. Billmeyer, *Textbook of Polymer Science*, Wiley, New York, (1984).

55. L.H. Sperling, *Introduction to Physical Polymer Science,* Hoboken, New York, (2005).

56. T. Liu, I.Y. Phang, L. Shen, S.Y. Chow, W.D. Zhang, *Macromolecules,* **37**, 7214 (2004).

57. L. Valentini, J. Biagiotti, M.A. López-Manchado, S. Santucci, J.M. Kenny, *Polymer Engineering & Science,* **44**, 303 (2004).

58. S.L. Kodjie, L. Li, B. Li, W. Cai, C.Y. Li, M. Keating, *Journal of Macromolecular Science, Part B,* **45**, 231 (2006).

59. Y. Li, H. Shimizu, *Macromolecular Rapid Communications,* **26**, 710 (2005).

60. A. Nuzzo, E. Bilotti, T. Peijs, D. Acierno, G. Filippone, *Polymer,* **55**, 4908 (2014).

Chapter 3

Transfer Phenomenon of CNTs between Polyethylene and Polycarbonate Blends

3.1 Introduction

Carbon nanotubes (CNTs) have been extensively investigated in many research fields recently due to their high aspect ratio and specific surface area [1]. Therefore, mechanical and electrical properties of a polymeric material can be greatly improved by adding CNTs [2-4]. Based on the above characteristics, it is appropriate to employ CNTs as a conductive filler in polymer composites for many potential applications in the manufacturing such as electrostatic dissipation, interference shielding, and so on [5-7]. Of course, the electrical properties of polymer composites are strongly affected by the dispersion of CNTs in the material, therefore it is important to understand and control the CNT dispersion [8].

Sumita et al. described the concept of double percolation, in which the amount of carbon blacks (CBs) is beyond the critical value for percolation in one continuous phase of an immiscible polymer blend [9, 10]. This method makes it possible to prepare a conductive composite with a small amount of CBs. They also revealed that CBs selectively reside in polyethylene (PE) phase in the blend of PE and poly(methyl

methacrylate) (PMMA), although PE is a non-polar polymer [10]. Furthermore, Wu et al. found that the addition of PE reduces the percolation threshold of the composite with vapor-grown carbon fibers (VGCFs) in PMMA [11]. They described that it is attributed to the self-assembled conductive network constructed by selective adsorption of PE on the end part of the VGCF filament. Later, they explained that this phenomenon is attributed to the flexibility of PE chains, which leads to the preferential adsorption at the rough ends of VGCF by entropic favor [12]. Similarly, Pötschke et al. prepared a conductive blend using polycarbonate (PC) and PE with MWCNTs and found that MWCNTs behave as a bridge between two polymers by the adsorption of chain ends [13]. In contrast, Mamunya et al. reported that the selective localization of conductive fillers in an immiscible polymer blend can be predicted by the interfacial tension between polymers and conductive fillers [14]. Typically, CNTs immigrate from a polymer with high interfacial tension to another with low interfacial tension through the boundary between the phases [15]. Besides, Gubbels et al. demonstrated that the selective localization of CBs at the interphase between PE and polystyrene (PS) in the co-continuous blend can greatly reduce the content of CBs required for the percolation threshold [16]. This selective localization occurs at the specific balance of interfacial tension among polymers and nanofillers.

Recently, the imprinting technique of nanofillers from one polymer to another has been developed to modify the surface properties of polymers [17-20]. Doan et al. conducted the annealing procedure using piled sheets comprised of pure PE and polypropylene (PP) containing nanofibers of poly(butylene terephthalate) (PBT) [19]. They found that PBT fibers are transferred from molten PP to PE, which results in the surface-modified PE sheet after separation of the laminated sheets. Similarly, nanofibers of polytetrafluoroethylene (PTFE) in a molten poly(lactic acid) (PLA) are transferred from PLA to PP during the annealing procedure, although PTFE does not transfer from PP to PLA [19]. These results indicate that the localization phenomenon is attributed to the compatibility with nanofillers. Furthermore, they reported that silica nanoparticles preferentially migrate from poly(styrene-*co*-butadiene) (SBR) to poly(butadiene) (BR) during annealing beyond their glass transition temperatures [20]. Nevertheless, the migration from BR to SBR does not occur, demonstrating that the interfacial tension between silica and BR is lower than that between silica and SBR, *i.e.*, the compatibility between silica and a rubber is the main driving force for the transfer.

Besides, Yoon et al. found that the interphase diffusion of MWCNTs from PP to PC occurs during the annealing treatment of laminated sheets composed of PP/MWCNT and PC, leading to a conductive film of PC with a significantly small amount of

MWCNTs. In contrast, the transfer is not detected at all from PC to PP. The results directly indicate that the interfacial tension between PC and MWCNT is lower than that between PP and MWCNT [21].

In this chapter, the interphase transfer of MWCNTs between immiscible polymers, *i.e.*, PC and PE, is studied. Two methods, *i.e.*, laminating and melt mixing, were employed to investigate the transfer behavior of MWCNTs. Moreover, the adsorption of PE on the surface of MWCNTs is shown, which will provide useful information for material design.

3.2 Experiments

3.2.1 Materials

The polymers used in this study were commercially available bisphenol A polycarbonate (PC) (Panlite L-1225Y, Teijin, Japan, MFR = 11 [g/10 min]) and high-density polyethylene (PE) (HJ590N, Japan Polyethylene, MFR = 40 [g/10 min]). The number- and weight-average molecular weights, characterized by a size exclusion chromatograph (SEC) (Tosoh, HLC-8020) using chloroform as an eluent, of PC are 1.9×10^4 and 9.7×10^4, respectively, as a polystyrene standard. Moreover, M_n and M_w of PE were also characterized by SEC using 1,2,4-trichlorobenzene at 140 °C and found to be 0.87×10^4 and 4.9×10^4, respectively as a polyethylene standard. The density of PE is

960 [kg/m^3] at room temperature.

The details of MWCNTs (NT-7, Hodogaya Chemical, Japan) are mentioned in the previous chapter. Two types of composites with 20 wt.% of multi-walled carbon nanotubes (MWCNTs), *i.e.*, PC/MWCNT and PE/MWCNT, were kindly provided by Hodogaya Chemical as a pellet form.

3.2.2 Sample preparation

Pure PC and its composite with 20 wt.% of MWCNTs were dried at 120 °C for 8 h in a vacuum oven before processing.

Melt-mixing experiment

A composite of PC/MWCNT (80/20) was mixed with pure PE in the molten state using a 30 cc internal mixer at 250 °C for 10 min at a blade rotation speed of 50 rpm. The blend ratio of PC/MWCNT and PE was 80:20 in weight fraction, *i.e.*, PC/MWCNT/PE = 64/16/20. In addition, another blend composed of pure PC and pure PE at a blend ratio of 76/24 (= 64/20) was also prepared under the same condition without MWCNTs. The obtained samples were compressed into flat sheets with a thickness of 1 mm using a laboratory compression-molding machine (Table-type test-press, Tester Sangyo, Japan)

at 200 °C under 10 MPa for 3 min.

Laminating experiment

Flat sheets of PE, PC, PE/MWCNT (80/20) and PC/MWCNT (80/20) were also prepared using the compression-molding machine at 200 °C under 10 MPa for 3 min. Then, the sheets with 1 mm thickness were subsequently cooled at 25 °C. The transfer experiment in the laminated sheets was conducted by placing a pure PC sheet on a PE/MWCNT (80/20) sheet (PC – PE/MWCNT). After the annealing treatment at 250 °C for 10 min, the sheets were immediately cooled and separated. The procedure is presented in Fig. 3-1. The same experiment was performed using a pure PE sheet and a PC/MWCNT (80/20) sheet (PE – PC/MWCNT).

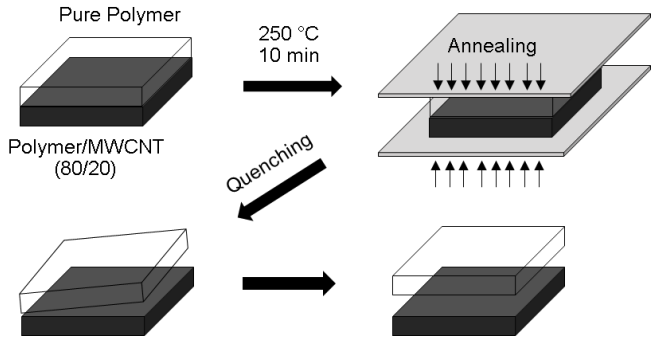

Fig. 3-1 Schematic illustration of experimental procedure for MWCNT transfer.

3.2.3 Measurements

The flat sheets of PC/PE and PC/MWCNT/PE with a thickness of about 1 mm were immersed in chloroform to remove PC fraction at room temperature for three days. Afterward, the insoluble part in chloroform was immersed into hot-xylene to remove PE fraction at 140 °C for 6 h. The chloroform and xylene solutions with dissolved polymers were collected and subsequently dried up to characterize the dissolved parts. Furthermore, the insoluble part was dried and weighed to determine the soluble fraction *S*, defined by equation 3.1:

$$S = \frac{w_i - w_f}{w_i} \times 100 \tag{3.1}$$

where w_i is the initial weight of the sample and w_f is the weight of the dry sample after immersion.

In addition, the MWCNT distribution on the surface of the insoluble part in chloroform and xylene and the surface of cryogenically fractured PC/MWCNT/PE was observed by a scanning electron microscope (SEM) (Hitachi, S4100). The surfaces of the separated PC and PE sheets at laminated experiments were also examined. Prior to the observation, all specimens were coated with Pt-Pd by a sputter coating machine.

The infrared (IR) spectra of pure PC and the dissolved part of the samples after extraction were measured by a Fourier-transform infrared spectroscopy (FTIR) analyzer

(Perkin Elmer, Spectrum 100). In addition, the insoluble part after extracted by chloroform and xylene was determined by an attenuated total reflectance (ATR) mode using a diamond (KRS) as an ATR crystal.

Electrical resistivity was measured on the surface of the separated sheets using constant-voltage supplied resistivity meters (MCP-HT450 and MCP-T610, Mitsubishi Chemical Analytech, Japan). The measurements were performed five times for each sample at room temperature, and the average value was calculated.

The thermal analysis was conducted by a differential scanning calorimetry (DSC) (DSC820, Mettler-Toledo International, Japan) under nitrogen atmosphere. The sample was heated from room temperature to 200 °C and kept at this temperature for 3 min. Then, the sample was cooled to 50 °C to evaluate crystallization temperature. The heating and cooling rates are carried out at 10 °C/min.

3.3 Results and discussion

3.3.1 MWCNT transfer in laminated sheets

The laminated sheets composed of a pure polymer and the other polymer with MWCNTs (20 wt.%), *i.e.*, PE - PC/MWCNT and PC - PE/MWCNT, were annealed at 250 ºC for 10 min to study the transfer behavior of MWCNTs. After quenching, the sheets

were able to be separated without any difficulty due to the immiscible nature of PE and PC. The surface resistivity of the separated PC sheet is found to be 10^6 Ω/sq., which is significantly lower than that of pure PC (>10^{15} Ω/sq.). This result indicates that MWCNTs migrate from PE to PC during the applied annealing procedure. However, the surface resistivity of the separated PE sheet after annealing is higher than 10^{15} Ω/sq., which is the same level as that for pure PE. It suggests that MWCNT transfer does not occur from PC to PE because of the difference in the compatibility of MWCNT with polymers.

SEM observation was performed to characterize the MWCNT distribution on the surface of the separated polymer sheets. As seen in Fig. 3-2(a), MWCNTs are dispersed on the PC surface, corresponding to the electrical resistivity measurement. On the contrary, the MWCNT transfer is not detected from PC to PE as shown in Fig. 3-2(b).

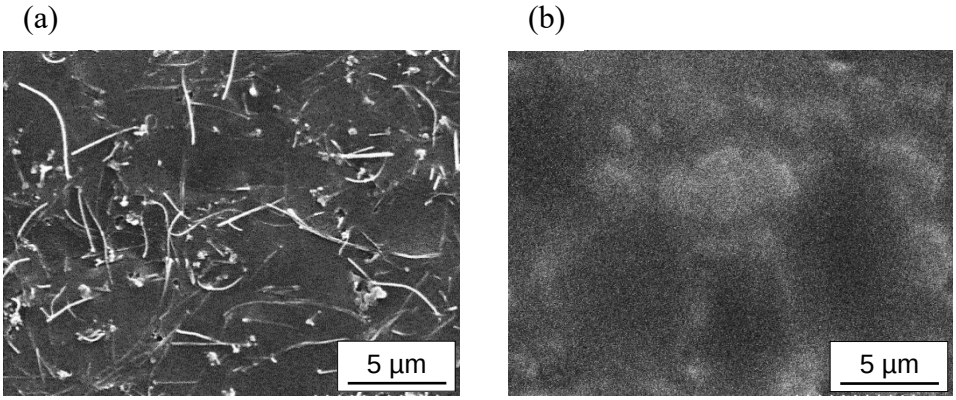

Fig. 3-2 SEM images of (a) PC surface separated from PE/MWCNT (80/20) and (b) PE surface separated from PC/MWCNT (80/20) after annealing at 250 ºC for 10 min.

In general, the transfer phenomenon can be explained by interfacial tension between the MWCNT and the polymer components, which is estimated by the theoretical model like Girifalco-Good equation [22, 23] as follows:

$$\Gamma_{1\text{-}2} = \gamma_1 + \gamma_2 - 2\sqrt{\gamma_1 \gamma_2} \tag{3.2}$$

where $\Gamma_{1\text{-}2}$ is the interfacial tension between components and γ_i is the surface free energy of *i-th* component.

It is known that the surface free energies of PE and PC at 200 °C are 25.4 and 32.1 mN/m, respectively [24]. Further, the surface free energy of MWCNTs has been reported by several researchers which depends on the production method and treatment history [15, 25, 26]. The interfacial tension between the polymer and MWCNT is calculated and listed in Table 3-1, assuming that surface free energy of MWCNT is 45.3 [mN/m] [15].

Table 3-1 Interfacial tension Γ between polymers and MWCNT

	Γ **(mN/m)**
PC – PE	0.391
PC - MWCNT	1.133
PE - MWCNT	2.858

It is clearly seen that the interfacial tension between PE and MWCNT is significantly higher than that between PC and MWCNT. Hence, the interphase diffusion

of MWCNTs occurs only from PE to PC. The results obtained in this experiment correspond with the previous report [21].

3.3.2 MWCNT transfer during melt-mixing

The localization behavior of MWCNTs in an immiscible blend composed of PE and PC was studied using an internal mixer. In this study, MWCNTs were dispersed in PC at first (PC/MWCNT = 80/20). Then pure PE was introduced into the blend at 250 ºC for 10 min. After compression-molding of the obtained composite (PC/MWCNT/PE = 64/16/20) at 200 ºC, the sheet with 1 mm thickness was immersed into chloroform at room temperature for three days. The solution is shown in Fig. 3-3 with the reference samples, *i.e.*, PC/MWCNT (80/20) and PC/PE (64/20) without MWCNTs.

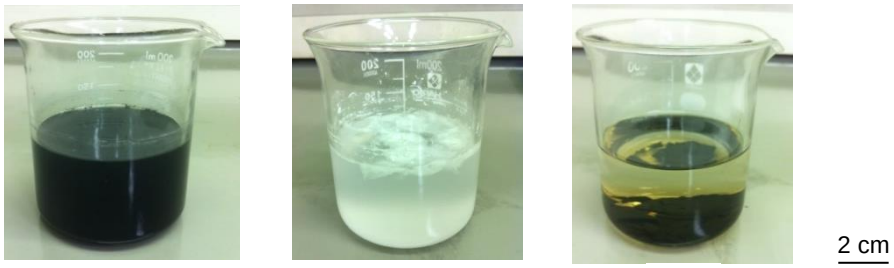

(a) (b) (c)

Fig. 3-3 Photographs of the immersion experiment in chloroform; (a) PC/MWCNT (80/20), (b) PC/PE (64/20) and (c) PC/MWCNT/PE (64/16/20).

In the case of PC/MWCNT, the solution is black. This is reasonable because MWCNTs are dispersed in the solution after PC is dissolved in the solvent. For the same reason, the solution of PC/PE (64/20) is opaque due to the light scattering of dispersed PE particles. In contrast, the solution of PC/MWCNT/PE (64/16/20) is fairly transparent, although PC is fully dissolved into chloroform. It should be noted because the result suggests that MWCNTs are barely dispersed in the PC phase in the blend. Furthermore, it is found from the weight measurement that the insoluble part is approximately 36 wt.%, which corresponds with the total amount of PE and MWCNT. Then, the solution was filtrated to remove MWCNTs and/or PE by a filter paper. The filtrate solution was dried and subsequently compressed into a flat film. Thereafter, the film sample was characterized by FTIR. It is demonstrated from the spectra in Fig. 3-4 that the peak at 1,462 cm^{-1}, which is assigned to CH_2 bending in PE, cannot be observed in the sample's spectra ((a) and (b)). It indicates that only PC fraction is dissolved in chloroform.

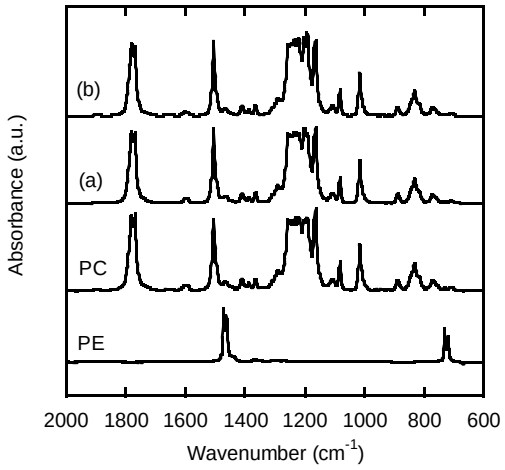

Fig. 3-4 Infrared spectra of soluble parts in chloroform at room temperature for (a) PC/PE (64/20) and (b) PC/MWCNT/PE (64/16/20).

Considering the weight measurement, PC fraction in PC/MWCNT/PE (64/16/20) is completely dissolved in chloroform, although MWCNTs are barely dispersed in the solution. Therefore, it can be concluded that MWCNTs are dispersed in PE phase in the blend of PC/MWCNT/PE (64/16/20). In other words, MWCNT transfer occurs from PC to PE during mixing, which is completely opposite to that detected at the laminated sheets.

The cryofractured surface of the blend, *i.e.*, PC/MWCNT/PE, is also characterized by SEM, as shown in Fig. 3-5. The co-continuous phase-separated structure is detected, in which only one phase, *i.e.*, PE, contains MWCNTs.

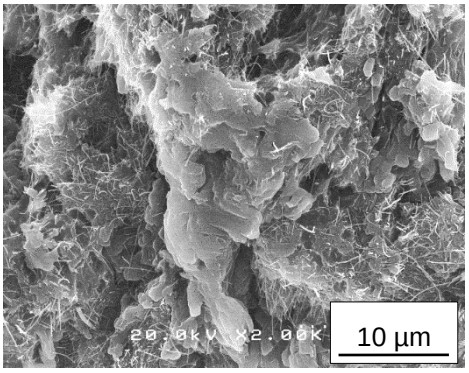

Fig. 3-5 SEM image of fractured surface of PC/MWCNT/PE (64/16/20).

To clarify the mechanism of the contradictory results, the insoluble part in chloroform is immersed into hot-xylene. Prior to the experiment, it was confirmed that pure PE is totally dissolved into hot-xylene at the same experimental condition. However, the insoluble part in chloroform, *i.e.*, PE/MWCNT, is not completely dissolved into hot-xylene. The weight of the remaining insoluble part in hot-xylene is 23.6 wt.% of the original blend (PC/MWCNT/PE). The dissolved part in hot-xylene (12.4 wt.% of the original blend) is PE, which is confirmed by FTIR. Moreover, it should be noted that the solution is transparent as shown in Fig. 3-6, demonstrating that there are two types of PE; one is free from MWCNTs and the other is adsorbed on the MWCNT surface and forms network structure.

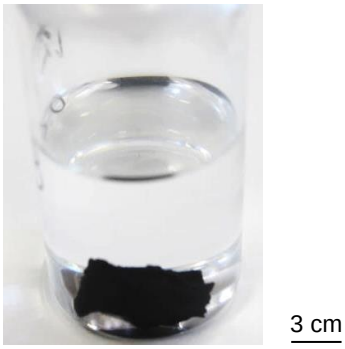

Fig. 3-6 Photograph of the immersion experiment in hot-xylene at 140 °C for 6 h using the insoluble part in chloroform of PC/MWCNT/PE (64/16/20).

The surface morphology of the insoluble part after immersed in hot-xylene is demonstrated in Fig. 3-7. It is clearly seen that the shish-kebab structure, which must be PE crystals, is detected on MWCNTs. Thermal behavior of the sample is investigated by DSC to support a selective adhesion of PE on the MWCNT surface, as presented in Fig. 3-8.

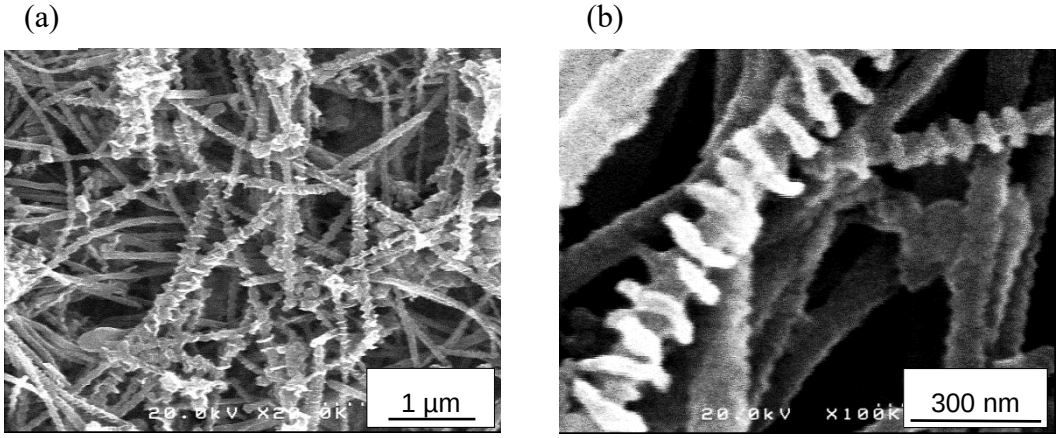

Fig. 3-7 SEM images of the surface of insoluble part in chloroform and hot-xylene, *i.e.*, PE/MWCNT in hot-xylene, at different magnifications.

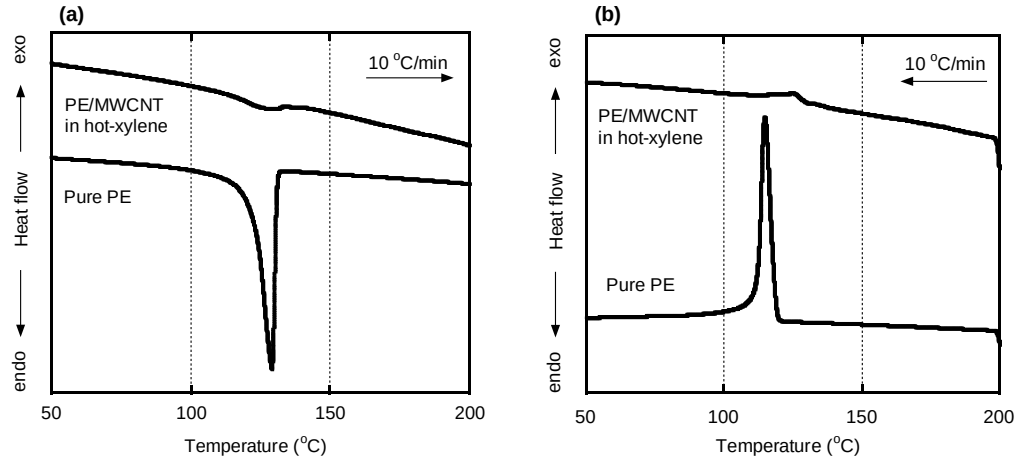

Fig. 3-8 DSC (a) heating and (b) cooling curves at 10 °C/min for pure PE and PE/MWCNT in hot-xylene.

It is found that the presence of MWCNTs does not affect T_m of PE. Nevertheless, a significant increase in crystallization temperature T_c is detected. The T_c of PE is increased from 115 to 125 °C, revealing that crystallization process occurs more easily. The result confirms that PE molecules adsorbed on the MWCNT surface are crystallized from MWCNTs because of the marked nucleation ability of MWCNTs as reported previously [27, 28].

These experimental results suggest that PE molecules are adsorbed on MWCNTs during melt-mixing, presumably with the aid of oxygen. In the rubber industry, it is well known that some molecules are adsorbed on carbon blacks, which are called "bound rubber" [29-31]. The detail mechanism of the present system is attributed to the functional groups containing oxygen on the surface of MWCNTs, which are responsible for the reaction and/or adsorption. In fact, PE is known to show the branching reaction with the aid of oxygen [32]. During processing, the thermal oxidation of PE occurs and subsequently forms free radicals in a chain. These radicals will rapidly react with oxygen and transform to alkylperoxy free radical (ROO•). The ROO• may abstract a hydrogen from the PE chain and yields hydroperoxide (ROOH) attached to carbon atom in the polymer backbone. Then, ROOH will cleave immediately because its life-time is short, and results to alkoxy (RO•) and hydroxyl (•OH) radicals. Both radicals will rapidly

abstract the hydrogen atom from the PE chain to generate more alkyl radicals by the following mechanism [32-34].

$$RH + O_2 \rightarrow ROOH$$

$$ROOH \rightarrow RO^{\bullet} + {}^{\bullet}OH$$

$$HO^{\bullet} + RH \rightarrow H_2O + R^{\bullet}$$

$$R^{\bullet} + O_2 \rightarrow RO_2^{\bullet}$$

$$RO_2^{\bullet} + RH \rightarrow ROOH + R^{\bullet}$$

$$ROOH \rightarrow RO^{\bullet} + {}^{\bullet}OH$$

$$RO^{\bullet} + RH \rightarrow ROH + R^{\bullet}$$

Because the alkoxy radical is unstable, it will decompose spontaneously to form ketones and aldehydes. Then, they will change further to produce acids and esters.

The product with carbonyl groups resulting from the oxidation of PE is usually monitored by the presence of carbonyl peaks. Fig. 3-9 shows the spectrum of insoluble part in chloroform and hot-xylene, *i.e.*, PE/MWCNT in hot-xylene.

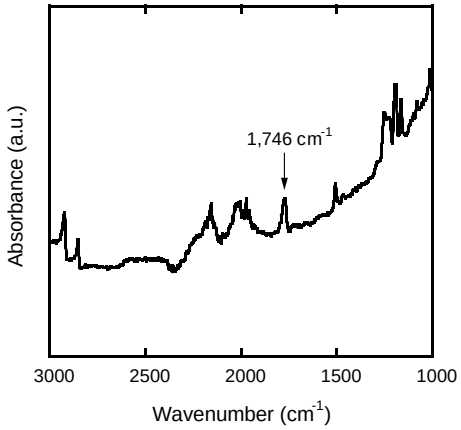

Fig. 3-9 ATR spectrum of PE/MWCNT in hot-xylene.

It is found that the peak at 1,746 cm^{-1}, which is assigned to an ester group, is detected, demonstrating an oxidation of PE during melt-mixing process. Afterward, the MWCNTs covered by PE molecules are expelled from PC phase and move to PE because of high interfacial energy between PE and PC. Therefore, mixing condition will play an important role in the distribution of MWCNTs in PC/PE blends, which greatly affects the mechanical properties in the solid state. Although the selective adsorption of PE on VGCF and MWCNT was already reported [10-13], the present results are completely different from those of the previous studies. In the case of the previous studies, PE molecules are absorbed on the rough edge of fibers owing to the flexibility of PE chains. In contrast, our results demonstrate that PE molecules can be absorbed even on the flat surface of the carbon fillers. This "*in-situ* surface modification" of MWCNTs will be available for the

material design of CNT-reinforced multi-components systems because CNTs can be localized in a specific phase.

3.4 Conclusion

The interphase transfer of MWCNTs in the immiscible blend of PE and PC is studied by two methods: (1) annealing in the laminated sheets and (2) melt-mixing in the mixer. It is found that MWCNTs move from PE to PC during the annealing treatment in the laminated sheets. On the contrary, the interphase diffusion from PC to PE does not occur due to a large difference in the surface tension between PE and MWCNT.

In the case of melt-mixing, it is interesting to note that MWCNT transfer occurs from PC to PE, not from PE to PC, which has been confirmed by solvent immersion, FTIR and SEM measurements. The contradict phenomenon is attributed to the strong adsorption of PE chains on the whole surface of MWCNTs, which will occur by the chemical reaction with the aid of oxygen during melt-mixing. The grafted PE chains on MWCNTs lead to the interphase transfer from PC to PE.

3.5 References

1. S. Iijima, *Nature,* **354**, 56 (1991).
2. A.K.T. Lau, D. Hui, *Composites Part B: Engineering,* **33**, 263 (2002).
3. P. Pötschke, T.D. Fornes, D.R. Paul, *Polymer,* **43**, 3247 (2002).
4. F. Gardea, D.C. Lagoudas, *Composites Part B: Engineering,* **56**, 611 (2014).
5. R.S. Ruoff, D.C. Lorents, *Carbon,* **33**, 925 (1995).
6. P.C. Ma, N.A. Siddiqui, G. Marom, J.K. Kim, *Composites Part A: Applied Science and Manufacturing,* **41**, 1345 (2010).
7. H. Rokni, A.S. Milani, R.J. Seethaler, *Composites Part B: Engineering,* **43**, 779 (2012).
8. K. Ke, Y. Wang, X.Q. Liu, J. Cao, Y. Luo, W. Yang, B.H. Xie, M.B. Yang, *Composites Part B: Engineering,* **43**, 1425 (2012).
9. M. Sumita, K. Sakata, S. Asai, K. Miyasaka, H. Nakagawa, *Polymer Bulletin,* **25**, 265 (1991).
10. M. Sumita, K. Sakata, Y. Hayakawa, S. Asai, K. Miyasaka, M. Tanemura, *Colloid Polymer Science,* **270**, 134 (1992).
11. G. Wu, S. Asai, M. Sumita, *Macromolecules,* **32**, 3534 (1999).
12. G. Wu, S. Asai, M. Sumita, *Mcromolecules,* **35**, 945 (2002).
13. P. Pötschke, A.R. Bhattacharyya, A. Janke, *Polymer,* **44**, 8061 (2003).
14. Y.P. Mamunya, *Journal of Macromolecular Science, Part B,* **38**, 615 (1999).
15. S. Nuriel, L. Liu, A.H. Barber, H.D. Wagner, *Chemical Physics Letters,* **404**, 263 (2005).
16. F. Gubbels, R. Jerome, P. Teyssie, E. Vanlathem, R. Deltour, A. Calderone, V. Parente, J.L. Bredas, *Macromolecules,* **27**, 1972 (1994).

17. B.D. Gates, Q. Xu, M. Stewart, D. Ryan, C.G. Willson, G.M. Whitesides, *Chemical Reviews,* **105**, 1171 (2005).

18. Z. Nie, E. Kumacheva, *Nature Materials,* **7**, 277 (2008).

19. V.A. Doan, S. Nobukawa, M. Yamaguchi, *Composites Part B: Engineering,* **43**, 1218 (2012).

20. V.A. Doan, S. Nobukawa, S. Ohtsubo, T. Tada, M. Yamaguchi, *Journal of Polymer Research,* **20**, 1 (2013).

21. H. Yoon, K. Okamoto, M. Yamaguchi, *Carbon,* **47**, 2840 (2009).

22. A.W. Adamson, A.P. Gast, *Physical Chemistry of Surfaces,* Wiley, New York, (1997).

23. S. Ross, I.D. Morrison, *Colloidal Systems and Interfaces,* Wiley, New York, (1998).

24. J. Brandrup, E.H. Immergut, E.A. Grulke, D.R. Bloch, *Polymer Handbook,* Wiley, New York, (1999).

25. E. Dujardin, T.W. Ebbesen, A. Krishnan, M.M.J. Treacy, *Advanced Materials,* **10**, 1472 (1998).

26. A.H. Barber, S.R. Cohen, H.D. Wagner, *Physical Review Letters,* **92**, 186103 (2004).

27. S. Liang, K. Wang, D. Chen, Q. Zhang, R. Du, Q. Fu, *Polymer,* **49**, 4925 (2008).

28. L. Li, W. Wang, E.D. Laird, C.Y. Li, M. Defaux, D.A. Ivanov, *Polymer,* **52**, 3633 (2011).

29. J.E. Callan, W.M. Hess, C.E. Scott, *Rubber Chemistry and Technology,* **44**, 814 (1971).

30. B.L. Lee, C. Singleton, *Journal of Applied Polymer Science,* **24**, 2169 (1979).

31. K. Yurekli, R. Krishnamoorti, M.F. Tse, K.O. Mcelrath, A.H. Tsou, H.C. Wang, *Journal of Polymer Science, Part B,* **39**, 256 (2001).

32. A.J. Peacock, *Handbook of Polyethylene Structures, Properties, and Applications,* Marcel Dekker, New York, (2000).

33. R.T. Johnston, E.J. Morrison, *Polymer Durability: Degradation, Stabilization, and Lifetime Prediction*, American Chemical Society, Washington, DC, (1996).

34. D.M. Wiles, *Biodegradable Polymers for Industrial Applications*, Woodhead, Cambridge, (2005).

Chapter 4

Improvement of Rigidity for Polypropylene and Ethylene-Propylene Copolymer Blend by CNT Localization

4.1 Introduction

Carbon nanotube (CNT) has received great attention in both academia and industry and is recognized as a proper candidate as a high-performance filler for both thermoplastic and thermosetting resins to enhance the modulus and strength effectively, which significantly expands the range of potential applications [1-3]. In the case of immiscible polymer blends having phase-separated structure, the selective localization of CNTs in one of polymer phases or at the interface is a key factor to achieve a material with desired properties [4-6]. For example, the rigidity and electrical conductivity can be efficiently enhanced when CNTs are selectively dispersed in a continuous phase. It has been known that the migration of fillers to a favored polymer phase during mixing usually occurs when fillers are pre-dispersed in a thermodynamically unfavored polymer [4, 6, 7]. Moreover, processing conditions and/or mixing protocol have a great impact on the final morphology [4, 8, 9]. Furthermore, it was reported that the addition of multi-walled carbon nanotubes (MWCNTs) can change the morphology of a polymer blend during

processing, leading to the modification of electrical and mechanical properties [9-11].

Isotactic polypropylene (PP) is one of the most conventional thermoplastics. In particular, PP with an impact modifier such as ethylene-propylene copolymer (EPR) is widely employed in industry because of its excellent balance of both rigidity and high-impact strength [12-15]. Recently, however, the demand to enhance the rigidity is increasing intensively especially in the automobile applications to reduce the thickness and weight. Hence, the addition of MWCNTs is focused because it enhances the rigidity further. For such a composite, fillers have to be localized in the continuous phase to enhance the rigidity effectively without losing the impact strength [16]. Moreover, controlling phase morphology in an immiscible blend is the important route to improve the stiffness and toughness [17]. It has been reported that carbon materials such as carbon black (CB), vapor-grown carbon fiber (VGCF), and CNT tend to reside in polyethylene (PE) and ethylene copolymer in an immiscible blend, although interfacial tension between them and carbon fillers is high. According to Wu et al., the entropy penalty plays an important role in the selective adsorption of PE chains on the rough ends of VGCF filaments due to the flexibility of polymer chains, leading to a self-assembled conductive network in a poly(methyl methacrylate) (PMMA) matrix. Similarly, CBs were found to be selectively located in the PE phase in the blend of PE and PP [17-19]. Yui et al. obtained

the same result using PE/PP/CB composites prepared by various processing methods [20]. Sumita et al. found that CBs preferentially localize in the PE phase in the blend of PE and PMMA [21, 22]. Haddadi-Asl studied the structure and properties of PP/EPR blends containing both CB and graphite fibers. He found that conductive carbon fillers are found in the EPR phase, resulting in few fillers residing in the PP phase. However, the characteristics of the composite can be modified greatly by controlling the processing conditions [23]. Hemmati et al. studied the effect of concentration of single-walled carbon nanotubes (SWCNTs) and its compatibilizer with PP, *i.e.*, PP-*graft*-maleic anhydride (PP-*g*-MA), on the morphology and mechanical properties of PP/ethylene-propylene-diene terpolymer (EPDM) blends. The tensile modulus was enhanced with increasing the SWCNT content, which is more pronounced in the compatibilized composite. They also demonstrated that the dispersed EPDM has uniform distribution in the PP matrix, where the fillers reside in the matrix, at a low SWCNT and compatibilizer concentration. However, with increasing the filler content, the concentration of PP-*g*-MA has to be increased to keep the fillers in the matrix. As a result, the viscosity ratio of EPDM to PP is increased. Therefore, the EPDM droplet becomes more difficult to break up, resulting in coarse morphology [24].

The localization of CNTs in the matrix is a key technology also for electro-

conductive composites. Meincke et al. showed that the selective localization of CNTs in polyamide 6 (PA6) in the blend with acrylonitrile-butadiene-styrene terpolymer (ABS) greatly reduces the concentration of CNTs required for the conductive network formation [25]. Phromdee et al. found that the volume resistivity of a PP/EPR blend with CBs is apparently low compared with that of a CB-filled PP homopolymer due to double percolation, in which CBs make a conductive path in the continuous EPR phase [26].

In Chapter 3, the interphase diffusion of MWCNTs between immiscible polymers during annealing treatment is studied. The result demonstrated that the transfer of MWCNTs from PP or PE to polycarbonate (PC) occurs during the annealing of laminated sheets composed of PP/MWCNT or PE/MWCNT and PC, as repeated by Yoon et al. [27]. On the contrary, the transfer is not detected from PC to PP or PE. The results indicate that the interfacial tension between PC and MWCNT is lower than that between polyolefin and MWCNT. In contrast, it was found that MWCNTs prefer to move from PC to PE during mixing at high temperature, even though the interfacial tension between PE and MWCNT is high. This phenomenon occurs by the adsorption of PE molecules on the surface of MWCNTs, and suggests that the adsorption of PE is pronounced at the high-temperature-mixing with the aid of oxygen.

In this chapter, the MWCNT distribution in PP/EPR and PC/EPR blends by the processing/mixing conditions such as temperature, purging of N_2 gas, and thermal stabilizer is considered. The information obtained will be applicable to enhance the rigidity of rubber-toughened plastics effectively by the selective localization of MWCNTs in the matrix phase.

4.2 Experiments

4.2.1 Materials

The polymers used in this research were bisphenol A polycarbonate (PC) (Panlite L-1225Y, Teijin, Japan), isotactic polypropylene (PP) (J108M, Prime Polymer, Japan), and ethylene-propylene copolymer (EPR) (EP11, JSR, Japan) with an ethylene content of 52 wt.%. Information on the materials, as provided in the manufacture's data sheets, is given in Table 4-1. The number- and weight-average molecular weights characterized by a size exclusion chromatography (SEC) (HLC-8020, Tosoh, Japan) using chloroform as an eluent are 1.9×10^4 and 9.7×10^4 for PC and 4.0×10^6 and 4.7×10^6 for EPR, as a polystyrene standard. For PP, M_n and M_w were also characterized by SEC using *o*-dichlorobenzene as a solvent and found to be 3.6×10^4 and 2.5×10^5, respectively, as a polypropylene standard.

Table 4-1 Characteristics of materials used in this work

Polymers	**Density (kg/m^3)**	**MFR (g/10 min)**	**Mooney viscosity ML_{1+4} (100 °C)**
PC	1200	11 [a]	-
PP	910	45 [b]	-
EPR	-	-	40

a) at 300 °C, 1.20 kg
b) at 230 °C, 2.16 kg

The composites with 20 wt.% of multi-walled carbon nanotubes, *i.e.*, PC/MWCNT and PP/MWCNT, were kindly provided by Hodogaya Chemical, Japan in pellet form. The detail of MWCNTs (NT-7, Hodogaya Chemical, Japan) is provided in the Chapter 2.

4.2.2 Sample preparation

Prior to mixing, PC/MWCNT was dried for 4 h at 120 °C in a vacuum oven to remove moisture. Either PP/MWCNT or PC/MWCNT was mixed with EPR in the weight fraction of 80/20, *i.e.*, PC/MWCNT/EPR or PP/MWCNT/EPR = 64/16/20.

PC/MWCNT (80/20) was melt blended with neat EPR in the molten state using a 30 cc internal-batch mixer at various temperatures, *i.e.*, 190, 220 and 250 °C, for 2 min with a blade rotation speed of 50 rpm. A small amount of a thermal stabilizer, 2-(tert-butyl)-6-

methyl-4-(3-((2,4,8,10-tetrakis(tert-butyl)dibenzo[d,f][1,3,2]dioxaphosphepin-6-yl)oxy) propyl)phenol (Sumilizer-GP, Sumitomo Chemical, Japan) was added.

PP/MWCNT (80/20) was mixed with neat EPR with/without the addition of the thermal stabilizer at 190 or 280 °C for 10 min with the same blade rotation speed. Furthermore, the effect of purging of N_2 gas on the structure was investigated. Additionally, a neat blend of PP/EPR at a blend ratio of 76/24 (= 64/20) in weight was also prepared at 190 °C for 10 min with a small amount of the thermal stabilizer (no N_2 gas).

All samples were compressed into flat sheets with a thickness of 1 mm using a laboratory compression-molding machine (Table-type test-press, Tester Sangyo, Japan) at 190 and 200 °C for composites of PP and PC, respectively, under 10 MPa for 3 min and subsequently cooled at 25 °C for 3 min.

4.2.3 Measurements

The flat films of PC/MWCNT/EPR composites were immersed in dichloromethane (CH_2Cl_2) at room temperature for three days. Thereafter, the insoluble part was taken out and dried up to quantify the weight. The collected solution was also

dried to obtain the soluble part. The weight fraction of the soluble part *S* was calculated using equation 4.1:

$$S = \frac{w_i - w_f}{w_i} \times 100 \tag{4.1}$$

where w_i and w_f are the weights of the initial sample and the dried insoluble part, respectively.

The infrared spectra of PC, EPR and the soluble part in CH_2Cl_2 were measured using a Fourier-transform infrared (FTIR) spectrometer (Spectrum 100, Perkin Elmer, USA).

The rheological measurements for PP, EPR, PP/EPR and PP/MWCNT/EPR were carried out using a rheometer (AR 2000ex, TA Instruments, Japan) at 190 °C under N_2 atmosphere with parallel-plate geometry. The diameter of plates is 8 mm for the composites and 25 mm for the samples without MWCNTs. All samples were kept in the rheometer for 10 min at 190 °C prior to the measurements.

The morphology and localization of MWCNTs in PP/MWCNT/EPR was investigated using a scanning electron microscope (SEM) (S4100, Hitachi, Japan). The sheets were fractured in a liquid N_2 and etched with xylene at room temperature for three days to remove EPR fraction on the surface of the blend. The etched samples were coated with Pt-Pd by a sputter coating machine prior to the observation.

The electrical resistivity measurement was carried out on the surface of the compressed films using a constant-current supplied resistivity meter (MCP-T610, Mitsubishi Chemical Analytech, Japan). The resistivity was measured five times for each sample at room temperature and the average value was calculated.

The temperature dependence of the dynamic tensile moduli was measured using a dynamic mechanical analyzer (Rheogel-E4000, UBM, Japan) at a heating rate of 2 °C/min in the temperature range from -80 to 160 °C. The frequency applied was 10 Hz.

The tensile test was performed at room temperature by a universal tensile testing instrument (LSC-50/300, Tokyo Testing Machine, Japan) at a constant crosshead speed of 50 mm/min (strain rate of 0.1 min^{-1}) according to ASTM D638. The specimens were in dumbbell shape (ASTM D638-V) with 0.5 mm thickness and had a gauge length of 10 mm. The detail of specimen dimension is mentioned in the Chapter 2.

4.3 Results and discussion

4.3.1 PC/EPR with MWCNTs

In order to investigate the dispersion state of MWCNTs in the composites, the sample sheets, *i.e.*, PC/MWCNT (80/20) and PC/MWCNT/EPR (64/16/20), were immersed into CH_2Cl_2 at room temperature for three days to remove PC fraction. It was

confirmed that EPR is not dissolved in the solvent at this condition, although it shows swelling. The photographs of solutions are presented in Fig. 4-1. In addition, the soluble part in CH_2Cl_2 was checked by FTIR after evaporating CH_2Cl_2, as shown in Fig.4-2.

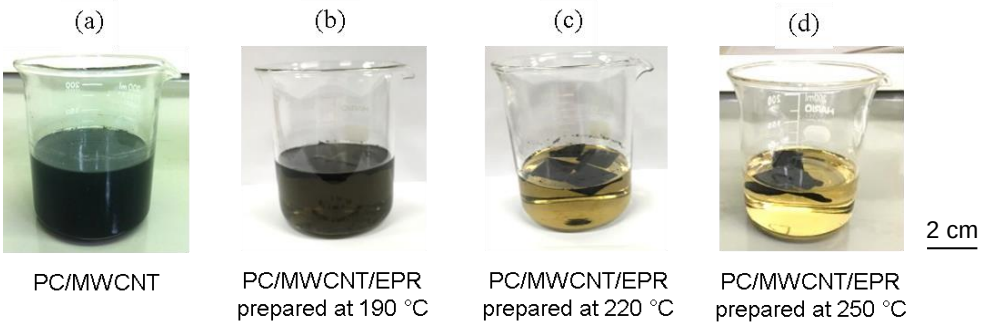

Fig. 4-1 Photographs of solvent immersion experiments; (a) PC/MWCNT (80/20) and PC/MWCNT/EPR (64/16/20) prepared at (b) 190 °C, (c) 220 °C and (d) 250 °C. The samples were immersed into CH_2Cl_2 at room temperature for three days.

It is obvious from Fig. 4-1(a) that the solution of PC/MWCNT is black because MWCNTs are dispersed in CH_2Cl_2 with the dissolution of PC. For the PC/MWCNT/EPR composites, it is clearly observed that the solution of the sample mixed at 190 °C (Fig. 4-1(b)) is black, indicating that MWCNTs are distributed in the PC phase. In contrast, the solution color becomes fairy transparent when the mixing temperature is high, *i.e.*, 220 and 250 °C, as shown in Figs. 4-1(c) and (d). Although the yellow solution implies that a

small amount of MWCNTs are dissolved into the solvent with PC, it demonstrates that the transfer of MWCNTs from PC to EPR occurs during melt-mixing at the high temperatures.

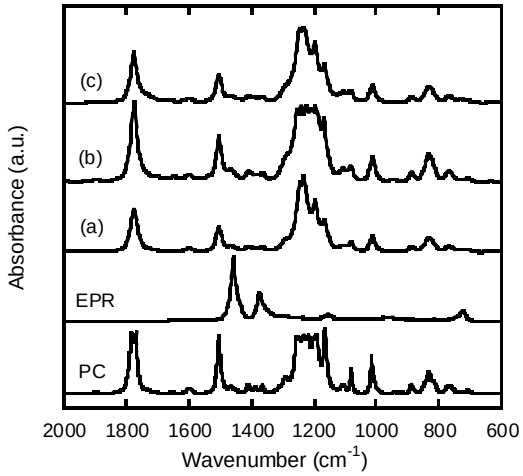

Fig. 4-2 Infrared spectra of soluble parts in CH_2Cl_2 for PC/MWCNT/EPR (64/16/20) prepared at (a) 190 °C, (b) 220 °C and (c) 250 °C. In the figure, the spectra of pure PC and EPR are also shown as references.

In the infrared spectra of pure EPR, ethylene sequence -CH_2- has a characteristic bending absorption peak at 1,462 cm^{-1}, while the adsorption peak of methyl group -CH_3 in the propylene unit is located at 1,375 cm^{-1}. There is no indication of both CH_2 and CH_3 adsorption peaks in the FTIR spectra of the soluble fractions ((a) - (c)), revealing that EPR is not dissolved in CH_2Cl_2. The weights of soluble part are approximately 65.8, 63.0

and 61.6 wt.% for PC/MWCNT/EPR prepared at 190, 220 and 250 °C, respectively. Therefore, it is suggested that MWCNTs immigrated from PC has network structure with EPR.

In addition, it is found that the weight fraction of the insoluble part in CH_2Cl_2 in the sample prepared at the low temperature is 34.2 wt.%, while those of the samples mixed at 220 and 250 °C are approximately 37.0 and 38.4 wt.%, respectively. The obtained result suggests that the adsorption of EPR on the surface of MWCNTs is accelerated by the high-temperature-mixing, presumably with the aid of oxygen which promotes the generation of the free radicals from the ethylene unit in EPR molecular chains [6, 28, 29]. The adhesion of rubber molecules on the MWCNT surface leads to the selective localization of MWCNTs in the EPR phase. For rubber-toughened plastics, in general, fillers should be dispersed only in the matrix by the following two reasons [30-32]: the one is to enhance the rigidity, *i.e.*, modulus, effectively. The other is to leave rubber phase without fillers, which allows the cavitation process under stress, *i.e.*, decrease in dilatational stress. The difference in the modulus between the matrix and dispersions is also responsible for the plastic deformation due to the stress concentration. Hence, the localization of fillers in the dispersed rubber phase should be avoided for mechanical properties.

4.3.2 PP/EPR with MWCNTs

A similar experiment is conducted using PP/EPR, one of the most important rubber-toughened plastics in industry.

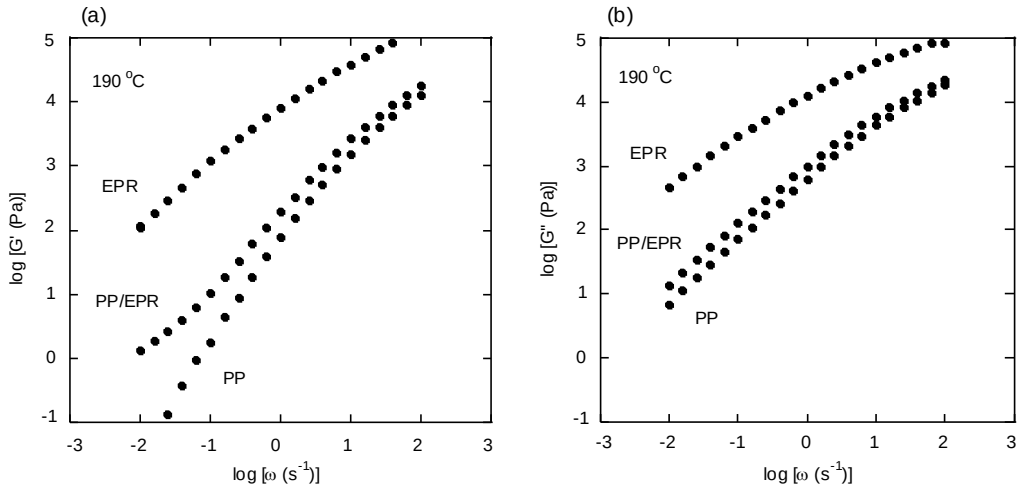

Fig. 4-3 Frequency dependence of oscillatory shear moduli such as (a) storage modulus *G'* and (b) loss modulus *G"* for PP, EPR and PP/EPR (64/20) at 190 °C.

Fig. 4-3 shows the shear storage modulus *G'* and loss modulus *G"* as a function of angular frequency ω for individual pure polymers and their blend at 190 °C.

It is shown that both moduli for EPR are significantly higher than those for PP because of a longer relaxation time due to its high molecular weight. The zero-shear viscosities of the polymers at 190 °C are 730 [Pa.s] for PP and 45,000 [Pa.s] for EPR. In the case of the PP/EPR blend, a long relaxation mechanism ascribed to the phase

separation is clearly detected in the *G'* curve.

The morphology of the PP/EPR blend is observed by SEM using the cryofractured surface of the sample. The EPR fraction was removed by stirring the fractured sheets in xylene at room temperature for three days. Prior to the experiment, it was confirmed that pure EPR is totally dissolved in xylene at the same experimental condition. Fig. 4-4 shows the SEM image of the PP/EPR (64/20) blend.

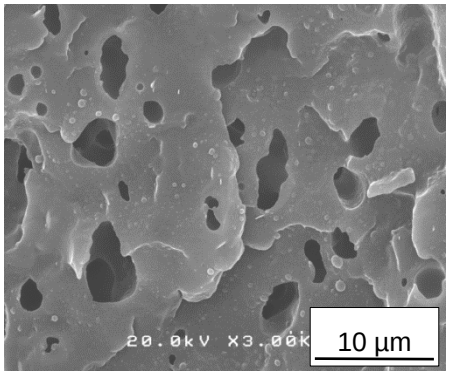

Fig. 4-4 SEM image of fractured surface of PP/EPR (64/20) after removal of EPR.

A sea-island structure in which EPR domains are dispersed in the PP matrix is clearly detected. It is observed that the size of the dispersed EPR is large and irregular in shape due to the long relaxation time.

PP/MWCNT and EPR were mixed at various mixing conditions in order to establish the mixing technique to control the distribution of MWCNTs and thus the

mechanical properties of the PP/EPR blend with MWCNTs. Besides, the effect of the addition of thermal stabilizer and/or N_2 purging on the distribution state is also examined in this study.

Melt rheological responses for the PP/MWCNT/EPR composites prepared by various mixing conditions are evaluated at 190 °C to obtain the information on the structure, as presented in Fig. 4-5.

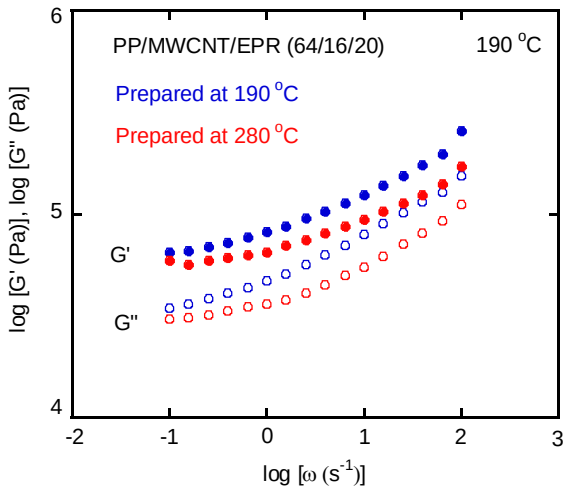

Fig. 4-5 Frequency dependence of oscillatory shear moduli for PP/MWCNT/EPR prepared at 190 °C and 280 °C. Both samples were prepared without thermal stabilizer and N_2 gas.

It is demonstrated that both *G'* and *G"* for the composite prepared at 190 °C are higher than those at 280 °C. Both samples were prepared without thermal stabilizer and

N_2 purging. The results suggest that the mixing temperature greatly affects the rheological responses, which would be ascribed to the difference in the distribution state of MWCNTs. Since the moduli for the sample prepared at the low temperature are higher than those at the high temperature, more MWCNTs are distributed in the continuous phase by the low-temperature-mixing. It is also found that the change in the shear moduli by the introduction of either thermal stabilizer or N_2 gas for the composites is barely detected, as shown in Fig. 4-6.

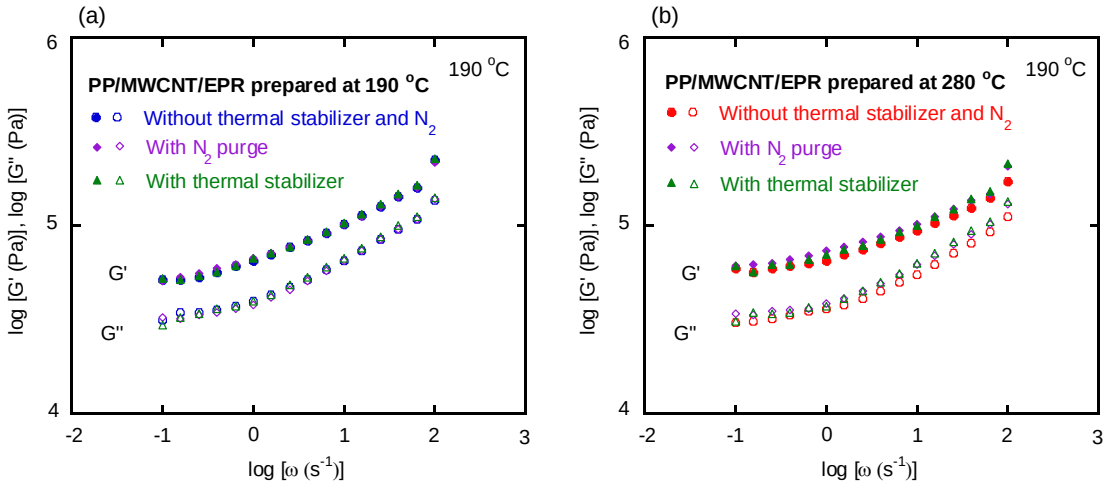

Fig. 4-6 Frequency dependence of oscillatory shear moduli for PP/MWCNT/EPR prepared at (a) 190 °C and (b) 280 °C. Either thermal stabilizer or N_2 gas was introduced into the composites during melt mixing.

The results reveal that the effect of mixing temperature on the rheological

behavior of the composites is stronger than the introduction of thermal stabilizer or N_2 gas. Although the rheological responses are similar irrespective of the introduction of either thermal stabilizer or N_2 gas, a slight change in the surface resistivity is detected, as demonstrated in Fig. 4-7. It suggests that the surface resistivity is more sensitive to the distribution states of MWCNTs.

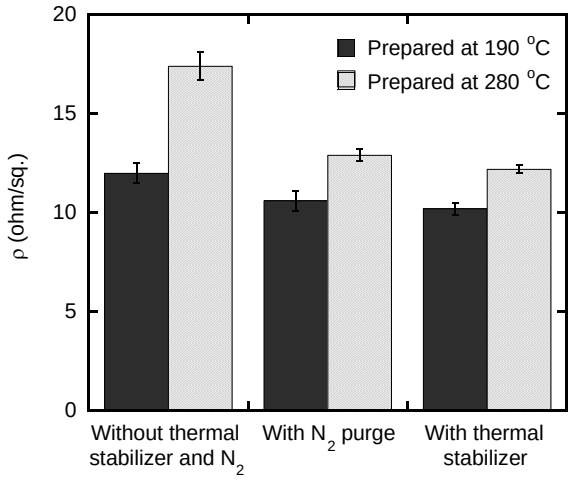

Fig. 4-7 Surface resistivity for PP/MWCNT/EPR (64/16/20) blends prepared by various mixing conditions.

When comparing the samples prepared at the same mixing temperature, it is found that the surface resistivity is low for the samples prepared with thermal stabilizer or N_2 purging. It implies that both thermal stabilizer and N_2 purging presumably enhance the MWCNT dispersion in the matrix.

Furthermore, the dispersion state of MWCNTs was investigated by SEM. Fig. 4-8 shows SEM images of the PP/MWCNT/EPR composites prepared with different mixing conditions.

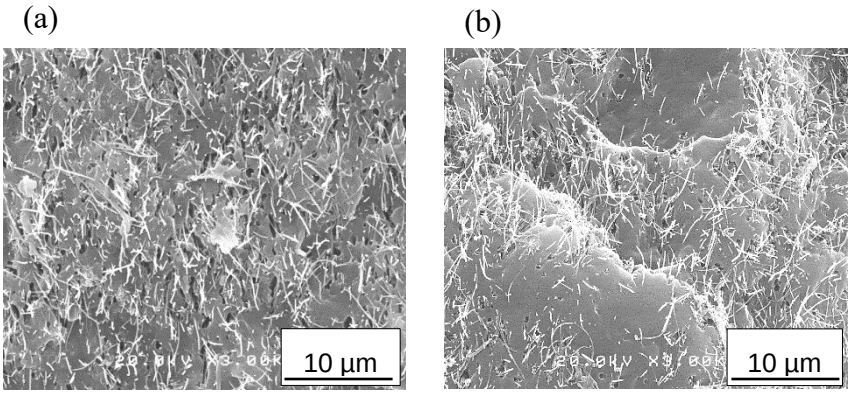

Fig. 4-8 SEM images of fractured surfaces of PP/MWCNT/EPR (64/16/20) prepared at (a) 190 °C with thermal stabilizer under N_2 gas and (b) 280 °C without thermal stabilizer and N_2 gas. EPR fraction is removed by xylene prior to Pt-Pd coating.

As seen in the figure, the sample prepared at the low temperature has a lot of holes on the surface. Since the fractured sample was immersed into xylene, *i.e.*, good solvent for EPR, the holes will be attributed to the EPR dispersion. As compared with the blend without MWCNTs (Fig. 4-4), the domain size of EPR obviously becomes smaller after the incorporation of MWCNTs. Considering that MWCNTs were added in PP at first, this would be attributed to the change in the viscosity ratio between PP and EPR phases. It is

well known that fine dispersion is obtained when the viscosity ratio is closed to 1 [33, 34]. In contrast, fewer holes are detected on the surface of the composite sample prepared at 280 °C. This result implies that most EPR are not dissolved into xylene similar to the PC/MWCNT/EPR composite prepared at the high temperature. Moreover, the MWCNT distribution is not homogeneous for this sample. Once MWCNTs move to EPR, the viscosity ratio becomes significantly large and therefore the morphology should be coarse.

These results indicate that MWCNTs are selectively localized in the PP phase when PP/MWCNT/EPR was prepared at the low temperature with the introduction of thermal stabilizer and N_2 gas. In contrast, most MWCNTs seem to be transferred from PP and distributed in the EPR phase, *i.e.*, the migration of MWCNTs occurs during mixing process at the high temperature, as similar to the PC/MWCNT/EPR system mentioned previously.

The localization of MWCNTs in polymer blends depends on both thermodynamic and kinetic effects. The thermodynamics of PP/MWCNT/EPR is considered based on the concept proposed by Sumita et al. using Young's equation, which is expressed by the calculation of the wetting coefficient ω_a [21],

$$\omega_a = \frac{\Gamma_{MWCNT-PP} - \Gamma_{MWCNT-EPR}}{\Gamma_{PP-EPR}} \tag{4.2}$$

where Γ_{A-B} is the interfacial tension between A and B. For $\omega_a > 1$, MWCNTs are only

dispersed within the EPR phase. For $\omega_a < -1$, they are only presented in the PP phase, and MWCNTs are localized at the interface between PP and EPR phases at $-1 < \omega_a < 1$.

The surface free energies of PP and EPR at 200 °C are 19.3 and 20.8 mN/m, respectively [35]. For MWCNT, the two values, *i.e.*, 27.8 [36] and 45.3 [37] mN/m, obtained from two different studies are used. The interfacial tension is calculated by the Girifalco-Good equation [38, 39].

$$\Gamma_{1-2} = \gamma_1 + \gamma_2 - 2\sqrt{\gamma_1\gamma_2} \tag{4.3}$$

where $\Gamma_{1\text{-}2}$ is the interfacial tension between components and γ_i is the surface free energy of *i-th* component.

The calculated wetting coefficients for the PP/MWCNT/EPR composite are 9.3 for γ_{MWCNT} = 27.8 mN/m and 26.8 for γ_{MWCNT} = 45.3 mN/m, indicating that MWCNTs should be localized in the EPR phase in both cases. However, they are dispersed in the PP phase as shown in Fig. 4-8(a). It should be noted that the PP sample used in this study has significantly lower viscosity than EPR. Hence, the reason for the actual distribution of MWCNTs could be the mixing sequence, mixing condition and high viscosity of EPR. Nevertheless, the location of MWCNTs is changed through the mixing at high temperature without the introduction of thermal stabilizer and N_2 gas.

The dispersion state of MWCNTs is a factor affecting the surface resistivity of the

composites. The values of the samples with MWCNTs are found to be between 10^1 and 10^2 Ω/sq. Furthermore, it is detected that the high-temperature-mixing gives higher electrical resistivity (ρ = 17.4 Ω/sq.) than the low-temperature-mixing (ρ = 6.5 Ω/sq.). This trend is attributed to the MWCNT localization in the blend; when more MWCNTs reside in the PP phase, the conductive path is easily built up in the matrix, leading to low electrical resistivity. On the contrary, when MWCNTs are confined in the dispersed EPR phase, the conductive path in the matrix is difficult to form, which results in high electrical resistivity. The obtained result corresponds with the rheological properties and morphology observation. The selective localization of MWCNTs in the continuous matrix is beneficial for forming an interconnecting conductive network in the matrix.

The dynamic tensile properties such as storage modulus *E'* and loss modulus *E"* of PP/EPR and PP/MWCNT/EPR prepared with different mixing conditions are evaluated as shown in Fig. 4-9. Glass transition temperatures T_g's of the samples obtained from the peak temperature in the *E"* curves are listed in Table 4-2.

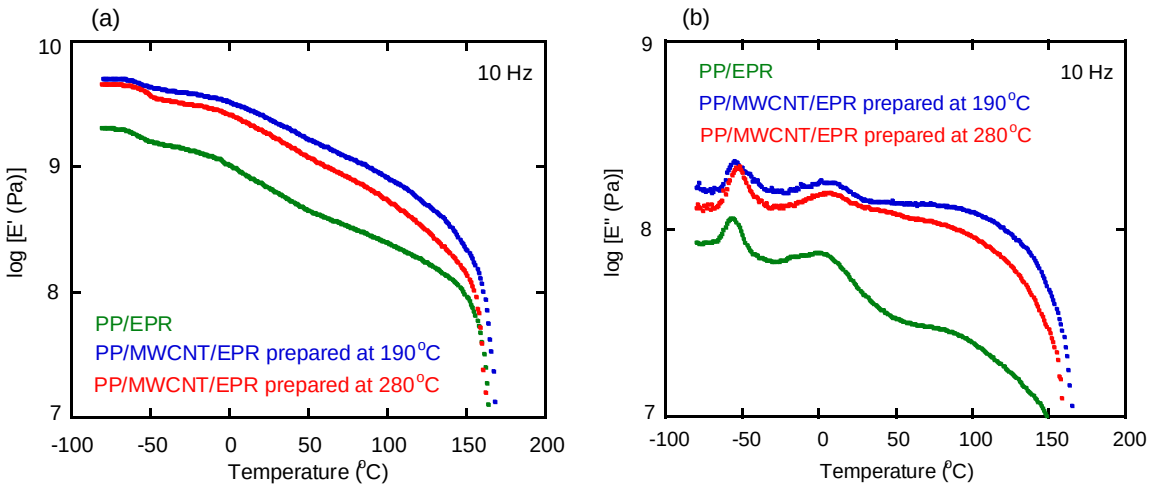

Fig. 4-9 Temperature dependence of tensile moduli such as (a) storage modulus *E'* and (b) loss modulus *E"* for PP/EPR and PP/MWCNT/EPR prepared by various mixing conditions.

Table 4-2 Glass transition temperature of PP/EPR and PP/MWCNT/EPR nanocomposites obtained from the peaks of *E"*

Samples	T_g (°C)	
	EPR	**PP**
PP/EPR	-56.1	4.8
PP/MWCNT/EPR prepared at 190 °C with thermal stabilizer under N_2 gas	-55.3	5.3
PP/MWCNT/EPR prepared at 280 °C without thermal stabilizer and N_2 gas	-52.2	5.4

It is found that *E'* is greatly enhanced by the addition of MWCNTs due to the filling effect, which is more pronounced for the composite prepared at the low temperature. This is reasonable because more MWCNTs reside in the matrix. Moreover, all the samples show double peaks in the *E"* curve, corresponding to T_g's of EPR and PP phases. As seen in Fig. 4-9(b), T_g's of EPR and PP are located at -56.1 and 4.8 °C, respectively. Furthermore, T_g of PP is slightly shifted to higher temperature by the addition of MWCNTs with enhanced α relaxation mode. The well-developed crystalline structure, presumably due to the nucleating ability of MWCNTs [24, 40, 41], is responsible for the marked α relaxation mode and also the T_g shift of PP owing to the restricted motion of amorphous chains by the crystals. Moreover, it should be noted that T_g of EPR in the composite prepared at 280 °C is located at higher temperature than that in the PP/EPR blend without MWCNTs. This is attributed to the reduced motion of EPR molecules adsorbed on the surface of MWCNTs.

Morphological, rheological and electrical properties give the evidence of the difference in the MWCNT localization. Especially, the variation of surface resistivity, oscillatory modulus in the molten state, and T_g agrees well with the morphology change. Thus, it is suggested that the mixing condition with combining the addition of thermal stabilizer and introduction of inert gas contributes to the morphology control of the

immiscible MWCNT-filled PP/EPR blend. This is significantly important because the localization of MWCNTs decides the mechanical properties in the solid state of an immiscible polymer blend.

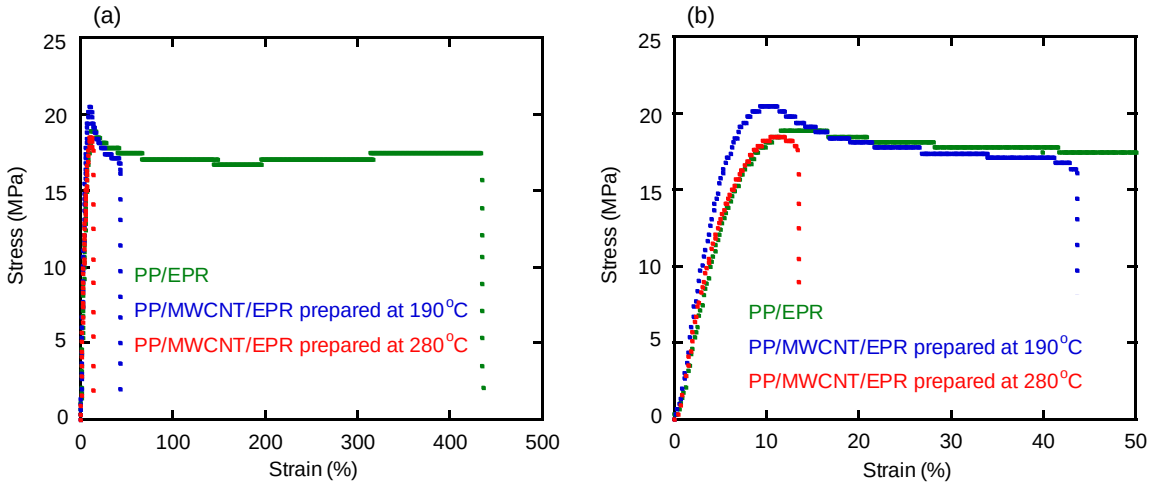

Fig. 4-10 Stress-strain curves of PP/EPR and PP/MWCNT/EPR prepared by various mixing conditions. The initial parts in the small strain region are shown in (b).

Table 4-3 Tensile properties of PP/EPR and PP/MWCNT/EPR nanocomposites

Samples	Yield strength (MPa)	Young's modulus (MPa)	Elongation at break (%)
PP/EPR	18.6±0.3	260±22	487±65
PP/MWCNT/EPR prepared at 190 °C with thermal stabilizer under N_2 gas	20.6±0.8	361±31	47±10
PP/MWCNT/EPR prepared at 280 °C without thermal stabilizer under N_2 gas	18.7±0.3	308±16	13±1

Fig. 4-10 shows the stress-strain curves of the PP/EPR blend and the PP/MWCNT/EPR composites having different structure. The tensile properties are summarized in Table 4-3. The PP/EPR blend shows ductile behavior with a large elongation at break. It is reasonably found that the PP/MWCNT/EPR composites have higher yield strength and Young's modulus than the PP/EPR blend due to the reinforcing ability of MWCNTs [1, 33, 42, 43]. Moreover, Young's modulus and yield strength of the composite prepared by the low-temperature-mixing are higher because MWCNTs, which are dispersed in the matrix, enhance the stiffness with a consequent increase in the modulus. Further, it should be noted that the sample shows a large elongation at break although it has higher modulus, demonstrating that the fracture energy is significantly larger than that for the composite prepared at the high temperature. On the other hand, more MWCNTs are found to be confined in the EPR phase and thus enhance the modulus of rubber dispersions for the composite prepared by the high-temperature-mixing. As a result, the reinforcing capability of rubber dispersion is reduced greatly because the introduction of MWCNTs enhances the cohesive energy to prevent the cavitation. Poor cavitation of rubbery dispersions loses the ability to decrease the dilatational stress and thus leads to brittle fracture. The result indicates that the tensile properties is dependent on the mixing condition.

Overall findings in this study demonstrate that the localization of MWCNTs can be controlled by mixing temperature as presented in PC/MWCNT/EPR and PP/MWCNT/EPR. Moreover, mixing at low temperature with the addition of thermal stabilizer under N_2 purging is effective to control the preferential localization of MWCNTs in a PP matrix of the PP/EPR blend with sea-island structure. This technique will be available for other polymer blends, at least, those containing EPR as an impact modifier, because the adsorption of EPR molecules on the surface of MWCNTs is responsible for the unfavored localization of MWCNTs in the rubbery phase. This concept will widen the material design to develop an advanced rubber-toughened plastic with high rigidity and high impact strength.

4.4 Conclusion

The effect of mixing temperature accompanying with the addition of thermal stabilizer and introduction of N_2 gas on the localization of MWCNTs in the immiscible polymer blends is studied. For the PC/MWCNT/EPR composites, the change of solvent color in dichloromethane from black to fairly transparent demonstrates that the transfer of MWCNTs from PC to EPR phase takes place at high mixing temperature. In the case of PP/MWCNT/EPR, MWCNTs are dispersed in the continuous PP phase when the composite was prepared by the low-temperature-mixing accompanying with the use of thermal stabilizer under N_2 purging. With increasing the mixing temperature up to 280 ℃ without the use of thermal stabilizer and N_2 gas, more MWCNTs are distributed in the dispersed EPR phase, which is attributed to the adsorption of EPR molecules on the MWCNT surface during melt mixing. As expected, when MWCNTs are localized in the PP matrix, Young's modulus and tensile strength are higher than those of the sample having MWCNTs confined in the EPR phase. Moreover, the elongation at break is larger than that for the composite prepared by the high-temperature-mixing.

4.5 References

1. S. Iijima, *Nature,* **354**, 56 (1991).
2. E. Logakis, C. Pandis, V. Peoglos, P. Pissis, C. Stergiou, J. Pionteck, P. Pötschke, M. Mičušík, M. Omastová, *Journal of Polymer Science Part B: Polymer Physics,* **47**, 764 (2009).
3. M.H. Al-Saleh, U. Sundararaj, *Journal of Polymer Science Part B: Polymer Physics,* **50**, 1356 (2012).
4. Y.P. Mamunya, *Journal of Macromolecular Science, Part B,* **38**, 615 (1999).
5. K. Prashantha, J. Soulestin, M.F. Lacrampe, P. Krawczak, G. Dupin, M. Claes, *Composites Science and Technology,* **69**, 1756 (2009).
6. P. Médéric, J. Ville, J. Huitric, M. Moan, T. Aubry, *Polymer Engineering & Science,* **51**, 969 (2011).
7. V.A. Doan, S. Nobukawa, S. Ohtsubo, T. Tada, M. Yamaguchi, *Journal of Polymer Research,* **20**, 1 (2013).
8. A. Göldel, G. Kasaliwal, P. Pötschke, *Macromolecular Rapid Communications,* **30**, 423 (2009).
9. A.C. Baudouin, J. Devaux, C. Bailly, *Polymer,* **51**, 1341 (2010).
10. P. Pötschke, S. Pegel, M. Claes, D. Bonduel, *Macromolecular Rapid Communications,* **29**, 244 (2008).
11. L. Zonder, A. Ophir, S. Kenig, S. McCarthy, *Polymer,* **52**, 5085 (2011).
12. M. Jaziri, N. Mnif, V. Massardier-Nageotte, H. Perier-Camby, *Polymer Engineering & Science,* **47**, 1009 (2007).
13. N. Mnif, V. Massardier, T. Kallel, B. Elleuch, *International Journal of Material Forming,* **1**, 639 (2008).

14. M. Yamaguchi, Y. Irie, P. Phulkerd, H. Hagihara, S. Hirayama, S. Sasaki, *Polymer,* **51**, 5983 (2010).

15. L. Moballegh, S. Hakim, J. Morshedian, M. Nekoomanesh, *Journal of Polymer Research,* **22**, 1 (2015).

16. Y. Liu, M. Kontopoulou, *Polymer,* **47**, 7731 (2006).

17. R. Uotila, U. Hippi, S. Paavola, J. Seppälä, *Polymer,* **46**, 7923 (2005).

18. G. Wu, S. Asai, M. Sumita, *Macromolecules,* **32**, 3534 (1999).

19. G. Wu, S. Asai, M. Sumita, *Macromolecules,* **35**, 945 (2002).

20. H. Yui, G. Wu, H. Sano, M. Sumita, K. Kino, *Polymer,* **47**, 3599 (2006).

21. M. Sumita, K. Sakata, S. Asai, K. Miyasaka, H. Nakagawa, *Polymer Bulletin,* **25**, 265 (1991).

22. M. Sumita, K. Sakata, Y. Hayakawa, S. Asai, K. Miyasaka, M. Tanemura, *Colloid Polymer Science,* **270**, 134 (1992).

23. V. Haddadi-Asl, *Iran Polymer Journal,* **5**, 75 (1996).

24. M. Hemmati, A. Narimani, H. Shariatpanahi, A. Fereidoon, M.G. Ahangari, *International Journal of Polymeric Materials and Polymeric Biomaterials,* **60**, 384 (2011).

25. O. Meincke, D. Kaempfer, H. Weickmann, C. Friedrich, M. Vathauer, H. Warth, *Polymer,* **45**, 739 (2004).

26. S. Phromdee, P. Larjai, S. Tiptipakorn, S. Rimdusit, *Journal of Metals Materials and Minerals,* **24**, 33 (2014).

27. H. Yoon, K. Okamoto, M. Yamaguchi, *Carbon,* **47**, 2840 (2009).

28. A.J. Peacock, *Handbook of Polyethylene Structures, Properties, and Applications,* Marcel Dekker, New York, (2000).

29. M. Siriprumpoonthum, S. Nobukawa, Y. Satoh, H. Sasaki, M. Yamaguchi, *Journal of Rheology,* **58**, 449 (2014).

30. H.H. Kausch, *Polymer Fracture,* Springer-Verlag, Berlin, (1987).

31. C.B. Bucknal, *Polymer Blends*, Wiley-Interscience, New York, (1999).

32. M. Yamaguchi, *Encyclopedia of Polymeric Nanomaterials*, Springer-Verlag, Berlin, (2015).

33. X.Q. Liu, W. Yang, B.H. Xie, M.B. Yang, *Materials & Design,* **34**, 355 (2012).

34. J.P. Cao, J. Zhao, X. Zhao, F. You, H. Yu, G.H. Hu, Z.M. Dang, *Composites Science and Technology,* **89**, 142 (2013).

35. J. Brandrup, E.H. Immergut, E.A. Grulke, D.R. Bloch, *Polymer Handbook*, Wiley, New York, (1999).

36. A.H. Barber, S.R. Cohen, H.D. Wagner, *Physical Review Letters*, 92, 186103 (2004).

37. S. Nuriel, L. Liu, A.H. Barber, H.D. Wagner, *Chemical Physics Letters*, 404, 263 (2005).

38. A.W. Adamson, A.P. Gast, *Physical Chemistry of Surfaces*, Wiley, New York, (1997).

39. S. Ross, I.D. Morrison, *Colloidal Systems and Interfaces,* Wiley, New York, (1998).

40. L. Valentini, J. Biagiotti, M.A. López-Manchado, S. Santucci, J.M. Kenny, *Polymer Engineering & Science,* **44**, 303 (2004).

41. B.P. Grady, *Carbon Nanotube-Polymer Composites: Maufacture, Properties, and Applications,* Wiley, Hoboken, (2011).

42. Y. Wang, J. Deng, K. Wang, Q. Zhang, Q. Fu, *Journal of Applied Polymer Science,*

104, 3695 (2007).

43. V.J. Cruz-Delgado, C.A. Ávila-Orta, A.B. Espinoza-Martínez, J.M. Mata-Padilla, S.G. Solis-Rosales, A.F. Jalbout, F.J. Medellín-Rodríguez, B.S. Hsiao, *Polymer,* **55**, 642 (2014).

Chapter 5

General Conclusions

CNT filled-immiscible polymer blends are of great interest because the mechanical and electrical properties are significantly improved compared to those of a composite with a single polymer. The effective utilization of CNTs in composite applications depends on the dispersion state of CNTs in a polymer blend, which greatly affects overall properties of the materials. The preferential localization of CNTs mainly occurs due to the difference in interfacial tension between CNTs and polymer phase. CNTs will move from a less preferred polymer phase to a more preferred one to minimize the interfacial energy of the blend when the Brownian motion is allowed. However, the equilibrium state of the filler dispersion is not easy to be obtained. Hence, the effect of applied flow field and processing conditions, *e.g.*, mixing period and mixing temperature, should be also taken into consideration.

The influence of mixing process on the localization of multi-walled carbon nanotubes (MWCNTs) in immiscible polymer blends during melt-mixing process is also presented in this dissertation. Furthermore, the effect of their localization on the resulting mechanical properties of the composites is shown.

In Chapter 2, the localization of MWCNTs in polycarbonate (PC)/poly(ethylene terephthalate) (PET) blends is demonstrated. It is found that MWCNTs preferentially localize in the favorable PET phase in all PC/MWCNT/PET composites, which are confirmed by SEM characterization and solvent extraction experiments. Although the incorporation of MWCNTs slightly influences the miscibility of the blend, it significantly affects the thermal and mechanical properties. Crystallization temperature of PET apparently shifts to a higher temperature. It clearly indicates that MWCNTs act as a strong nucleating agent for PET, resulting in the acceleration of crystallization. Due to their reinforcing ability combined with high aspect ratio, tensile properties, *i.e.*, Young's modulus and ultimate strength, of PC/PET blends are increased by the addition of MWCNTs.

For Chapter 3, a contradictory transfer phenomenon of MWCNTs is presented in the immiscible polymer pairs of PC and polyethylene (PE). MWCNTs prefer to immigrate from PE to PC through phase boundary during annealing in the laminated sheets, whereas the transfer of MWCNTs from PC to PE does not occur at all. The MWCNT transfer is attributed to the difference in the interfacial tension between each polymer and MWCNT with the aid of Brownian motion. In contrast, it is found that MWCNTs move from PC to PE phase during melt mixing, which is revealed by solvent

extraction, SEM observation, and DSC measurements. Moreover, the selective adsorption of PE molecules on the surface of MWCNTs is clearly detected by the solvent extraction experiments, which is presumably generated by the aid of oxygen during melt-mixing process. These results suggest that the distribution state of MWCNTs can be tailored by controlling the processing condition.

A methodology for controlling the MWCNT localization in either matrix or dispersed phase is further shown in Chapter 4. There are two types of polymer blends, *i.e.*, PC/ethylene-propylene copolymer (EPR) and polypropylene (PP)/EPR, used in this study. For the PC/EPR blend, it is found that MWCNTs reside in the PC phase at low mixing temperature. On the contrary, MWCNTs move from PC toward EPR droplets when the mixing temperature is high, which is attributed to the adsorption of EPR on the MWCNT surface. In the case of PP/EPR blends, most of MWCNTs are dispersed in EPR in the composite prepared at high temperature, while some MWCNTs are still remained in the matrix. Because of MWCNTs are dispersed in the EPR droplets, a conductive path by CNTs in the PP matrix is difficult to form, leading to high surface resistivity. In contrast, when the composite is prepared by the low mixing temperature accompanying with the introduction of thermal stabilizer and N_2 gas purging, MWCNTs are found to be selectively localized within the PP matrix, resulting in low surface resistivity and the

enhancement in Young's modulus and yield strength.

From the results obtained in this work, it is concluded that the appropriate mixing condition, *i.e.*, low-temperature-mixing combined with the addition of thermal stabilizer under N_2 gas, can efficiently provide the high rigidity and toughness for a polymeric composite. I hope that the acquired knowledge can be useful for a further control of CNT-filled polymer blends and toward their practical applications.

Once the MWCNT localization in either the matrix or dispersed phase can be controlled by using the concept employed in this thesis, the applications of polymer nanocomposites will be widened. Moreover, graphene is currently of a great interest as an effective filler for polymer nanocomposites due to its impressive properties and cost effective. Therefore, the presented method is possible to be utilized for controlling the graphene localization in a polymeric composite.

Achievements

Publications

1. **R. Wiwattananukul**, Y. Hachiya, T. Endo, S. Nobukawa and M. Yamaguchi Anomalous Transfer Phenomenon of Carbon Nanotube in the Blend of Polyethylene and Polycarbonate
   Composists Part B: Engineering, (2015), 78, 409-414.

2. **R. Wiwattananukul**, Y. Hachiya, T. Endo, S. Nobukawa and M. Yamaguchi Selective Localization of Carbon Nanotubes in PC/PET Blends.
   Polymer Composites, (2015), in press, DOI: 10.1002/pc.23672.

3. **R. Wiwattananukul**, Y. Tanigawa and M. Yamaguchi
   Improvement of Rigidity for Rubber-Toughened Plastics by Localization of Carbon Nanotubes. Submitted.

4. M. Yamaguchi, Y. Hachiya, H. Yoon, **R. Wiwattananukul** and S. Nobukawa Interphase Transfer of Carbon Nanotube between Two Polymer Sheets
   Journal of Material Testing Research. Association of Japan, (2015), 60, 140-143.

Others

1. J. Seemork, T. Itoh, T. Sako, **R. Wiwattananukul**, S. Nobukawa, H. Sasaki, Y. Satoh and M. Yamaguchi
   Impact of Mixing Method on Flow Instability for Binary Mixture of Linear Low-Density Polyethylene. Submitted.

Presentations

International Conference:

1. **R. Wiwattananukul**, S. Nobukawa and M. Yamaguchi
   "Anomalous Transfer of Carbon Nanotube between Immiscible Polymers"
   Eurofillers Polymer Blends 2015, Montpellier, France, April 2015

2. **R. Wiwattananukul**, S. Nobukawa and M. Yamaguchi
   "Contradictory Transfer Phenomenon of Carbon Nanotubes in Immiscible Polymers"
   31st International Conference of the Polymer Processing Society (PPS-31), Jeju island, Korea, June 2015

3. **R. Wiwattananukul**, S. Nobukawa and M. Yamaguchi
   "Control of MWCNT Distribution in Immiscible Polymers"
   Polymer Processing Society Conference 2015 (PPS2015), Graz, Austria, September 2015

4. **R. Wiwattananukul** and M. Yamaguchi
   "Localization Behaviour of Carbon Nanotubes in Melt-Mixed Immiscible Polymer Blend"
   Asian Polyolefin Workshop 2015 (APO2015), Tokyo, Japan, November 2015

5. **R. Wiwattananukul** and M. Yamaguchi
   "Localized Distribution of Carbon Nanotube in a Rubber-Modified Plastic"
   The 3rd International Symposium for Green-Innovation Polymers (GRIP2016), Nomi, Japan, March 2016

6. **R. Wiwattananukul** and M. Yamaguchi
   "Selective Localization of Carbon Nanotube and Effect on Mechanical properties of Immiscible Polymer Blends"
   The XVIIth International Congress on Rheology (ICR2016), Kyoto, Japan, August 2016

Domestic Conference:

1. **R. Wiwattananukul**, Y. Hachiya, T. Endo, S. Nobukawa and M. Yamaguchi
   "Contradictory Phenomenon of Carbon Nanotube Transfer in an Immiscible Polymer Blend"
   63rd Symposium on Macromolecules (SPSJ), Nagasaki University, Japan, September 2014

Awards:

1st Prize of Springer Poster Award
Eurofillers Polymer Blends 2015 conference at Montpellier, France April, 2015

JAIST President's Award, July 2015

JAIST Doctoral Research Fellow (DRF)
October 2013 – September 2016

Improvement of fuel cells with carbon nanotube based electrode thin films using layer by layer assembly

1. Introduction

Due to extraordinary and unique properties of carbon nanotube (CNT), this material is one of the most promising materials for functional thin film application, transistors, photoresponsive devices, electrochemical energy conversion and storage devices [1- 4]. High surface area combined with superior properties of CNTs shows that CNTs have good ability to promote electron transfer reaction when used as electrode materials in electrochemical reaction [5, 6]. However, an oxygen reduction on the electrode surface takes place in various electrochemical energy conversion processes [7]. It is well-known that metalloporphyrins and their derivatives are found to be versatile compounds with use in many fields involving redox process, which is the central metal has been clarified to a large extent. Therefore, they can be used as an appropriate catalyst for oxygen reduction [8, 9]. Metalloporphyrins generally catalyze oxygen reduction via the 2-electron reduction of oxygen to hydrogen peroxide, followed by further 2-electron reduction to generate water. This reaction is a requirement for proton conducting membrane fuel cells (PCMFCs) [10]. Many studies have been shown that

platinum dispersed in polymer and CNT/porphyrin composite enhance the efficiently of oxygen reduction [11, 12]. Generally, porphyrin derivatives can be dissolved in suitable solutions, but in most case, they are assembled on solid substrates, *i.e.*, glass, quartz and several electrode surfaces, because layers of porphyrins on solid surfaces are practical in various applications [13, 14]. Recently, one of the most useful method to assemble CNTs and porphyrins into thin films is layer-by-layer (LBL) assembly.

The LBL assembly technique has been reported approach to prepare thin films, which involves the alternate adsorption of oppositely charged species via an interlayer coordinative bond or an electrostatic interaction. The LBL method is a simple but effective approach to develop a homogeneous and stable film because the films could be constructed directly on the substrate surface, which shows strong stability and potential application [15, 16]. Moreover, this method cannot be only incorporated large amount of CNTs but also control the composition and nanostructure of the composite, including molecular framework and thickness.

In this work, thin film for the electrode in fuel cell based on LBL method is prepared employing single-walled carbon nanotube (SWCNT) and cobalt (II) porphyrin of 5, 10, 15, 20-tetrakis-(4-aminophenyl) (Co(II)(T(*p*-NH_2)PP)). SWCNTs were functionalized on their exterior walls with carboxylic acid group, SWCNT-COOH, in

order to achieve good dispersion in solvent and prevent aggregation of CNT bundles. The negatively charged SWCNT will assemble to the positively charged porphyrin yielding SWCNT-COOH/Co(II)(T(*p*-NH_2)PP) on the substrate surface. The prepared films were characterized using UV-vis spectroscopy and X-ray photoelectron spectroscopy.

2. Experimental

2.1 Material

Single-walled carbon nanotube functionalized with carboxylic acid group (SWCNT-COOH) (4-5 nm diameters and 0.5-1.5 μm length, C > 90 %, carboxylic extent 1.0-3.0 %) was purchased from Sigma-Aldrich Co. LLC. Cobalt (II) porphyrin of 5, 10, 15, 20-tetrakis-(4-aminophenyl) (Co(II)(T(*p*-NH_2)PP)) (M_w = 731.73 g/mol) was obtained from Porphyrin System. (3-Aminopropyl) trimethoxysilane (APTMS) (M_w = 179.29 g/mol) was used in silanization processes as a silane coupling agent. The structure of materials is shown in Fig. 1.

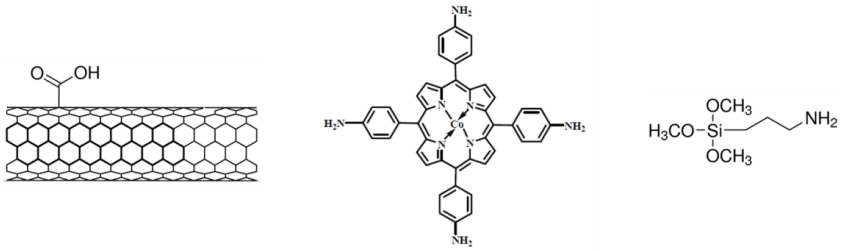

Fig. 1 Structures of (a) SWCNT-COOH, (b) Co(II)(T(*p*-NH_2)PP) and (c) APTMS.

Other aqueous solutions such as dimethylformamide (DMF), dimethyl sulfoxide (DMSO), 2-propanol, ethanol and toluene were employed in this study. The solvents, *i.e.*, 2-propanol and ethanol in HPLC grade, were used to clean the substrates, whereas ethanol and toluene in Analytical grade were used in substrate modification.

2.2 Layer-by-layer assembly

Cationic 0.05 mM Co(II)(T(*p*-NH_2)PP was prepared by dissolving in DMSO in an ultrasonic bath for 30 min. The 0.1 mg/ml anionic SWCNT solution was also prepared by dissolving in DMF, followed by sonication for 30 min to remove large nanotube bundles and form stable suspension. All solutions were used without adjusting pH. In this study, two different substrate species, indium tin oxide (ITO) and quartz, were employed for LBL assembling of the multilayer thin films. Due to the difference of substrate species, a difference of modification method was used.

For ITO substrate, the substrate was cut to 10×50 mm^2 size, ultrasonically cleaned in 2-propanol for 15 min and then dried. The freshly clean substrate was then refluxed in 0.4475 ml ATPMS : 250 ml toluene at 100 °C for 30 min to form amine group on the surface. A positively charged surface (covered with $–C_6H_{17}NO_3Si$) was obtained, which will be used to adsorb negatively charged polyelectrolytes. Thereafter, the positively charged ITO-ATPMS was washed and sonicated with 2-propanol before use.

In case of quartz, the substrate was cleaned in 2-propanol for 20 and 10 min each, and then dried. The clean substrate was also formed amine group in 0.4475 ml APTMS : 250 ml ethanol at room temperature for 1 h with a mild shaking. Then, the amine functionalized quartz substrate was washed with ethanol for 5 and 5 min each, followed by 2-propanol for 5 and 5 min each. All of washing sequences were performed under mild sonication. After the modification of the substrate surface, multilayers of SWCNT-COOH/Co(II)(T(*p*-NH_2)PP were prepared.

The SWCNT-COOH/Co(II)(T(*p*-NH_2)PP assemblies were deposited on either the ITO- or quartz-silane modified substrate by a LBL technique, as demonstrated in Fig. 2. Selective deposition of each monolayer is attributed to an opposite charged electrostatic interactions.

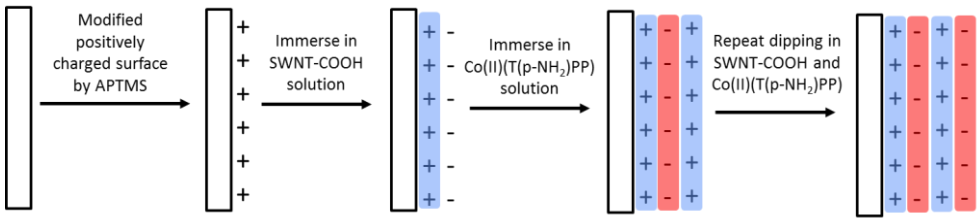

Fig. 2 The LBL assembled SWCNT-COOH/Co(II)(T(*p*-NH_2)PP thin film by altered dipping the substrate in negatively and positively charged ions, respectively.

Modified substrate was firstly dipped into the SWCNT-COOH solution for 5 min, then four baths of DMF for 1, 1, 1 and 1 min each in order to rinse off excessively large particulates. After that, the substrate was dried to prevent cross-contamination between the oppositely charged solutions. The substrate was then dipped into Co(II)(T(*p*-NH_2)PP solution for 5 min, and washed in four baths of DMSO for 1, 1, 1 and 1 min each. Then, the sample was dried again by air blower for 5 min. This cycle makes one bilayer of SWCNT-COOH and Co(II)(T(*p*-NH_2)PP, denoted SWCNT-COOH/Co(II)(T(*p*-NH_2)PP. The cycle was repeated to reach desired number of bilayers. Furthermore, the assembly times for each layer were changed from 5 min to 1 h for SWCNT-COOH and 30 min for Co(II)(T(*p*-NH_2)PP. The number of washing times was decreased from four to three times. Further, for ITO substrate, one more experiment was conducted. After the modification of substrate surface, ITO was immersed into SWCNT-COOH solution and then refluxed at 150 °C for 30 min.

Thereafter, the obtained substrate was washed, followed by dipping in cobalt (II) porphyrin solution for 30 min.

2.3 Characterization

UV-vis spectra of metalloporphyrin, Co(II)(T(*p*-NH_2)PP, in DMSO solution and LBL multilayers were acquired with the use of UV-visible spectrophotometer (UV-vis) (V-630 BIO, JASCO, Japan). In order to determine the adsorb of CNT per adsorption cycle on the substrates, the absorbance of Co(II)(T(*p*-NH_2)PP was determined because Co(II)(T(*p*-NH_2)PP correlates to the amount of SWCNT-COOH deposition.

The composition and surface chemistry of SWCNT-COOH/Co(II)(T(*p*-NH_2)PP were analyzed using X-ray photoelectron spectrophotometer (XPS) (AXIS-ULTRA DLD, Shimadzu, Japan). The XPS measurement was done with a monochromatic Al K_α X-ray source for excitation. The Casa XPS software with a Gaussian-Lorentzian mix function and Shirley background subtraction were used to deconvolute the data.

3. Results and Discussion

3.1 Absorbance of Co(II)(T(p-NH_2)PP in solution

To examine the characteristic peaks of metalloporphyrin, an absorbance peak of Co(II)(T(*p*-NH_2)PP solution was measured using UV-vis spectroscopy, as shown in Fig. 3. Since CNT does not absorb in the visible region (300-1100 nm), the obtained absorbance is only due to the Co(II)(T(*p*-NH_2)PP.

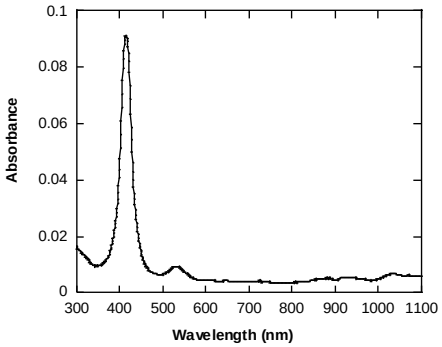

Fig. 3 UV-vis spectrum of Co(II)(T(*p*-NH_2)PP solution.

Fig. 3 shows strong adsorption peaks of Co(II)(T(*p*-NH_2)PP at 415 and 533 nm, which are Soret and Q-bands absorption characteristics of the porphyrin.

3.2 LBL assembly

3.2.1 ITO substrate

XPS results for ITO substrate after silanization with aminosilane, *i.e.*, APTMS, are presented in Fig. 4.

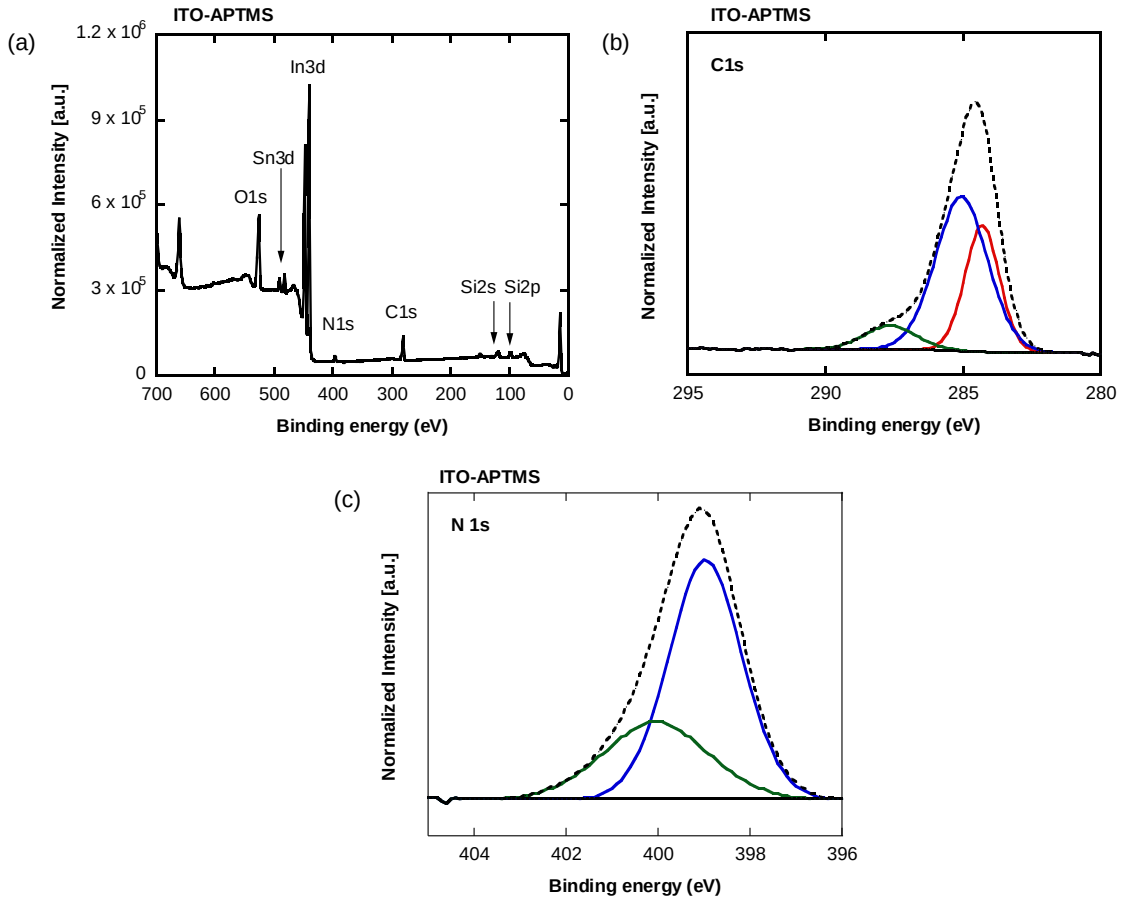

Fig. 4 XPS (a) survey scan, and deconvoluted spectra of (b) C1s and (c) N1s of ITO after silanization with APTMS.

Peaks of carbon (C), silicon (Si) and oxygen (O) are detected. In addition, nitrogen (N) peak related to the amino group appears, revealing the aminosilane is formed on the substrate surface. Deconvoluted XPS C1s spectra show three contributions that are related to different types of carbon-atoms bonds. The component at 284.3 eV represents the backbone and/or the methyl carbon bonds (C-C and/or C-H);

the peak at 285.1 eV corresponds to the carbon atom connected to oxygen (C-O) or to nitrogen (C-N); the peak at 287.6 eV corresponds to O-C-O and C=O bonds. Here, the N1s can be fitted by two components, *i.e.*, the peaks at 398.9 eV and 400.0 eV. The first peak is believed to assign the nitrogen atoms in the form of NH_2, and the second peak is attributed to the protonated aliphatic amino group (NH_3^+) [17-19].

Furthermore, the formation of SWCNT-COOH/Co(II)(T(*p*-NH_2)PP films on ITO was characterized using UV-vis absorption spectroscopy and XPS, as demonstrated in Fig. 5.

The increase in the number of multilayer catalyst, *i.e.*, Co(II)(T(*p*-NH_2)PP, is expected to be increased the possibility to give higher density of catalytic sites on the electrode surface. However, the achieved result shows that the absorption peak of Co(II)(T(*p*-NH_2)PP cannot be detected. The C1s spectrum (Fig. 5(c)) shows three contributions at 284.3, 285.6 and 287.8 eV, denoting C-C/C-H, C-N, and C=O, respectively. The new carbon peak at 285.6 is assigned to the C-NH_2 moieties. This is also proved by the occurrence of two major peaks in N1s spectra at 399.3 and 400.9 eV. The binding energy at 399.3 eV is assigned to the amine (-NH_2) bonds, while the peak at 400.9 eV is probably due to the nitrogen contamination by nitrogen gas adsorption [19]. Even though the spectrum of bilayer film (Fig. 5(b)) shows the presence of C, N

and O, the cobalt (Co) peak is not detected at 780.8 and 795.6 eV.

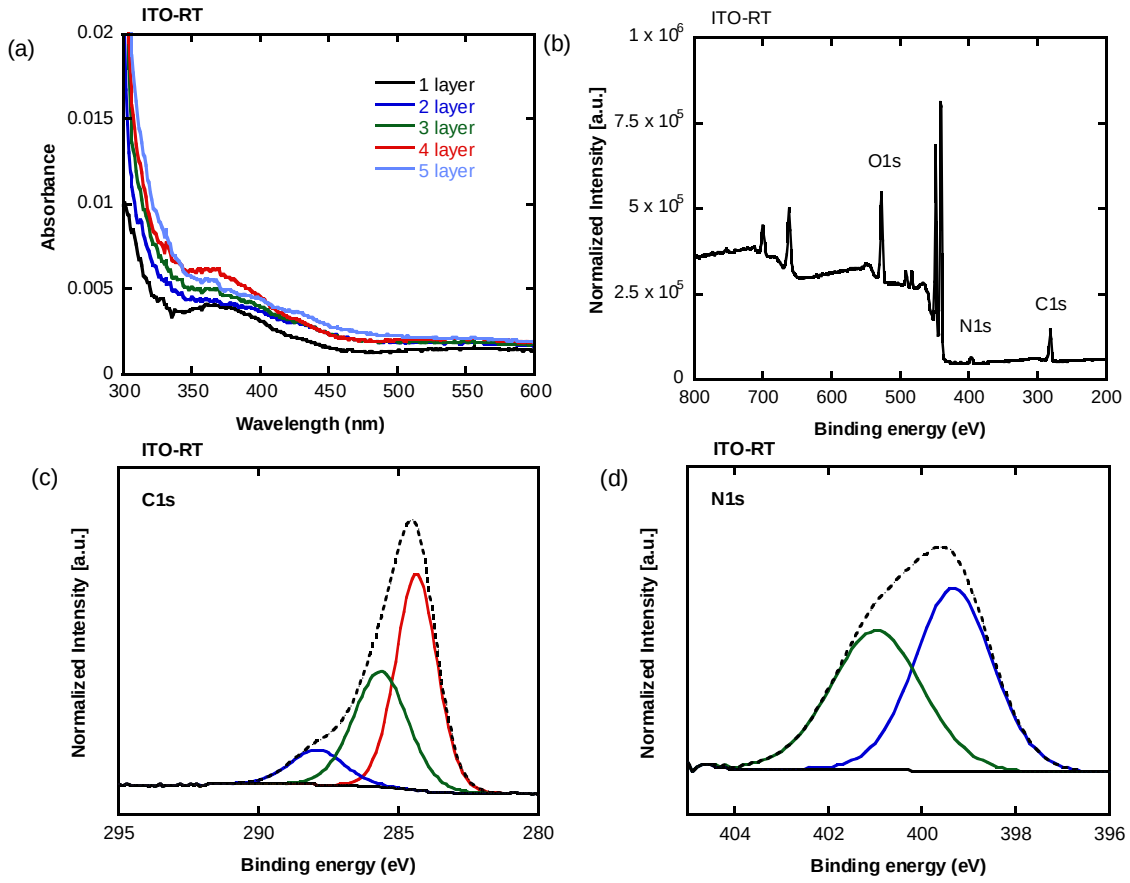

Fig. 5 (a) UV-vis spectra and (b) XPS survey scan of SWCNT-COOH/Co(II)(T(*p*-NH_2)PP film. Deconvoluted XPS spectra of (c) C1s and (d) N1s are also shown. The experiment was conducted at room temperature.

It suggests that only small amount of SWCNT can adsorb on the substrate, resulting in a difficulty for forming the interaction between positively charged-Co(II)(T(*p*-NH_2)PP and negatively charged-SWCNT. This is presumably

because the dipping time (5 min) is insufficient. Considering this assumption, the dipping time in both solutions is increased to 1 h for SWCNT and 30 min for Co(II)(T(*p*-NH_2)PP solutions. Additionally, the number of washing times in pure solvents, DMF and DMSO, are reduced to avoid the dissociation of nanotube and cobalt (II) porphyrin during LBL process.

It is found that, even prolonged dipping time, the Co(II)(T(*p*-NH_2)PP peaks cannot be observed (the result not shown here), demonstrating that the interaction between Co(II)(T(*p*-NH_2)PP and SWCNT is hardly formed. The main reason of these unexpected results is, probably, that only small amount of functionalized SWCNTs can form interaction with APTMS on the substrate because the extent of carboxylic functionalized on SWCNT surface is extremely low (1-3 wt.%). Further, it can be assumed that an electrostatic interaction in this study is easily dissociated.

In order to enhance the probability of the formation between SWCNT-COOH and APTMS, reflux technique is used to generate a reaction between carboxylic acids and amines, resulting in a strong hydrogen bonding interaction. Afterward, the ITO substrate was submersed into Co(II) porphyrin solution. The result is shown in Fig. 6.

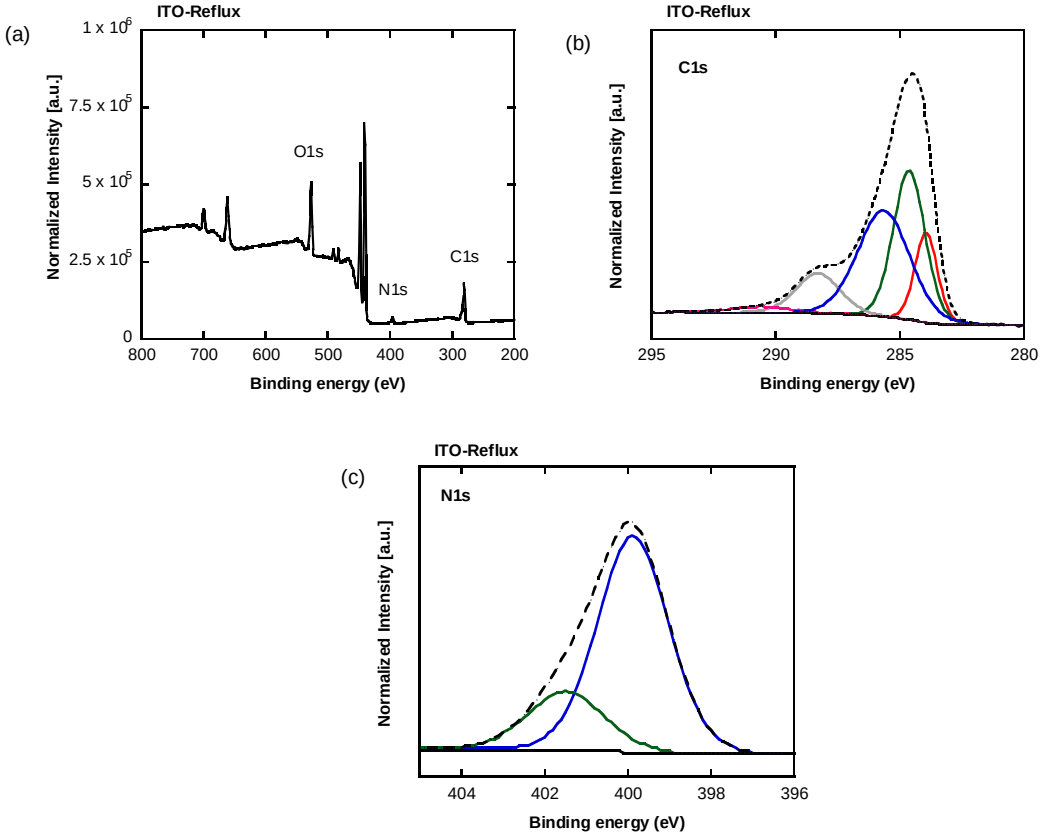

Fig. 6 (a) XPS survey scan, and deconvoluted spectra of the (b) C1s and (c) N1s of SWCNT-COOH/Co(II)(T(*p*-NH_2)PP film. The ITO was refluxed in nanotube solution and then dipped into cobalt (II) porphyrin solution.

The C1s spectrum shows five contributions. The binding energy at 283.9 eV represents the C-C/C-H; however, the binding energy shift to lower energy as compared to the previous result (284.3 eV). Aside from the C-C/C-H peak, the main two peaks at 284.6 and 285.6 eV are presumably related to the aromatic carbon of the porphyrin

molecules and phenyl rings, and carbon atom connected to nitrogen atom in amine ($C\text{-}NH_2$), respectively. The peaks at 288.2 and 290.5 eV are assigned to the -COO and the π- π^*, which is the characteristic of carbon in aromatic compounds, respectively. The deconvolution of N1s spectrum results in two peaks, in which the N-C bond is at 399.8 eV and the second peak at 401.4 eV shows the presence of N atom in the amino group (NH_3^+). This peak may be associated to the NH_2 binds with hydrogen from -OH group on the surface of substrate or hydrogen atom from another alky amine unit. Another possibility is the reaction between NH_2 and carboxylic group on the surface of SWCNT.

In addition, the surface atomic concentrations of C, O and N of the films on ITO substrates are calculated from the corresponding peak areas and summarized in Table 1.

Table 1 XPS surface atomic concentrations of C, N and O of LBL-multilayer films on ITO substrates after LBL assembly at different conditions.

Condition	Dipping time (min)		C (%)	N (%)	O (%)
	SWCNT-COOH	Co(II)(T(*p*-NH_2)PP			
Reference (APTMS)	-	-	17.5	4.6	77.9
RT	5	5	21.1	4.1	74.8
Reflux (150 °C)	30	30	28.9	4.6	66.5

It is found that the increase of C (36.9%) and N (12.2%) is detected after heat treatment accompanying with the prolonged dipping time. The result reveals that the extent of amine group increases, which can be referred to the interaction between carbon and nitrogen. Furthermore, a sharp decrease of oxygen concentration is obvious in reflux condition than in room temperature condition, indicating that the SWCNT-porphyrin binding occurs on the ITO surface.

3.2.2 Quartz substrate

Multilayers of SWCNT-COOH/Co(II)(T(*p*-NH_2)PP were also prepared on silane-modified quartz substrate surfaces. The modified substrate was submersed into

SWCNT and Co(II)(T(*p*-NH_2)PP solutions for 1 h and 30 min, respectively, at room temperature. The surface atomic concentrations of C, O and N are listed in Table 2. Besides, the UV-vis and XPS spectra of obtained sample are shown in Fig. 7.

Table 2 XPS surface atomic concentrations of C, N and O of LBL-multilayer films on quartz substrates after self-assembly.

Condition (°C)	Dipping time (min)		C (%)	N (%)	O (%)
	SWCNT-COOH	Co(II)(T(*p*-NH_2)PP			
Reference (APTMS)	-	-	4.2	0.9	94.9
RT	60	30	7.8	1.3	90.9

Apparent increase of C (85.7%) and N (44.4%) are shown in Table 2. At the same time, the O amount on the sample is reduced, as compared to reference, *i.e.*, APTMS coated on quartz. It suggests that the interaction between porphyrin and SWCNT exists.

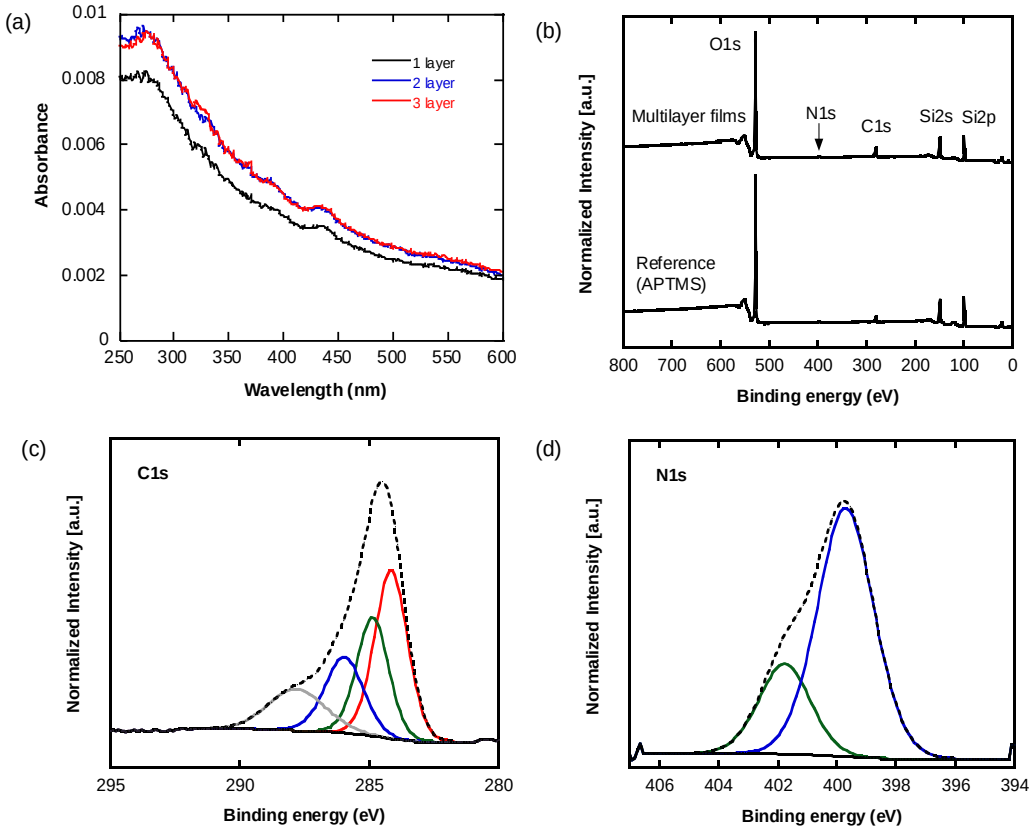

Fig. 7 (a) absorption spectra and (b) XPS survey scan for the multilayers after assembly on quartz substrate. XPS of (c) C1s and (d) N1s spectra are also presented.

Fig. 7(a) reveals only one group of absorption band at about 436 nm corresponding to the Soret band of porphyrins. It can be found that the Soret absorption band of porphyrin in the DMSO solution appears at about 415 nm (Fig. 3) and this band shifts to about 436 nm in the films of SWCNT-COOH/Co(II)(T(*p*-NH_2)PP. This shift has been observed in the ultrathin films of porphyrins or macrocyclic molecules and has been ascribed to a closely packed arrangement of porphyrin in macromolecular

assemblies [20]. Additionally, the deconvoluted XPS spectrum of C1s presents different components that are related to different types of C atom bonds. The component at 284.8 eV corresponds to C-C/C-H bonds; the component at 285.9 eV corresponds to C-O bonds; and the component at 287.8 eV is related to O-C-O and C=O bonds. In the N1s spectrum obtained after self-assembly, there are two different components related to NH bonds, as demonstrated in Fig. 7(d). The peak at 399.6 eV is related to -NH_2 bonds, and the component at 401.7 eV corresponds to (NH_3^+) bonds [18]. The results are in good agreement with the UV-vis spectra that cobalt (II) porphyrin binds to SWCNT.

4. Conclusion

It is found that the formation of thin films between cobalt (II) porphyrin and SWCNT is uneasy to be reached although the substrate types and experimental condition are changed. The results of this present study suggest that the main reason for unsuccessful LBL assembly is owing to the low concentration of COOH on SWCNT surface and/or non-appropriate assembly condition. Considering all of the results, high concentration of negatively charged on the SWCNT surface should be selected for self-assembly technique. Moreover, prolonged dipping time is also recommended.

5. References

1. S. Iijima, *Nature*. **354,** 56 (1991).
2. R.H. Baughman, A.A. Zakhidov, W.A. de Heer, *Science*. **297,** 787 (2002).
3. M.S. Dresselhaus, K.A. William, P.C. Eklund, *Material Research Bulletin,* **24,** 45 (2000).
4. A.C. Dillon, M.J. Heben, *Apply Physics A*, **72,** 133 (2001).
5. P.J.F. Harris, *Carbon Nanotubes and Related Structures*, Cambridge university press, Cambridge (1999).
6. B.P. Grady, *Carbon Nanotube-Polymer Composites: Manufacture, Properties, and Applications*, Willey, Hoboken (2011).
7. E. Song, C. Shi, F.C. Anson, *Langmuir*, **144,** 315 (1998).
8. E. Song, F.C. Anson, *Journal of the American Chemical Society,* **113,** 9564 (1991).
9. R.J.H. Chan, Y.O. Su, T. Kuwana, *Inorganic Chemistry,* **24,** 3777 (1985).
10. K.D. Kreuer, *Journal of Membrane Science,* **185,** 29 (2001).
11. J. Qu, Y. Shen, X. Qu, S. Dong, *Electroanalysis*. **16,** 1444 (2004).
12. Q. Zhou, C. Li, J. Li, X. Cui, D. Gervasio, *Journal of Physical Chemistry C,* **111,** 11216 (2007).
13. H.L. Wang, Q. Sun, M. Chen, J. Miyake, D.J. Qian, *Langmuir,* **27,** 9880 (2011).
14. K.S. Lokesh, M.D. Keersmaecker, A. Adriaens, *Molecules*, **17,** 7824 (2012).
15. D.G. Fuzzy, *Science*, **277,** 1232 (1997).
16. M.N. Zhang, L. Su, L.Q. Mao, *Carbon,* **44,** 276 (2006).
17. Y. Bai, M. Sekita, M. Schmid, T. Bischof, H.P. Steinrück, J.M. Gottfried, *Physical Chemistry Chemical Physics,* **12,** 4336 (2010).
18. G. Jakša, B. Štefane and J. Kavač, *Surface Interface Analysis,* **45,** 1709 (2013).

19. L. Zhang, J. Liu, J. Yang, Q. Yang and C. Li, *Microporous and Mesoporous Materials,* **109,** 172 (2008).
20. K.S. Lokesh, K. De Wael, A. Adriaens, *Langmuir,* **26,** 17665 (2010).
21. M. Kasha, *Journal of Radiation Research,* **20,** 55 (1963).

Acknowledgement

First and foremost, I would like to express my gratitude to my supervisor, Prof. Masayuki Yamaguchi for all of his support and patient guidance. He is always willing to answer my questions and provides valuables advice during the study. I am always encouraged and inspired by his enthusiasm toward research and insightful suggestions. Without his help, this thesis would not be accomplished.

I also appreciate of my committees: Prof. Tatsuo Kaneko, Associate Professor Ken-ichi Shinnohara, Associate Professor Kazuaki Matsumura of JAIST, and Prof. Shuichi Maeda of Yamaguchi University for their helpful comments.

I am grateful to Associate Professor Yuki Nagao, Ms. Salinthip Laokroekkiat and Mr. Md. Abu Rashed for their warm welcome and helpful suggestions on my minor research. They helped me greatly to finish my experimental and characterization parts in the minor research.

I also would like to express my gratitude to Hodogaya Chemical Co., Ltd. for the kind supply of the samples employed in this study.

A sincere appreciation goes to my colleagues and friends in Yamaguchi laboratory for their help, sharing their knowledge and meaningful contribution to this thesis. Their friendship makes my daily life in JAIST enjoyable in these years. I also

deeply appreciate Assistant Professor Dr. Shogo Nobukawa for his valuable guidance and technical supports.

The most important, I would like to convey my heartfelt thanks to my family who have been a great source of strength all through this work during the time far from home. Without their love and encouragement, I would not have finished this thesis.

Rujirek Wiwattananukul

August 2016

Ishikawa, Japan